PH.D. THESIS

The QCD Phase Diagram from Strong Coupling Expansion

Author:
Giuseppe Gagliardi

Supervisor & Examiner:
Dr. Wolfgang Unger
Examiner:
Prof. Dr. Owe Philipsen

UNIVERSITÄT
BIELEFELD

Declaration of Authorship

I, Giuseppe Gagliardi, declare that this thesis titled, "The QCD Phase Diagram from Strong Coupling Expansion" and the work presented in it are my own. I confirm that:

- This work was done wholly or mainly while in candidature for a research degree at this University.

- Where I have consulted the published work of others, this is always clearly attributed.

- Where I have quoted from the work of others, the source is always given. With the exception of such quotations, this thesis is entirely my own work.

- I have acknowledged all main sources of help.

- Where the thesis is based on work done by myself jointly with others, I have made clear exactly what was done by others and what I have contributed myself.

Signed:

_____

Date:

_____

Abstract

In this thesis we investigate dualization strategies in SU(N) lattice gauge theories making use of the strong coupling expansion. The conventional representation of the lattice QCD path-integral, which is obtained by considering the gauge links as the fundamental degrees of freedom after having integrated out the fermion fields, suffers from the so-called finite density sign problem: when a non-zero chemical potential μ_q is switched on, the QCD action is no longer real and the thermodynamic properties of the QCD medium at finite temperature and density cannot be reached by means of standard Monte Carlo methods which relies on the interpretation of the path-integral as a probability distribution. The severity and the existence of the sign problem is however representation dependent: using a different representation, replacing the gauge links by a different set of integration variables might produce a mild enough sign problem that can be handled in Monte Carlo simulations via sign reweighting. A dual representation with a mild sign problem was so far only known in the so-called strong coupling limit $\beta = 2Nc/g_s^2 = 0$ and more recently including $\mathcal{O}(\beta)$ gauge corrections. Going beyond this approximation is challenging as non-trivial and coupled gauge integrals over the invariant Haar measure are involved. We will show how group theoretical techniques can be applied to perform an exact dualization of the theory in an all-order strong coupling expansion in the β parameter. For pedagogical purposes, the dualization of the pure Yang-Mills theory will be presented first, while the inclusion of the staggered quark fields will be treated as a generalization of the Yang-Mills result. The formalism and the results obtained here can be used for future investigations of the QCD phase diagram at non-zero μ, helping unraveling its structure and the location of the conjectured critical endpoint.

Contents

Dedicated to my parents, my girlfriend, and all my friends…

Chapter 1

Introduction

Quantum chromodynamics (abbr. QCD) is the fundamental theory of the strong interactions. It is a Yang-Mills theory with gauge group $SU(3)_c$ coupled to $N_f = 6$ fermions in the fundamental representation, named by Murray Gell-Mann, the quarks. Remarkably, such a simple theory containing only seven free parameters (six quark masses and the strong coupling constant α_s) describes accurately the dynamics and properties of all hadrons, from protons and neutrons to pions and heavy resonances. Qualitatively, the building blocks of the theory are represented by the aforementioned six quarks, along with eight spin-1 massless particles, the gluons, which constitute the mediators of the strong force. Together with the electroweak sector, QCD forms the so-called Standard Model of particle physics, our most fundamental understanding of the laws of nature. Being a quantum field theory, quantum fluctuations in the form of creation/annihilation of virtual particles make the strong coupling constant α_s a function of the energy scale μ of the process under consideration. When compared to its electroweak counterpart, the evolution (or running) of α_s with the energy scale μ is very peculiar: it goes asymptotically to zero at high-energy and becomes of order one at an energy scale $\Lambda_{QCD} \approx 10^2$ MeV, which separates the perturbative and non-perturbative regimes of the theory. These two properties, usually referred to as asymptotic freedom and infrared slavery, reflect the phenomenon of quark confinement into color singlet hadronic bound states, which seems to be a fundamental property of the QCD Lagrangian.

When dealing with the low-energy non-perturbative regime, the standard analytic techniques based on a perturbative expansion in the strong coupling constant α_s become ineffective, and one has to rely on alternative methods to compute measurable quantities. The lattice formulation of quantum chromodynamics, in combination with the use of Monte Carlo methods and high performance computers, provides a powerful non-perturbative tool to perform ab-initio calculations in the regime where the running coupling cannot be considered as small. Since it was proposed by Kenneth Wilson in 1974, lattice QCD has undergone tremendous improvement due to a better understanding of the formulation, algorithmic

developments and larger computing resources. Despite its success, several questions regarding the thermodynamic behavior of the theory in particular regions of its parameter space are still unanswered.

One of the most relevant open problems concerns the phase structure of the QCD medium at finite temperature and baryon chemical potential μ_B. At zero density, the transition between the hadronic chirally broken phase, and the quark-gluon plasma phase with restored chiral symmetry, is known to be an analytic crossover which takes place at a pseudocritical temperature $T_c = 155.5 \pm 1.5$ MeV for physical quark masses [1]. It is conjectured that this crossover extends also at finite chemical potential, defining a pseudocritical line that terminates in a critical endpoint followed by a line of first-order phase transitions. The existence and location of the conjectured critical endpoint is however still unknown. From the experimental side, heavy ion collision experiments are being carried out at the relativistic heavy ion collider (RHIC), and at the large hadron collider (LHC) in order to find signatures of these phase transitions. At RHIC the second beam energy scan (BES-II) for Au+Au collisions in the energy range 7.7 GeV $< \sqrt{s_{NN}} < 19.6$ GeV is being performed[1]. Due to the increased luminosity of the low energy beams, higher precision measurements will be produced. Besides the critical endpoint, there are additional phases which were conjectured on the basis of model calculations. At low temperature, by increasing the baryon chemical potential, after encountering the nuclear liquid phase, a quarkyonic matter phase [2] and a superconducting phase [3], signaled by the presence of a non-zero di-quark condensate, were conjectured. The existence of these states of matter could play an important role in neutron stars. Providing first principle calculations from lattice QCD at finite density is thus crucial to verify these conjectures and to interpret the experimental data.

The finite density sign problem however hinders a straightforward application of the standard stochastic techniques used to compute lattice QCD observables. While several new methods were proposed and exploited in the last decades in order to solve or circument the sign problem, an ultimate solution is still missing. In Fig. 1.1 a sketch of the conjectured phase diagram, along with its current determination from first principle calculations, is reported. In this thesis, we will discuss dual representations as a possible tool to make the finite density sign problem manageable. In the past years, dual methods have proven to be successful in solving the finite density sign problem in several models. Some of the hallmarks in the context of statistical physics are the $O(N)$ and CP^{N-1} models [4, 5], and in quantum field theory the Abelian gauge-Higgs model and the massless Schwinger model [6, 7]. Dualizing non-Abelian gauge theories such as QCD seems to be instead a non-trivial task: polynomial integrals over the SU(N) invariant Haar measure and over the

---

[1] $\sqrt{s_{NN}}$ is the center of mass energy per nucleon.
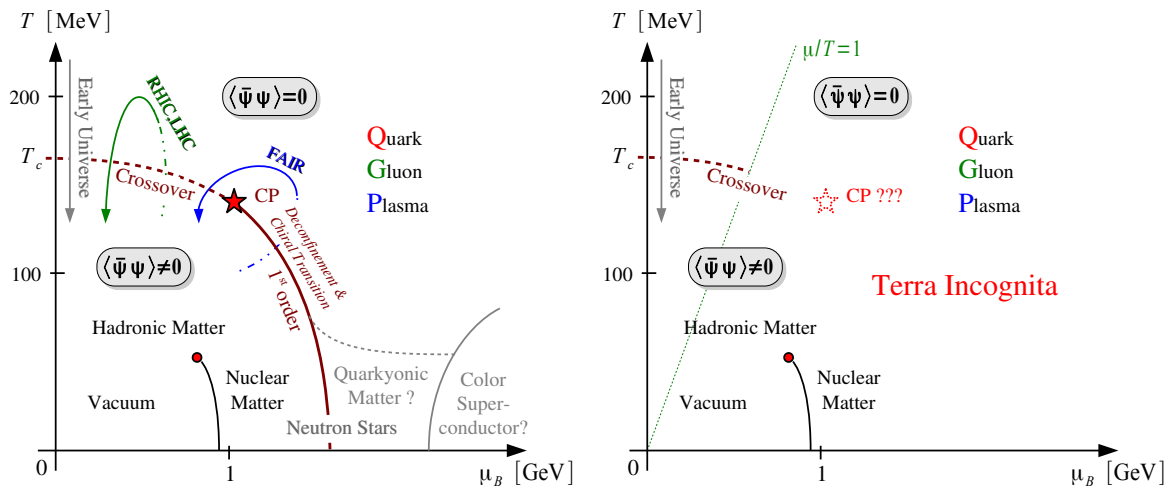
FIGURE 1.1: Sketch of the phase diagram in the $T - \mu_B$ plane. *Left*: The conjectured phase diagram. The crossover line departing from $\mu_B = 0$ ends in a critical endpoint (CEP). At low temperature, increasing μ_B one encounters in order, the hadron gas-to-liquid transition, the quarkyonic matter phase and the color superconducting phase. The regions of the phase diagram probed or targeted by heavy ion collision experiments are also shown. *Right*: What we know from first principle calculations. Courtesy of Wolfgang Unger.

fermionic Grassmann fields have to be performed analytically in order to obtain a dual representation of the partition function. This step cannot be performed by brute force, and it is necessary to introduce auxiliary variables in order to make it feasible. After having integrated out the fermion and gauge fields, the partition function shall be expressed as a sum over configurations identified by the dual variables, which are typically given by a set of constrained integers. In fact, constraints in the form of conservation laws on lattice sites and bonds naturally arise from the requirement that the gauge integrals have to be non-zero and from the nilpotency of the Grassmann measure.

In this work, we will show how to perform an exact dualization for staggered lattice gauge theories with an arbitrary number of colors. The partition function will be organized as a strong coupling series. Along with the usual dual variables already present in the dual representation of the Schwinger model and of strong coupling QCD, a new class of degrees of freedom, which we called *Decoupling Operator Indices* (DOI), will be introduced. The latter allows to deal with the non-Abelian nature of the theory and to perform the dualization without any approximation. The finite density sign problem in the resulting representation will not be absent: negative configurations usually appear due to the anti-commuting nature of the Grassmann variables (so-called fermionic sign) as well as from the gauge part. However, our preliminary analysis of the sign problem in small two-dimensional volumes suggests that the sign problem remains manageable for small to moderate values of the inverse bare gauge coupling β, and that the phase diagram including higher order gauge corrections can be in principle mapped out using the formalism developed in this thesis.

This thesis is organized as follows:

- **Chapter 2** contains an introduction to continuum QCD along with its lattice counterpart. The lattice discretization used in this thesis will be discussed, and the finite density sign problem presented, shortly reviewing the various approaches currently used to circumvent it, and our current understanding of the QCD phase diagram.

- **Chapter 3** focuses on dual representations in simple models. We will present the main concepts and the formalism behind every dual representations based on a strong coupling expansion.

- **Chapter 4** contains an introduction to gauge integration, which constitutes the first step towards dualization in non-Abelian gauge theories. Our main findings regarding polynomial integration over the $\mathrm{SU}(N)$ gauge group will be described in detail and cross checked against known results in specific limiting cases.

- **Chapter 5** gives the dual representation for non-Abelian gauge theories. As a preliminary step we will present the dualization of Yang-Mills theories with an arbitrary number of colors N. The generalization to staggered fermions will be then discussed and the final form of the QCD partition function presented. We will further show how to automate the computation of the higher order β corrections, cross checking our evaluation of the dual Boltzmann weights against hybrid Monte Carlo (HMC) results.

- **Chapter 6** contains a summary of the obtained results and a recap of the main features of QCD in the dual representation. Future perspectives will be finally discussed.

Chapter 2

QCD at finite temperature and density: a short review

2.1 The continuum theory

In quantum field theory, the information about all measurable quantities is contained in the Green functions, i.e. the vacuum expectation value of the time-ordered product of elementary or composite fields, which are determined using the Feynman path-integral. Collectively denoting the fields of a given theory by $\phi(x)$, the Green functions are defined as

$$G^n(x_1, \ldots, x_n) \equiv \langle\Omega|T\{\phi(x_1)\ldots\phi(x_n)\}|\Omega\rangle \equiv \langle\phi(x_1)\ldots\phi(x_n)\rangle, \tag{2.1}$$

where T is the time-ordering operator, $|\Omega\rangle$ the ground state of the theory, and the expectation value $\langle\,.\,\rangle$ of a generic observable $\mathcal{O}(\phi)$ function of the fields is obtained from the path-integral

$$\langle\mathcal{O}\rangle = \frac{\int\mathcal{D}[\phi]\mathcal{O}(\phi)\exp\left(iS\left[\phi\right]\right)}{\int\mathcal{D}[\phi]\exp\left(iS\left[\phi\right]\right)} = \frac{1}{\mathcal{Z}}\int\mathcal{D}[\phi]\mathcal{O}(\phi)\exp\left(iS\left[\phi\right]\right). \tag{2.2}$$

$\mathcal{D}[\phi]$ is the functional measure, and its explicit form depends on the nature of the fields, while $S\left[\phi\right]$ is the action of the theory, i.e. the $(D+1)$ spacetime integral of the Lagrangian density[1]

$$S\left[\phi\right] = \int dt \int d^D\vec{x}\,\mathcal{L}(\phi(\vec{x}, t)) \equiv \int d^{D+1}x\mathcal{L}(\phi(x)). \tag{2.3}$$

The denominator $\mathcal{Z}$ in Eq. (2.2) is called the *partition function* of the theory. It is an integral over all possible paths $\phi(x)$, every path being weighted by the exponential factor $\exp\left(iS[\phi]\right)$. Evaluating the path-integral Eq. (2.2) is the main task when studying a quantum field theory.

In the case of QCD, the elementary fields are given by $N_f = 6$ spin-1/2 fields ψ^f in the fundamental representation of the color gauge group SU(3) (the quarks), and a non-Abelian

---

[1] D is the number of spatial dimensions.

spin-1 gauge field A_μ that describes the gluons and lives in the adjoint representation of SU(3). The QCD Lagrangian, which describes the interaction between quarks and gluons, is given by the sum of the SU(3) Yang-Mills gauge term and the Dirac Lagrangian for the N_f quarks, which are minimally coupled to the gauge field

$$\mathcal{L}_{QCD} = -\frac{1}{2g^2} \text{Tr} F_{\mu\nu}(x) F^{\mu\nu}(x) + \sum_{f=1}^{N_f} \bar{\psi}_i^f(x) \left(i\gamma^\mu \left(D_\mu \right)_{ij} - m_f \delta_{ij} \right) \psi_j^f(x). \tag{2.4}$$

In the previous equation g is the bare gauge coupling, $i, j = 1, 2, 3$ are color indices and γ^μ are the usual Dirac matrices satisfying the anticommutation rules

$$\{\gamma^\mu, \gamma^\nu\} = 2g^{\mu\nu}. \tag{2.5}$$

To render the notation more compact, we did not write explicitly the Dirac indices in Eq. (2.4). The field strength tensor $F_{\mu\nu}$ and the covariant derivative D_μ are given in terms of the gauge field by

$$F_{\mu\nu}(x) = \partial_\mu A_\nu(x) - \partial_\nu A_\mu(x) + i \left[A_\mu(x), A_\nu(x) \right], \tag{2.6}$$

$$(D_\mu)_{ij} = \delta_{ij} \partial_\mu + i \left(A_\mu \right)_{ij}, \tag{2.7}$$

and the commutation rules of the gauge fields are obtained as usual expanding A_μ in a basis of the generators $\{T^a\}_{a=1,...,8}$ of the $\mathfrak{su}(3)$ Lie algebra

$$A_\mu(x) = A_\mu^a(x) T^a, \qquad \left[T^a, T^b \right] = i f^{abc} T^c, \qquad \text{Tr} \left(T^a T^b \right) = \frac{1}{2} \delta^{ab}, \tag{2.8}$$

where f^{abc} are the SU(3) structure constants and $A_\mu^a(x) \in \mathbb{R}$ are the gauge field components. The QCD Lagrangian Eq. (2.4) also enjoys a gauge symmetry, i.e. it is invariant under the following local transformations of the fundamental fields

$$\psi^f(x) \to G(x) \psi^f(x), \quad \bar{\psi}^f(x) \to \bar{\psi}^f(x) G(x)^\dagger, \tag{2.9}$$

$$A_\mu(x) \to G(x) A_\mu(x) G(x)^\dagger + i \left(\partial_\mu G(x) \right) G(x)^\dagger, \tag{2.10}$$

where $G(x) \in$ SU(3). The QCD partition function is obtained integrating $e^{i \int \mathcal{L}_{QCD}}$ over a suitably defined measure of the gauge and fermionic fields. For the gauge field, the functional integral is over all possible values of the gauge field components $A_\mu^a(x)$

$$\int \mathcal{D}[A_\mu] \equiv \prod_a \prod_{x,\mu} \int_{-\infty}^{+\infty} dA_\mu^a(x), \tag{2.11}$$

while the definition of the fermionic functional integral requires some additional work. The standard procedure is to implement directly Fermi statistics associating to each fermionic state $i \in [1, \ldots, N]$ a pair of Grassmann variables $\{\eta_i, \bar{\eta}_i\}$ fulfilling the anticommutation rules

$$\{\eta_i, \eta_j\} = \{\bar{\eta}_i, \bar{\eta}_j\} = \{\bar{\eta}_i, \eta_j\} = 0, \qquad \forall\, i, j = 1, \ldots, N. \tag{2.12}$$

Grassmann variables are nilpotent since the square of any of them gives zero. As a consequence, every function of a finite number of Grassmann variables is a finite polynomial in $\eta_i, \bar{\eta}_j$. Since we want to determine the functional measure, it is necessary to define the integral of a Grassmann variable. This can be done imposing

$$\int d\eta_i = \int d\bar{\eta}_i = 0, \qquad \int d\eta_i \eta_i = \int d\bar{\eta}_i \bar{\eta}_i = 1, \tag{2.13}$$

along with the usual linear properties of standard integration, and with $d\eta_i$ (resp. $d\bar{\eta}_i$) obeying the same anticommutation rules as η_i (resp. $\bar{\eta}_i$). The Grassmann integral of an arbitrary function F,

$$\mathcal{I}_F = \int \prod_{i=1}^{N} d\bar{\eta}_i d\eta_i \, F(\{\eta_i\}, \{\bar{\eta}_i\}), \tag{2.14}$$

can be then obtained expanding F in a Taylor series and retaining only the term of order $2N$ where every Grassmann variable appears exactly one time

$$F(\{\eta_i\}, \{\bar{\eta}_i\}) = \alpha(F) \prod_{i=1}^{N} \eta_i \bar{\eta}_i + \ldots. \tag{2.15}$$

Given Eqs. (2.12) and (2.13), all the other terms are indeed either vanishing or will give zero after integration. The value of the integral is then simply $\mathcal{I}_F = \alpha(F)$. Notice that to bring the non-vanishing expansion term in the canonical form Eq. (2.15), it might be necessary to reorder the Grassmann variables $\eta_i, \bar{\eta}_i$. In that case one has to take into account the minus signs from the anticommutation rules Eq. (2.12). Making use of these definitions, one can for instance show that the Gaussian integral over Grassmann variables is given by

$$\int \prod_{i=1}^{N} d\bar{\eta}_i d\eta_i \, \exp\left(\bar{\eta}_i M_{i,j} \eta_j\right) = \det M. \tag{2.16}$$

The fermionic fields $\bar{\psi}^f(x), \psi^f(x)$ are thus considered as Grassmann valued, and the corresponding functional integral is defined as

$$\int \mathcal{D}[\bar{\psi}, \psi] \equiv \prod_{f,i} \prod_{x} \int d\bar{\psi}_i^f(x) d\psi_i^f(x) \qquad i = 1, 2, 3. \tag{2.17}$$

Finally, the path-integral representation for the vacuum expectation value of a generic QCD observable $\langle \mathcal{O} \rangle$ is

$$\langle \mathcal{O} \rangle = \frac{1}{\mathcal{Z}_{QCD}} \int \mathcal{D}[A_\mu] \int \mathcal{D}[\bar{\psi}, \psi] \mathcal{O}(\bar{\psi}, \psi, A_\mu) \exp\left(i \int d^4 x \mathcal{L}_{QCD} \right), \qquad (2.18)$$

$$\mathcal{Z}_{QCD} = \int \mathcal{D}[A_\mu] \int \mathcal{D}[\bar{\psi}, \psi] \exp\left(i \int d^4 x \mathcal{L}_{QCD} \right). \qquad (2.19)$$

One can explicitly check that in the free field limit the Grassmann integral correctly reproduces the fermionic two-point function and that Wick theorem is implemented.

The path-integral in Eq. (2.19) is however ill-defined: its oscillatory nature makes it difficult to prove the convergence of the integral. In addition, the standard technique that allows for a direct evaluation in the continuum, consists in a perturbative expansion around the free field limit via

$$\langle \mathcal{O} \rangle = \frac{\int \mathcal{D}[A_\mu] \mathcal{D}[\bar{\psi}, \psi] e^{iS_{\text{free}}[A_\mu, \bar{\psi}, \psi] + igS_I[A_\mu, \bar{\psi}, \psi]} \mathcal{O}[A_\mu, \bar{\psi}, \psi]}{\int \mathcal{D}[A_\mu] \mathcal{D}[\bar{\psi}, \psi] e^{iS_{\text{free}}[A_\mu, \bar{\psi}, \psi] + igS_I[A_\mu, \bar{\psi}, \psi]}}$$

$$= \frac{\sum_{n=0}^{+\infty} \frac{(ig)^n}{n!} \int \mathcal{D}[A_\mu] \mathcal{D}[\bar{\psi}, \psi] e^{iS_{\text{free}}[A_\mu, \bar{\psi}, \psi]} \left(S_I[A_\mu, \bar{\psi}, \psi] \right)^n \mathcal{O}[A_\mu, \bar{\psi}, \psi]}{\sum_{n=0}^{+\infty} \frac{(ig)^n}{n!} \int \mathcal{D}[A_\mu] \mathcal{D}[\bar{\psi}, \psi] e^{iS_{\text{free}}[A_\mu, \bar{\psi}, \psi]} \left(S_I[A_\mu, \bar{\psi}, \psi] \right)^n} \qquad (2.20)$$

using then the Feynman diagrams technique to evaluate the perturbative series order by order[2]. However, when one tries to go beyond the leading order expansion term, the contribution to the functional integral coming from ultraviolet paths produces divergent expectation values $\langle \mathcal{O} \rangle$. For a certain class of field theories to which QCD belongs (so-called renormalizable theories), these divergencies are actually harmless. It can be shown that by introducing a regulator Λ to make all integrals convergent, it is possible to absorb the divergencies order by order into a redefinition of fields and couplings, in such a way that all the Green functions, when expressed in terms of *renormalized* fields and couplings, have a smooth finite limit when the regulator Λ is removed (see for instance [8, 9]). Physical observables are not affected by the specific way the regulator Λ is introduced (so-called regularization scheme), while their dependence on the original parameters appearing in the Lagrangian (bare parameters), disappears in favor of a dependence on the finite renormalized ones. This so-called *renormalization procedure* has extremely important consequences: renormalized couplings become functions of an energy scale μ, the functional dependence being described by the renormalization-group flow equations [10]. Once a renormalized quantity is fixed at some energy scale μ^* (e.g. by comparison with experiments), its evolution with μ is determined by the flow equations. A perturbative expansion in terms of renormalized quantities, for an observable $\mathcal{O}$ involving a typical energy scale E, produces

---

[2]To define the perturbative expansion in presence of gauge invariance, a gauge fixing condition must be supplied. This is usually done via the Faddeev-Popov gauge-fixing procedure.

reliable results only if the coupling constants at $\mu \approx E$ are small. In the case of QCD, the renormalized strong coupling constant $g^r(\mu)$ has the fundamental property

$$\lim_{\mu \to \infty} g^r(\mu) = 0 , \qquad (2.21)$$

so that the theory becomes free at asymptotically high energy. In contrast, $g^r(\mu)$ grows when decreasing the scale μ, reaching a point where the pertubative expansion is no longer reliable. This happens at an energy scale[3] $\mu = \Lambda_{QCD} \approx 10^2 \, \text{MeV}$, which sets a limit between the perturbative and the non-perturbative regime of the theory. Since low energy processes cannot be described by a perturbative expansion in $g^r(\mu)$, alternative techniques must be used to evaluate the path-integral. As will be described in the next sections, the lattice discretization provides a powerful, fully non-perturbative and gauge invariant method to evaluate the path-integral even when the perturbative expansion fails to provide reliable results.

2.1.1 QCD at finite temperature

In the previous subsection we introduced a path-integral representation for the vacuum expectation values. To perform thermodynamic calculations, we want to know how Eq. (2.18) gets modified when the system is in contact with a thermal reservoir. At equilibrium, we know from standard thermodynamic arguments that every energy eigenstate n of the system is visited a number of times $N(n)$ proportional to the Boltzmann factor

$$N(n) \propto \exp\left(-\frac{E_n}{T}\right), \qquad (2.22)$$

where E_n is the energy of the state n, T the temperature of the system and we set the Boltzmann constant $k_B = 1$. The canonical partition function of the system is defined as

$$\mathcal{Z}(T) \equiv \sum_n \exp\left(-\frac{E_n}{T}\right) = \sum_n \langle n | \exp\left(-\frac{\hat{H}}{T}\right) | n \rangle = \text{Tr} \exp\left(-\frac{\hat{H}}{T}\right), \qquad (2.23)$$

where $\hat{H}$ is the Hamiltonian of the system and we used the invariance of the trace. Thermodynamic quantities such as mean energy $\langle E \rangle$, pressure $\langle P \rangle$ and entropy $\langle S \rangle$ can be obtained as usual from $\mathcal{Z}(T)$ and its derivatives. The operator $\hat{\rho} = \exp\left(-\frac{\hat{H}}{T}\right)$ is called the density matrix, and any thermal expectation value can be computed via

$$\langle \mathcal{O} \rangle = \frac{\text{Tr}\left(\mathcal{O}\hat{\rho}\right)}{\text{Tr}\left(\hat{\rho}\right)} . \qquad (2.24)$$

---

[3]In contrast to Eq. (2.21), this value is regularization scheme dependent. In the $\overline{\text{MS}}$ scheme and for $N_f = 3$, $\Lambda_{QCD}^{\overline{\text{MS}}} = 332 \pm 17 \, \text{MeV}$ [11].

A path-integral representation of Eq. (2.24), can be obtained starting from the quantum amplitude $\langle q' | e^{-i\hat{H}t} | q \rangle$ written as

$$\langle q' | \exp\left(-i\hat{H}t\right) | q \rangle = \int \mathcal{D}[x] \exp\left(i \int_0^t dt' \mathcal{L}(x(t'))\right). \tag{2.25}$$

where q, q' are position eigenstates and the path-integral in the r.h.s is over all paths satisfying $x(0) = q, x(t) = q'$. Thermal averages can be thus expressed in the form of a path-integral, performing an analytic continuation to imaginary time $t \to i\tau$ (Wick rotation), and setting $\tau = \frac{1}{T}$.

The analytic continuation modifies the spacetime metric from Minkowskian to Euclidean. In the case of QCD, the analytically continued Euclidean Lagrangian $\mathcal{L}^E$, invariant under the Euclidean group $\mathbb{E}(4)$, is given by

$$\mathcal{L}^E_{QCD}(x) = \frac{1}{2g^2} \text{Tr}\, F_{\mu\nu}(x) F_{\mu\nu}(x) + \sum_{f=1}^{N_f} \bar{\psi}_i^f(x) \left(\gamma_E^\mu \left(D_\mu\right)_{ij} + m_f \delta_{ij}\right) \psi_j^f(x), \tag{2.26}$$

where the Euclidean gamma matrices satisfy the following anticommutation rules

$$\{\gamma_E^\mu, \gamma_E^\nu\} = 2\delta^{\mu\nu}. \tag{2.27}$$

In terms of $\mathcal{L}_E$, the canonical partition function and thermal averages can be written similarly to the zero temperature case, through

$$\langle \mathcal{O} \rangle = \frac{1}{\mathcal{Z}_{QCD}(T)} \int \mathcal{D}[A_\mu] \int \mathcal{D}[\bar{\psi}, \psi] \mathcal{O}(\bar{\psi}, \psi, A_\mu) \exp\left(-S^E_{QCD}(T)\right), \tag{2.28}$$

$$\mathcal{Z}_{QCD}(T) = \int \mathcal{D}[A_\mu] \int \mathcal{D}[\bar{\psi}, \psi] \exp\left(-S^E_{QCD}(T)\right), \tag{2.29}$$

$$S^E_{QCD}(T) \equiv \int_0^{\frac{1}{T}} d\tau \int d^3\vec{x}\, \mathcal{L}_E(\vec{x}, \tau). \tag{2.30}$$

In the following, the subscript/superscript E will be neglected where it is clear we are referring to the Euclidean theory. Given the trace in Eq. (2.23), the path-integral should now extend over all paths that are periodic in time direction. Actually this is not true for fermionic fields, which as a consequence of their statistics require antiperiodic boundary conditions in temporal direction[4]. Therefore the Path Integral is constrained to those field configurations satisfying

$$A_\mu(\vec{x}, 0) = A_\mu(\vec{x}, \frac{1}{T}), \tag{2.31}$$

$$\psi_f(\vec{x}, 0) = -\psi_f(\vec{x}, \frac{1}{T}). \tag{2.32}$$

---

[4]Equivalently this stems from the definition of trace for Grassmann variables [12].

The Euclidean path-integral has better convergence properties as compared to the one in Minkowski space. Every path is weighted by $\exp\left(-S^E(T)\right)$, which resembles the usual Boltzmann factor, and contributions corresponding to large values of the Euclidean action are now suppressed. This expression thus provides a better behaved definition for the vacuum expectation values in Eq. (2.18), which can be obtained by taking the zero temperature limit in Eq. (2.28) and performing the analytic continuation back to Minkowski space. The relations Eqs. (2.28) and (2.29) also establish the well known connection between the thermodynamics of a quantum field in D spatial dimensions and that of a classic system in (spatial) dimensions $D + 1$.

2.1.2 QCD at finite density

In the same spirit of the previous subsection, we can generalize Eq. (2.29) to the finite density case. In general, when an exactly conserved charge Q corresponding to a symmetry of the Lagrangian is allowed to be exchanged between the system and the reservoir, after reaching equilibrium, the system is described by the modified density matrix

$$\hat{\rho} = \exp\left(-\frac{\hat{H} - \mu_Q \hat{Q}}{T}\right), \tag{2.33}$$

where $\mu_Q \in \mathbb{R}$ is the *chemical potential* associated to the charge Q. In the following, we will be mainly interested in the case where Q is the net quark number relative to some flavor f. The corresponding μ_f are then called the quark number chemical potentials, and $\mu_f \neq 0$ corresponds to an asymmetry between quark and antiquarks of flavor f. This regime is called QCD at finite density. The $U(1)$ symmetry that gives rise to quark number conservation is given by

$$\psi_f(x) \to e^{i\alpha}\psi_f(x), \quad \bar{\psi}_f(x) \to \bar{\psi}_f(x)e^{-i\alpha} \qquad \alpha \in \mathbb{R}, \tag{2.34}$$

and the corresponding Noether current is

$$J_f^\mu(x) = \frac{\partial \mathcal{L}}{\partial(\partial_\mu \psi_f)}\delta\psi_f = \bar{\psi}_f(x)\gamma^\mu\psi_f(x). \tag{2.35}$$

The quark number operator $\hat{Q}_f$ is obtained from the spatial integral of the temporal component of J_f^μ, and the *grand canonical* partition function that generalizes Eq. (2.29) has thus the following path-integral representation

$$\mathcal{Z}_{QCD}(T, \{\mu_f\}) \equiv \int \mathcal{D}[A_\mu] \int \mathcal{D}[\bar{\psi}, \psi] \exp\left(-\int_T d^4x \, \mathcal{L}_{QCD}(x) - \sum_f \mu_f \bar{\psi}_f(x)\gamma^0\psi_f(x)\right). \tag{2.36}$$

As in the case of the canonical partition function, the integral in the imaginary time direction is over the compact interval $\left[0, \frac{1}{T}\right]$, and the fields satisfy identical boundary conditions.

Inserting a non-zero chemical potential is however not an innocent operation. The modified Lagrangian density in Eq. (2.36) can be written as a sum of two terms: the pure Yang-Mills part $\mathcal{L}_{Y.M.}$ and the fermion Lagrangian $\mathcal{L}_F$

$$\mathcal{L}_{Y.M.} = \frac{1}{2g^2} F_{\mu\nu}(x) F_{\mu\nu}(x) \tag{2.37}$$

$$\mathcal{L}_F = \sum_f \bar{\psi}_f(x) \left(\gamma_\mu D_\mu + m_f - \gamma^0 \mu_f\right) \psi_f(x) := \sum_f \bar{\psi}_f \, M_f \left(A_\mu, m_f, \mu_f\right) \psi_f. \tag{2.38}$$

The latter is a quadratic form in $\{\bar{\psi}_f, \psi_f\}$ and the functional integral over the fermion fields can be carried out exactly in favor of the determinant of M_f as in Eq. (2.16). The grand canonical partition function thus becomes

$$\mathcal{Z}_{QCD}(T, \{\mu_f\}) = \int \mathcal{D}[A_\mu] \exp\left(-S_{Y.M.}[A_\mu]\right) \prod_f \det M_f \left(A_\mu, m_f, \mu_f\right). \tag{2.39}$$

The fermion determinant $\det M_f$ at non-zero chemical potential is not real anymore as it can be seen directly from the identity

$$M_f(-\mu_f^*) = \gamma^5 M_f(\mu_f) \gamma^5, \qquad \gamma^5 \equiv \gamma^0 \gamma^1 \gamma^2 \gamma^3 ; \tag{2.40}$$

hence the integrand in Eq. (2.39) cannot be interpreted anymore as a Boltzmann factor since it is in general a complex number. This poses a serious problem when it comes to numerical evaluation of the path-integral, which we shall discuss in the next sections. The lack of positivity of the fermion determinant, usually referred to as the finite density *sign problem*, will be the driving motivation behind the whole thesis.

2.1.3 Chiral symmetry and confinement

Before entering the discussion on how to evaluate the path-integral, we introduce some of the observables relevant to studying the QCD phase diagram. As we outlined in the introduction, the QCD medium at zero temperature is in a confined chirally broken phase. This means that quarks are bound into color singlet hadrons and do not exist as asymptotic states, and that the $SU_A(N_f)$ (chiral) symmetry of the QCD Lagrangian

$$\psi'^f(x) = e^{i\gamma_5 \tau_{ff'}} \psi^{f'}(x), \quad \bar{\psi}'^f(x) = \bar{\psi}^{f'}(x) e^{i\gamma_5 \tau_{f'f}}, \quad \tau \in \mathfrak{su}(N_f), \tag{2.41}$$
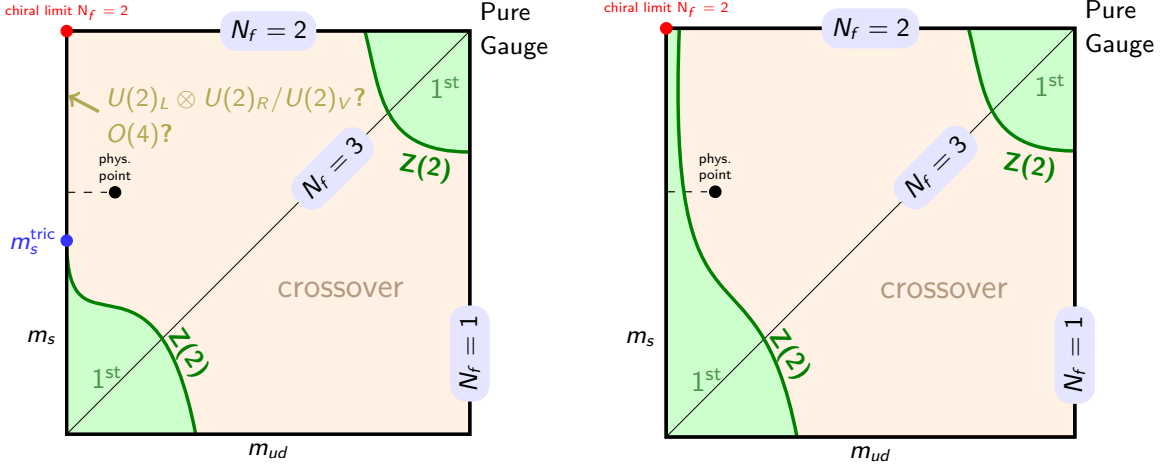
FIGURE 2.1: The behavior of the zero density thermal phase transition as a function of the light (m_{ud}) and strange (m_s) quark masses. The figures describe two different scenarios depending on the order of the $N_f = 2$ chiral transition. Taken from [13].

is spontaneously broken by the vacuum. Chiral symmetry is not an exact symmetry in the real world since quark masses are non-zero[5]. However, since the up and down quark masses m_u, m_d are small and there is no evidence for an approximate $SU_A(2)$ degeneracy in the hadron spectrum, we still talk of a spontaneously broken chiral symmetry. When studying the phase diagram as a function of chemical potential and temperature, one is mainly interested in knowing when chiral symmetry gets restored and when quarks and gluons start to behave as free particles (so-called quark-gluon-plasma phase). To probe these phases, commonly used observables are

$$\text{(Chiral condensate)} \qquad \langle \bar{\psi}\psi \rangle \equiv \frac{T}{V} \sum_f \frac{\partial \log{(\mathcal{Z})}}{\partial m_f} , \qquad (2.42)$$

$$\text{(Polyakov loop)} \qquad \langle L \rangle \equiv \frac{1}{V} \langle \frac{1}{3} \int_{\vec{x}} \text{Tr} \, \mathcal{P} \left\{ \exp \left(i \int_0^{\frac{1}{T}} A_0(\vec{x}, \tau) d\tau \right) \right\} \rangle , \qquad (2.43)$$

along with their *susceptibilities*, i.e. the second order connected momenta of their distributions

$$\chi_{\bar{\psi}\psi} \equiv \frac{V}{T} \left[\langle (\bar{\psi}\psi)^2 \rangle - \langle \bar{\psi}\psi \rangle^2 \right] = \frac{T}{V} \sum_f \frac{\partial^2 \log{(\mathcal{Z})}}{\partial^2 m_f} , \qquad \chi_L \equiv V \left[\langle |L|^2 \rangle - \langle |L| \rangle^2 \right] , \qquad (2.44)$$

where V is the spatial volume. The behavior of these quantities can be exactly related to the confinement and chiral properties of the system in particular limits. In pure gauge theory (i.e. $m_f \to \infty$), the Polyakov loop is the order parameter for the $Z(3)$ center symmetry associated to deconfinement. In particular $\langle L \rangle = 0$ implies confinement and $\langle L \rangle \neq 0$ deconfinement. In this limit, the Polyakov loop susceptibility diverges at the deconfinement

---

[5]The quark mass term in Eq. (2.4) is not invariant under the transformations in Eq. (2.41)

temperature $T_c \approx 270 \, \text{MeV}$, where a first order transition takes place [14]. The chiral condensate is instead the order parameter for chiral symmetry breaking in the limit $m_f \to 0$, and acquires a non-vanishing expectation value $\langle \bar{\psi}\psi \rangle \neq 0$ in the broken phase. The chiral susceptibility diverges at the transition temperature, but in this case the order of the transition depends on the number of chiral flavors [15, 16, 17]. In the real world, where quark masses are finite and non-zero, there are no real symmetries associated to these phases and these observables are only approximate order parameters. In particular we know that the zero density thermal transition, for physical quark masses, is not a real phase transition: the Polyakov loop susceptibility χ_L and the chiral susceptibility $\chi_{\bar{\psi}\psi}$ do not diverge at the transition point in the thermodynamic limit. What is observed[6] is an analytic rise in the Polyakov loop and a drop in the chiral condensate that are however not associated to critical behavior (so-called crossover) [18]. This takes place at a pseudocritical temperature that for chiral observables is $T_c = 155.5(1.5)$ MeV [1]. The quark mass dependence of the zero density thermal transition for $N_f = 2 + 1$ flavors is summarized in the so-called Columbia plot (Fig. 2.1). What happens at finite density $\mu_f \neq 0$ is instead largely unknown. As we will see in the next sections, the *sign problem* hinders a direct evaluation of thermodynamic quantities, and the structure of the phase diagram is only qualitatively understood on the basis of model calculations (e.g. [19]), and at non-zero baryon chemical potential $\mu_B \equiv \frac{1}{3} \sum\limits_{f=u,d,s} \mu_f$, only for small values of μ_B/T [20, 21]. In this context, the main open question regards the existence of a second order critical point in the $T - \mu_B$ plane that represents the ending point of the crossover line.

2.2 The lattice formulation

The lattice discretization is a non-perturbative way of regularizing the path-integral, which allows for numerical evaluations. It constitutes the only known method to perform ab-initio calculations in the regime where the perturbative expansion is not reliable. In this section we will describe the main concepts behind the lattice formulation of Euclidean QCD. This is not meant to be a detailed introduction, for which we refer to [22, 23]. Only the main aspects and the information needed for the understanding of the next chapters will be covered.

2.2.1 From continuum to discrete

The functional measure appearing in the path-integral representation of the partition function is infinite dimensional since paths of arbitrary wavelength contribute. In the lattice

---

[6]These calculations were made considering only the three lightest quarks u, d, s, since at the temperatures of interest the contribution of the c, b, t quarks is largely negligible.

discretization, this infinite number of integration variables is made finite (regularized), introducing a lattice spacing a such that the continuum spacetime x_μ is replaced by a lattice[7] Λ having a finite number of points (lattice sites)

$$x_\mu \in \mathbb{R} \to a n_\mu, \ n_\mu \in [1, \dots, N_\mu] \,, \tag{2.45}$$

and the spacetime integral by

$$\int d^{D+1}x \to a^{D+1} \sum_{n \in \Lambda} \,. \tag{2.46}$$

The lattice spacing a and the lattice size[8] $V = \prod_{\mu=0}^{D} N_\mu$ provide a natural cut-off for ultraviolet and infrared modes and the resulting path-integral is always finite. Basically we are replacing the infinite-dimensional functional integral by a finite number of integrals over all field configurations at discrete spacetime points.

Before discussing the more technical discretization of the QCD action, in order to show the main features of the lattice discretization, we consider the simpler case of the scalar ϕ^4 theory in four dimensions. In this case, the continuum Euclidean action is given by

$$S_{\phi^4}[\phi, \partial_\mu \phi] = \int d^4x \, \frac{1}{2} \partial_\mu \phi(x) \partial_\mu \phi(x) + \frac{1}{2} m^2 \phi^2(x) + \frac{\lambda}{4!} \phi^4(x) \,, \tag{2.47}$$

and the continuum functional measure is

$$\int \mathcal{D}[\phi] = \prod_x \int_{-\infty}^{+\infty} d\phi(x) \,. \tag{2.48}$$

After having discretized the spacetime, the domain of the field ϕ is the finite set of lattice sites $n = (n_0, \dots, n_3)$. Clearly, the continuum action must be now substituted with a discrete counterpart since differential operators such as ∂_μ are no longer well defined. A necessary condition when discretizing the Lagrangian is that in the limit $a \to 0$ its continuum counterpart must be recovered. Hence, possible candidates for the discretized derivative operator

---

[7]We will only consider hypercubic lattices.

[8]At finite temperature the lattice temporal extent is related to T via $N_0 = \frac{1}{aT}$. Oftentimes we will use the notation N_t in place of N_0.

are the forward, backward and symmetric derivatives

$$\nabla_\mu^{(f.)} \phi(n) = \frac{\phi(n+\hat{\mu}) - \phi(n)}{a}, \tag{2.49}$$

$$\nabla_\mu^{(b.)} \phi(n) = \frac{\phi(n) - \phi(n-\hat{\mu})}{a}, \tag{2.50}$$

$$\nabla_\mu^{(s.)} \phi(n) = \frac{\phi(n+\hat{\mu}) - \phi(n-\hat{\mu})}{2a}, \tag{2.51}$$

where $\hat{\mu}$ is the unit vector in direction $\mu = 0, \dots, D$. In the limit $a \to 0$ the usual derivative is obtained in all cases. Introducing the following dimensionless quantities

$$\hat{\phi}(n) \equiv a\phi(n), \qquad \hat{m} \equiv am, \qquad \hat{\lambda} \equiv \lambda, \qquad \hat{\nabla}_\mu \equiv a\nabla_\mu \tag{2.52}$$

the discretized Path Integral is

$$\mathcal{Z}_{\phi^4} = \prod_{n \in \Lambda} \int_{-\infty}^{+\infty} d\hat{\phi}(n) \exp\left(-\sum_{n \in \Lambda} \frac{1}{2} \hat{\nabla}_\mu^{(c)} \hat{\phi}(n) \hat{\nabla}_\mu^{(c)} \hat{\phi}(n) + \frac{1}{2} \hat{m} \hat{\phi}^2(n) + \frac{\hat{\lambda}}{4!} \hat{\phi}^4(n) \right), \tag{2.53}$$

where $c = \{f., b., s.\}$. The discretized system takes the form of a statistical model with a finite number of degrees of freedom, the derivative operators being replaced by couplings between fields at different lattice sites. The explicit dependency on the lattice spacing a completely disappeared from the action, which is written only in terms of dimensionless couplings and fields. The main advantage of the lattice discretization, as we will see, is that numerical techniques from statistical mechanics, in particular Monte Carlo methods, can be used to evaluate the partition function.

On the lattice, some of the symmetries of the continuum Lagrangian can be lost. For instance, this is the case of the Euclidean $O(4)$ symmetry in Eq. (2.47), which is reduced to a symmetry under the hypercubic group C_4 of Eq. (2.53). Symmetry transformations acting on the internal space of the fundamental fields may or may not survive the lattice discretization. When possible it is always better to choose a symmetry-preserving lattice discretization in order to avoid the spurious artifacts that would be introduced.

2.2.2 Recovering the continuum theory

At this point it is not clear whether and how a suitable limit of the partition function in Eq. (2.53) can be taken in order to recover the continuum theory. Indeed, we ended up with a statistical model where the lattice spacing completely disappeared from its description in terms of dimensionless couplings and fields. Naively, one would expect that by an appropriate tuning of the dimensionless parameters $\{\hat{m}, \hat{\lambda}\}$, the continuum theory is always

recovered in some limit

$$\hat{\lambda} \to \hat{\lambda}^*, \qquad \hat{m} \to \hat{m}^*, \qquad N_\mu \to \infty. \tag{2.54}$$

However, to define a proper continuum limit, we need to define first our target theory. The continuum ϕ^4 Lagrangian in four dimensions is a renormalizable theory having two free parameters that must be fixed imposing two conditions. One possible choice to fix them (but other choices might be more convenient for practical purposes) is requiring that the lightest particle of the system has a prescribed mass M, and that the scattering amplitude of the $\phi + \phi \to \phi + \phi$ process in the limit of zero external three-momenta is equal to some value λ_R. In terms of the renormalized vertex functions[9] this reads

$$\Gamma_R^{(2)}(p)\big|_{p^2=-M^2} = 0 \tag{2.55}$$

$$\Gamma_R^{(4)}(p_1, \ldots, p_4)\big|_{\vec{p}_i=0} = -\lambda_R. \tag{2.56}$$

On the lattice, the bare dimensionless parameters $\{\hat{m}, \hat{\lambda}\}$ have to be tuned in order to fulfill the condition in Eq. (2.56). This determines a trajectory in the $\hat{m} - \hat{\lambda}$ plane called the *line of constant physics* (LCP)

$$\hat{\lambda} = \hat{\lambda}(\hat{m}, \lambda_R), \qquad \lambda_R \text{ fixed.} \tag{2.57}$$

The lattice spacing a can be then defined on a given point of the LCP computing the correlation length $\hat{\xi}$ from the connected two-point function

$$\langle \hat{\phi}(n)\hat{\phi}(0)\rangle_c\big|_{|n|\to\infty} \propto \exp\left(-\frac{|n|}{\hat{\xi}}\right) \tag{2.58}$$

using $a = 1/\hat{\xi}M$. A proper, well defined, continuum limit requires therefore that the LCP possesses a critical point (i.e. a point where a second-order phase transition occurs) where the correlation length diverges

$$\hat{\xi} = \frac{1}{aM} \to \infty, \tag{2.59}$$

and $a \to 0$. Qualitatively we can say that close to the critical point the system loses memory of the underlying lattice structure since the only relevant scale is the diverging correlation length $\hat{\xi}$. The full $O(4)$ rotational symmetry is therefore recovered in this limit, while in the scaling region of the critical point the expectation value of a dimensionless quantity $\langle \hat{X} \rangle$

---

[9]For definitions and properties of the vertex functions see for instance [8].

evaluated on the lattice is related to its continuum counterpart via[10]

$$\langle \hat{X}(a) \rangle \big|_{\text{lat.}} \underset{a \to 0}{=} \langle \hat{X} \rangle \big|_{\text{cont.}} + \mathcal{O}(a^k), \quad k > 0. \tag{2.60}$$

The critical point picture of the continuum limit allows to understand the freedom when choosing the discretized action: in RG language, if the difference between two lattice actions corresponds to an irrelevant operator, the critical properties of the two systems are identical, i.e. they describe the same physics in the continuum limit[11]. At the same time it is not guaranteed that such a continuum limit exists for all systems and for every value of the renormalized couplings. For a general discretized theory with bare couplings $\{\hat{g}_i\}$ it is in fact possible that a given LCP does not contain a critical point. Hence not all theories admit a lattice discretization. We will not discuss further this issue and we refer to [22] for a more detailed presentation. Here we only want to mention that in the case of the ϕ^4 theory just discussed, an interacting continuum limit having $\lambda_R \neq 0$ does not exist. In the case of QCD, which we are going to analyze, the existence of a non-trivial continuum limit is guaranteed by the property of asymptotic freedom Eq. (2.21).

2.2.3 The naive fermion discretization

In this subsection we begin the discretization of the Euclidean QCD path-integral starting from the fermionic action in the free field limit (i.e. neglecting the coupling to the gauge field). Unlike the case of the ϕ^4 theory, an admissible discretization of the free Dirac Lagrangian for one flavor of quarks,

$$\mathcal{L}_f^{\text{free}}(x) = \bar{\psi}(x) \left(\gamma^\mu \partial_\mu + m \right) \psi(x), \tag{2.61}$$

can be only obtained using the symmetric derivative operator. Indeed, the forward and backward derivatives produce in this case a non-hermitian action. This (so-called naive) discretization has however a problem. The discretized path-integral is

$$\mathcal{Z}_F = \prod_{n \in \Lambda} \int d\hat{\bar{\psi}}(n) d\hat{\psi}(n) \exp \left(-\sum_n \hat{\bar{\psi}}(n) \left[\sum_\mu \frac{\gamma_\mu}{2} \left(\hat{\psi}(n+\hat{\mu}) - \hat{\psi}(n-\hat{\mu}) \right) + \hat{m}\hat{\psi}(n) \right] \right), \tag{2.62}$$

where, as in the scalar case, dimensionless couplings and fields have been introduced:

$$\hat{\psi}(n) \equiv a^{\frac{3}{2}} \psi(n), \qquad \hat{\bar{\psi}}(n) \equiv a^{\frac{3}{2}} \bar{\psi}(n), \qquad \hat{m} \equiv am. \tag{2.63}$$

---

[10]A renormalization of the operator $\hat{X}$ on the lattice might be required to subtract UV divergences.

[11]Although a clever choice of the action can considerably speed up the convergence [24, 25].

The lattice two-point function in the free field limit can be readily obtained inverting in momentum space the quadratic form in Eq. (2.62)

$$\langle \hat{\bar{\psi}}_\alpha(n_1)\hat{\psi}_\beta(n_2)\rangle = \int_{-\pi}^{\pi} \frac{d^4k}{(2\pi)^4} e^{ik(n_1-n_2)} \frac{-i\sum_\mu (\gamma_\mu)_{\alpha\beta} \sin(k_\mu) + \hat{m}\delta_{\alpha\beta}}{\sum_\mu \sin^2(k_\mu) + \hat{m}^2}. \tag{2.64}$$

We can see that a problem arises: the term $\sum_\mu \sin^2(k_\mu)$ in the r.h.s. of the previous equation goes to zero not only for $k_\mu \to 0$, but at every corner $|k_\mu| = \pi$ of the Brillouin zone. When moving towards the continuum limit $\hat{m} = am \to 0$, the contribution to the integral coming from the momentum region around these corners cannot be neglected, and the continuum Lagrangian describes 16 fermions with equal masses and different chiralities. This is the so-called *doubling problem* which afflicts the naive fermion discretization[12]. The origin of the doublers is actually deep, and this problem cannot be solved without paying a price. Indeed, the Nielsen-Ninomiya theorem [26] states a set of conditions that cannot be simultaneously satisfied by any discretization of the Dirac Lagrangian

$$\mathcal{L}_F[\hat{\bar{\psi}}, \hat{\psi}] = \sum_{n,m\in\Lambda} \hat{\bar{\psi}}(n)D(n,m)\hat{\psi}(m) : \tag{2.65}$$

- The operator $D(n,m)$ is translationally invariant, i.e. it depends only on the difference $|n - m|$.

- The matrix elements $D(n,m)$ decay at least exponentially fast when $|n - m|$ goes to infinity.

- The operator $D(n,m)$ is invariant under the full chiral group in the massless limit $\hat{m} = 0$. This condition can be rephrased as $\{\gamma^5, D(\hat{m} = 0)\} = 0$.

- The continuum theory describes only one free fermion without doublers.

The fermion discretizations we are going to describe will break in one way or another one or more of these conditions. Here we will only discuss those discretizations which are somehow more suited for a strong coupling expansion, namely the Wilson and the staggered discretization. However other discretizations have been introduced and used in other contexts, such as the twisted mass fermions, the overlap and the domain walls fermions. The latter two in particular have good chiral properties but the drawback is that the matrix elements $D(n,m)$ are not sufficiently local and too coumbersome to be treated analytically in a series expansion. From now on, we will not discuss further these discretizations, and we refer to the literature (e.g. [23]) for a more comprehensive presentation.

---

[12]In the case of a scalar theory, the symmetric derivative also produces doublers. In this case however the problem is easily solved by using either $\nabla^{(f.)}$ or $\nabla^{(b.)}$.

2.2.4 Wilson fermions

In the Wilson discretization, the naive fermion Lagrangian Eq. (2.62) is modified by adding a dimension five operator. This so-called *Wilson term* solves the doubling problem by giving to the doublers a mass proportional to $\frac{1}{a}$, while the low-momentum modes acquire a mass proportional to a, which vanishes in the continuum limit. In this way all doublers become infinitely heavy in the continuum limit and disappear from the spectrum. The price one has to pay is that at finite lattice spacing the Wilson term explicitly breaks the chiral symmetry, and the Nielsen-Ninomiya no-go theorem is thus satisfied. The free Wilson Lagrangian is given by

$$\mathcal{L}_F^{\text{Wilson}}[\hat{\bar{\psi}}, \hat{\psi}] = \sum_{n \in \Lambda} \hat{\bar{\psi}}_\alpha(n) \left[\hat{\nabla}_\mu^{(\text{s.})} \gamma_\mu^{\alpha\beta} + \hat{m}\delta^{\alpha\beta} - \frac{r}{2}\delta^{\alpha\beta}\hat{\nabla}_\mu^{(\text{b.})}\hat{\nabla}_\mu^{(\text{f.})} \right] \hat{\psi}_\beta(n), \qquad (2.66)$$

where a summation over $\mu = 0, \dots, 3$ is implied. The last term in square bracket is the *Wilson term* and $r \in (0,1]$ the Wilson parameter. Since it breaks explicitly chiral symmetry, lattice artifacts are usually quite sizable using this discretization, and the study of the chiral transition requires a fine tuning of the bare mass parameter $\hat{m}_q$ since additive mass renormalization terms are present.

2.2.5 Staggered fermions

The staggered discretization was first proposed by Kogut and Susskind in [27]. In some sense it is halfway between the naive and Wilson discretization, because chiral symmetry is not completely spoiled and the number of doublers is not maximal as in the naive discretization. The derivation of the staggered discretization starts with the so-called *spin-diagonalization* of the naive fermion Lagrangian. One performs a local transformation on the fermion fields

$$\chi(n) = \Omega(n)\hat{\psi}(n), \qquad \bar{\chi}(n) = \hat{\bar{\psi}}(n)\Omega^\dagger(n), \qquad (2.67)$$

where $\Omega(n)$ is a 4×4 unitary matrix acting on the spinor components of the fields $\{\hat{\bar{\psi}}, \hat{\psi}\}$, and chosen such that the following *spin-diagonalization* condition is satisfied

$$\Omega^\dagger(n)\gamma_\mu\Omega(n+\hat{\mu}) = \eta_\mu(n)\mathbb{1}_{4\times4}, \qquad \eta_\mu(n) \in \mathbb{R}. \qquad (2.68)$$

The usual choice of the matrices $\Omega(n)$ is

$$\Omega(n) = \gamma_0^{n_0}\gamma_1^{n_1}\gamma_2^{n_2}\gamma_3^{n_3}, \qquad \eta_\mu(n) = (-1)^{\sum_{\nu<\mu} n_\nu}. \qquad (2.69)$$

When the naive Lagrangian is written in terms of the *staggered* fields $\{\bar{\chi}, \chi\}$, the four Dirac components completely decouple as a consequence of the previous condition

$$\mathcal{L}_F^{\text{naive}}[\bar{\chi}, \chi] = \sum_{n \in \Lambda} \sum_{\alpha=0}^{3} \bar{\chi}_\alpha(n) \left[\eta_\mu(n) \nabla_\mu^{(s.)} + \hat{m} \right] \chi_\alpha(n), \qquad (2.70)$$

and the staggered Lagrangian is defined retaining only one term in the previous sum over α (e.g. the term with $\alpha = 0$). The resulting Lagrangian, in terms of a single component field $\{\bar{\chi}_0, \chi_0\}$ describes four (instead of sixteen) degenerate flavors of fermions, as we shall see in a moment. Dropping out the index 0, we can construct four Dirac fields ψ^f associated to the values of the staggered field $\{\bar{\chi}, \chi\}$ at the corners of the elementary hypercube of size a via[13]

$$\hat{\psi}_\alpha^f(n) = \frac{1}{8} \sum_y \Gamma_{y;\alpha,f} \chi(2n + y), \qquad \hat{\bar{\psi}}_\alpha^f(n) = \frac{1}{8} \sum_y \bar{\chi}(2n + y) \Gamma_{y;\alpha,f}^\dagger, \qquad (2.71)$$

where f stands for the four different flavors, α is again a Dirac index and y spans the corners of the hypercube. The matrices Γ_y are given by

$$\Gamma_y = \gamma_0^{y_0} \gamma_1^{y_1} \gamma_2^{y_2} \gamma_3^{y_3}. \qquad (2.72)$$

Notice that the lattice spacing for the fields $\hat{\psi}^f$ effectively doubled since the number of lattice sites where they are defined has been halved. In term of these new fields defined on the sublattice Λ' made only of the even sites, the staggered Lagrangian is

$$\mathcal{L}_F^{\text{stagg.}}[\hat{\bar{\psi}}^f, \hat{\psi}^f] \propto \sum_{n \in \Lambda'} \hat{\bar{\psi}}_\alpha^f(n) \left[\hat{m} \delta_{\alpha\beta} \delta_{ff'} + \left((\gamma_\mu)_{\alpha\beta} \delta_{ff'} \hat{\nabla}_\mu^{(s.)} - \frac{1}{2} (\gamma_5)_{\alpha\beta} (\gamma_5 \gamma_\mu^{\text{T}})_{ff'} \hat{\nabla}_\mu^2 \right) \right] \hat{\psi}_\beta^{f'}(n), \qquad (2.73)$$

where $\hat{\nabla}_\mu^2$ is the following discretized version of the second derivative

$$\hat{\nabla}_\mu^2 \hat{\psi}(n) = \frac{\hat{\psi}(n + \mu) + \hat{\psi}(n - \mu) - 2\hat{\psi}(n)}{2}. \qquad (2.74)$$

The mass and kinetic terms in the Lagrangian Eq. (2.73) describes four flavors of fermions (which are usually called tastes) in a similar way as in the naive discretization. The last term is a dimension five operator which vanishes in the continuum limit. However, at finite lattice spacing this term breaks the chiral symmetry of the four tastes (so-called *taste symmetry breaking*). Nevertheless the invariance under the chiral group is not completely lost, and a remnant of chiral symmetry in the massless limit still persists at finite lattice spacing. The

---

[13]We assume that the number of lattice sites in each direction is even.

Lagrangian Eq. (2.70) is indeed invariant under the following $U(1)$ transformations

$$\chi(n) \to e^{ia\epsilon(n)}\chi(n), \qquad \bar{\chi}(n) \to e^{ia\epsilon(n)}\bar{\chi}(n), \qquad \epsilon(n) = (-1)^{n_0+\ldots+n_3}, \qquad (2.75)$$

which in terms of the "physical field" in Eq. (2.71) reads

$$\hat{\psi}(n) \to e^{ia\gamma_5^{\text{Spin}}\otimes\gamma_5^{\text{Taste}}}\hat{\psi}(n), \qquad \hat{\bar{\psi}}(n) \to \hat{\bar{\psi}}(n)e^{ia\gamma_5^{\text{Spin}}\otimes\gamma_5^{\text{Taste}}}, \qquad (2.76)$$

where the notation $\gamma_5^{\text{Spin}} \otimes \gamma_5^{\text{Taste}}$ means the direct product between two γ^5 matrices acting on Dirac and taste components. The existence of this symmetry makes the staggered fermions more suited to the study of the QCD chiral transition. Notice that since $\text{Tr}\,\gamma_5^{\text{Taste}} = 0$ this symmetry is part of the $SU(4)$ chiral group.

Moreover, the four tastes in Eq. (2.73) do not produce doublers in the continuum limit. Computing the fermionic two-point function as in Eq. (2.64), one can show that the $\sin^2(k_\mu)$ term gets replaced by $\sin^2(k_\mu/2)$ which does not go to zero at the corners of the Brillouin zone. The reason behind this behavior is hidden in the fact that the lattice spacing for the fields in Eq. (2.71) is $2a$, and in units of their momenta the Brillouin zone is $[-\frac{\pi}{2}, \frac{\pi}{2}]$.

2.2.6 Gauge fields

We now describe the discretization of the gauge fields $A_\mu(x)$ and of the QCD action. Before analyzing the Yang-Mills term, we consider the modification of the minimal coupling between fermionic and gauge fields at finite lattice spacing. Any discretized free fermion Lagrangian, ignoring internal indices, takes the form

$$\mathcal{L}_F[\hat{\bar{\psi}}, \hat{\psi}] = \hat{\bar{\psi}}(n)\hat{\nabla}_\mu^{(\text{s.})}B^\mu\hat{\psi}(n) + \ldots, \qquad (2.77)$$

where the structure of the $4-$vector B^μ depends on the discretization adopted. In the case of the quark fields, we insist on having a Lagrangian that is invariant under the gauge transformations Eq. (2.9) at each lattice site n. As neighboring lattice points are separated by a finite distance a, a gauge invariant quantity can be constructed modifying the symmetric derivative operator via

$$\hat{\nabla}_\mu^U \hat{\psi}(n) = \frac{U_{n,\mu}\hat{\psi}(n+\hat{\mu}) - U_{n-\hat{\mu},\mu}^\dagger \hat{\psi}(n-\hat{\mu})}{2}, \qquad U_{n,\mu} \in SU(3). \qquad (2.78)$$

The quantities $U_{n,\mu}, U_{n,\mu}^\dagger$ are the *gauge links* in the forward ($U_{n,\mu}$) and backward ($U_{n,\mu}^\dagger$) directions. They are defined on every bond (or link) (n, μ) of the lattice Λ and transform under a

gauge transformation G as

$$U_{n,\mu} \to U'_{n,\mu} = G(n)\, U_{n,\mu}\, G(n + \hat{\mu})^{\dagger}. \tag{2.79}$$

In terms of the continuum gauge field $A_{\mu}(x)$, the gauge link $U_{n,\mu}$ corresponds to the Wilson line

$$U_{n,\mu} = \mathcal{P} \exp\left(i \int_{an}^{an+a\hat{\mu}} A_{\mu}(x) dx^{\mu} \right); \tag{2.80}$$

therefore it acts as a parallel transporter between the lattice sites n and $n + \hat{\mu}$. It is straightforward to show that in the limit $a \to 0$, Eq. (2.78) describes the usual minimal coupling of the continuum Lagrangian. The Euclidean Yang-Mills term

$$\mathcal{L}_{YM}(x) = \frac{1}{2g^2} \text{Tr}\left[F_{\mu\nu}(x) F_{\mu\nu}(x) \right], \tag{2.81}$$

$$F_{\mu\nu}(x) = \partial_{\mu} A_{\nu}(x) - \partial_{\nu} A_{\mu}(x) + i\left[A_{\mu}(x), A_{\nu}(x) \right], \tag{2.82}$$

must be also discretized in terms of gauge links. From the transformation rule Eq. (2.79), it follows that any trace of product of gauge links along a closed path is gauge invariant. Hence, they are good candidates to describe the Yang-Mills term. The first lattice version of Eq. (2.81), proposed by K. Wilson in [28], was obtained considering the smallest loop, i.e. the product of four gauge links around the elementary square of size a. This quantity is called the *plaquette*, and it is given by

$$U_{p=(n,\mu,\nu)} \equiv U_{n,\mu}\, U_{n+\hat{\mu},\nu}\, U_{n+\hat{\nu},\mu}^{\dagger}\, U_{n,\nu}^{\dagger}, \qquad \mu < \nu. \tag{2.83}$$

In terms of the plaquettes, the (Wilson) lattice gauge action is simply

$$S_G[U_p] = \frac{\beta}{6} \sum_p \text{Tr}\left[2 \cdot \mathbb{1} - U_p - U_p^{\dagger} \right] \in \mathbb{R}, \tag{2.84}$$

where the sum is over all (unoriented) plaquettes and β is a constant. One can verify that for $a \to 0$, substituting

$$U_{x,\mu} \simeq \exp\left(ia A_{\mu}(x) \right), \tag{2.85}$$

and using the Baker-Campbell-Hausdorff formula, the correct continuum limit for the action is approached,

$$S_G \overset{a \to 0}{=} \frac{\beta}{12} \int d^4x \, \text{Tr} \, F_{\mu\nu}(x) F^{\mu\nu}(x) + \mathcal{O}(a^2), \tag{2.86}$$

if β is related to the inverse bare gauge coupling via $\beta = \frac{6}{g^2}$. In the case of a $SU(N)$ or $U(N)$ Yang-Mills theory the same result holds true with $\frac{\beta}{6} \to \frac{\beta}{2N} = \frac{1}{g^2}$.

The discretized functional integral for QCD thus takes the form

$$\mathcal{Z}_{QCD} = \prod_n \int d\hat{\bar\psi}(n) d\hat\psi(n) \prod_{(n,\mu)} \int \mathcal{D}U_{n,\mu} \exp\left(-S_G[U_p] + S_F[\hat{\bar\psi}, \hat\psi, U]\right), \qquad (2.87)$$

where S_F is a not yet specified fermion discretization equipped with the modified derivative operator Eq. (2.78). The continuum gauge integral over the gauge components $A_\mu^a(x)$ is now replaced by a functional integral over the gauge links $U_{n,\mu} \in SU(3)$. The corresponding measure $\mathcal{D}U_{n,\mu}$ is the invariant $SU(3)$ Haar measure which will be described in more details in Ch. 4. For a general group $G = SU(N), U(N)$, the Haar measure of G satisfies the invariance property

$$\int \mathcal{D}U = 1, \qquad \mathcal{D}(UV) = \mathcal{D}(VU) = \mathcal{D}U, \qquad \forall V \in G. \qquad (2.88)$$

As we already outlined, lattice QCD has a well defined continuum limit which is obtained in the limits

$$\beta \to \infty, \qquad \hat{m} \to 0, \qquad N_\mu \to \infty, \qquad (2.89)$$

ensuring that for every value of $(\beta, \hat{m})$ on the LCP the lattice is large enough so that finite volume effects are under control. Since we will be limited to β values far from the continuum limit, we do not go into details concerning the determination of the LCP and the extraction of continuum physics from the discretized QCD partition function. For further reading we refer to [29, 30, 23, 22].

QCD thermodynamics can be studied on the lattice compactifying the temporal extent via $N_t = \frac{1}{aT}$. As in the continuum theory, the gauge links $U_{n,\mu}$ and fermion fields $\{\hat{\bar\psi}, \hat\psi\}$, must satisfy respectively periodic and antiperiodic boundary conditions in the temporal direction. To reduce finite size effect, periodic conditions for all fields are usually imposed on the spatial boundaries. In addition, a finite quark chemical potential μ_f can be introduced ([31]) via an exponential coupling to the gauge links (see [32] for an alternative discretization)

$$U_{n,\mu} \to e^{\hat\mu_f \delta_{\mu,0}} U_{n,\mu}, \qquad U_{n,\mu}^\dagger \to e^{-\hat\mu_f \delta_{\mu,0}} U_{n,\mu}^\dagger, \qquad (2.90)$$

where $\hat\mu_f = a\mu_f$. Again, the insertion of a finite chemical potential gives rise to a complex fermion determinant. Using for instance the Wilson or staggered discretization, it is easy to

show that the fermionic action still satisfies Eq. (2.40).

2.3 Numerical methods

The most powerful method used to compute lattice observables are Monte Carlo simulations. The main idea behind this technique is very easy: starting from the partition function Eq. (2.87), one integrates the fermion fields as in Eq. (2.39) arriving at

$$Z_{QCD} = \int \mathcal{D}[U] \exp\left(-S_G[U]\right) \prod_{f=1}^{N_f} \det M_f[U] \equiv \int \mathcal{D}[U] P[U]. \tag{2.91}$$

If the fermion determinant is positive (as at zero chemical potential), the integrand can be interpreted as a probability distribution over the gauge links $U_{n,\mu}$ that one can evaluate stochastically since the number of integrals is large but finite. Indeed, one can set up a Markov process

$$\{U_{n,\mu}\}_{(0)} \rightarrow \{U_{n,\mu}\}_{(1)} \rightarrow \cdots \rightarrow \{U_{n,\mu}\}_{(N)}, \tag{2.92}$$

such that after a number of equilibration steps $\tau_{\text{eq.}}$, it visits every gauge configuration $\{U_{n,\mu}\}$ a number of times proportional to the positive integrand in Eq. (2.91). This can be done choosing the transition probabilities $A_{\{U_{n,\mu}\}\to\{U'_{n,\mu}\}}$ from a state $\{U_{n,\mu}\}$ to a state $\{U'_{n,\mu}\}$ such that the *detailed balance* condition is fulfilled[14]

$$A_{\{U_{n,\mu}\}\to\{U'_{n,\mu}\}} P\left(\{U_{n,\mu}\}\right) = A_{\{U'_{n,\mu}\}\to\{U_{n,\mu}\}} P(\{U'_{n,\mu}\}). \tag{2.93}$$

An estimate for an observable $\langle \mathcal{O} \rangle$, is then obtained from the generated set of gauge configurations via

$$\langle \mathcal{O} \rangle = \frac{1}{\mathcal{Z}_{QCD}} \int \mathcal{D}[U] \exp\left(-S_G[U]\right) \prod_{f=1}^{N_f} \left(\det M_f[U]\right) \mathcal{O}[U] \approx \frac{1}{N} \sum_{i=1}^{N} \mathcal{O}\left[\{U_{n,\mu}\}_{(\tau_{\text{eq.}}+i)}\right], \tag{2.94}$$

with the statistical error on $\mathcal{O}$ decreasing as the square root of the sample size $\frac{1}{\sqrt{N}}$[15]. The rational hybrid Monte Carlo algorithm (RHMC) [33] along with its improved versions (for instance [34]), when combined with the use of high performance computers, represents the

---

[14]In addition the Markov process must be ergodic and aperiodic [22].
[15]Assuming that the gauge configurations are sufficiently decorrelated.

fastest way to compute lattice QCD observables, and led in the past years to continuum extrapolated results for realistic quark masses.

At finite chemical potential, the RHMC algorithm cannot be directly used as the integrand cannot be interpreted anymore as a probability distribution. In this case a "conservative" variation on the standard Monte Carlo algorithms is obtained via *reweighting*. This is done introducing a fictitious, positive defined, function of the gauge fields $P_{\text{rew.}}[U]$, determining the expectation value $\langle \mathcal{O} \rangle$ via

$$\langle \mathcal{O} \rangle = \frac{\int \mathcal{D}[U] P_{\text{rew.}}[U] \frac{P[U]}{P_{\text{rew.}}[U]} \mathcal{O}[U]}{\int \mathcal{D}[U] P_{\text{rew.}}[U] \frac{P[U]}{P_{\text{rew.}}[U]}} = \frac{\langle \frac{P}{P_{\text{rew.}}} \mathcal{O} \rangle_{\text{rew.}}}{\langle \frac{P}{P_{\text{rew.}}} \rangle_{\text{rew.}}} , \tag{2.95}$$

where $\langle . \rangle_{\text{rew.}}$ means average over the probability distribution $P_{\text{rew.}}$. The drawback of this method is that when the two functions P and $P_{\text{rew.}}$ are not peaked around the same region of the phase space $\{U_{n,\mu}\}$, an *overlap* problem arises: the denominator in the r.h.s. of the previous equation is

$$\langle \frac{P}{P_{\text{rew.}}} \rangle_{\text{rew.}} = \exp\left(-(f - f_{\text{rew.}}) \frac{V}{T} \right) , \tag{2.96}$$

which is exponentially suppressed with the lattice volume if the free energy densities of the full (f) and reweighted ($f_{\text{rew.}}$) systems are too different. Basically the overlap between the two probability distributions gets suppressed at large volumes as a consequence of the central limit theorem. In this case the number of gauge configurations to generate in order to get a fixed statistical accuracy can be prohibitively large, and reweighting becomes ineffective. Common choices for the reweighted function $P_{\text{rew.}}$ in the case of QCD at finite density are

$$P_{\text{p.q.}}[U] = \exp\left(-S_G[U]\right) \left| \prod_{f=1}^{N_f} \det M_f[U, \mu_f] \right| , \tag{2.97}$$

$$P_{\mu_f=0}[U] = \exp\left(-S_G[U]\right) \prod_{f=1}^{N_f} \det M_f[U, \mu_f = 0] , \tag{2.98}$$

or the multi-parameter reweighting [35], but none of these has led so far to a determination of the finite density phase diagram. Many other strategies are available to circumvent the sign problem for small values of the chemical potential, like the Taylor expansion method [36] or the use of an imaginary chemical potential [37, 38, 39]. More recently, other approaches that are not limited to small μ_q have been proposed, such as the complex Langevin approach [40, 41], the Lefschetz thimble approach [42, 43, 44, 45], the density of states method [46]

and the use of 3*d* effective theories [47, 48, 49]. All these approaches have their advantages and shortcomings, but a method that allows to simulate lattice QCD at finite density has not yet been established. Instead among the methods that are not lattice based, the functional approach is recently playing a prominent role [50]. In the next chapters we will discuss the application of *dual methods* as a possible way to solve or mitigate the QCD sign problem.

Chapter 3

Dual representations

In this chapter we illustrate the main ideas behind *dual representations*. A number of concepts and quantities which will enter the dualization of non-Abelian gauge theories will be introduced. Before going through the involved process of dualization in QCD, which will be covered in the next chapters, a fully dualized version of the multi-flavor lattice Schwinger model, and of lattice QCD in the strong coupling limit $\beta = 0$, will be presented. This is meant to be a pedagogical introduction that aims to show the main features of dualizations based on series expansion and their usefulness: the finite density sign problem that afflicts the conventional formulation of the multi-flavor Schwinger model is absent in the dual representation in the massless limit, whereas in the case of lattice QCD at strong coupling, although a residual sign problem is still present, it is mild enough that the phase diagram can be studied via sign reweighting.

3.1 Definition and general considerations

Historically duality transformations were introduced and used for the first time by Krammers and Wannier in 1941 [51, 52]. They discovered a self-duality property of the two-dimensional Ising model, i.e. a mapping between the high and low temperature phase, and were able, under a mild assumption, to locate exactly and for the first time the ferromagnetic-to-paramagnetic transition temperature. Since then duality transformations were extended to a large number of systems, and a number of relations connecting different statistical models have been discovered (see [53] for a review). In the context of lattice field theories, the term *dual representations* was introduced, and the corresponding dual transformations, which bring one from the original to the dual system, are generally different from the Krammers-Wannier ones. Typically, to obtain a dual representation, one integrates out the original degrees of freedom that parameterize the partition function (e.g. the gauge links in a pure gauge theory) after a Taylor or character expansion of the local Boltzmann factors. The integer variables that identify a given order of the Taylor expansion or a given

irreducible representation in the character expansion correspond to the new set of degrees of freedom in the dual representation (so-called dual variables). In the case of non-Abelian gauge theories, the set of dual variables must be augmented by an additional set of *auxiliary* degrees of freedom that allow to express the dualized partition function as a product of local weights distributed over lattice sites and bonds. The particle content of the original formulation is usually translated into constraints on the admissible set of dual variables, which are then crucial in Monte Carlo simulations, where it is fundamental to build an ergodic Markov process capable of proposing updates only between admissible configurations.

The driving force behind the use of dual representations comes from the observation that the sign problem is representation-dependent. Indeed, it does not have a physical origin and only stems from the choice of the basis in which the matrix elements of the density matrix are expressed. Therefore, a different parameterization of the partition function produces a sign problem with a different magnitude, which in some cases can be even absent. Before entering the discussion about dualization in QCD, we will re-examine two models: the multi-flavor lattice Schwinger model (i.e. two-dimensional quantum electrodynamics on the lattice) and lattice QCD at strong coupling, where the dualization process can be carried out quite easily, without struggling with the non-Abelian Yang-Mills term.

3.2 The lattice Schwinger model

3.2.1 Formulation

The Euclidean action of the multi-flavor Schwinger model in the continuum is given by

$$S_{\text{S.M.}} = - \int d^2x \; \frac{1}{2e^2} F_{\mu\nu}(x) F_{\mu\nu}(x) + \sum_{a=1}^{N_f} \bar{\psi}^a(x) \left[\sum_{\mu=0,1} \gamma_\mu D_\mu + m_a \right] \psi^a(x) , \quad (3.1)$$

$$F_{\mu\nu}(x) = \partial_\mu A_\nu(x) - \partial_\nu A_\mu(x), \qquad A_\mu \in \mathbb{R}, \qquad \mu, \nu = 0, 1 , \quad (3.2)$$

where e is the bare electric charge, A_μ the Abelian photon field and $\gamma_{\mu=0,1}$ are the two-dimensional gamma matrices. This model shares important properties with QCD: it exhibits confinement, spontaneous chiral symmetry breaking and has a non-trivial topology. Apart from gauge and chiral symmetry, the action Eq. (3.1) is invariant under $U(1)$ transformations corresponding to independent global phase rotations of the different flavors. The corresponding N_f conserved quantities

$$Q^a(x_0) = \int dx_1 \bar{\psi}^a(x_0, x_1) \gamma^0 \psi^a(x_0, x_1) , \qquad \partial_{x_0} Q^a(x_0) = 0 , \qquad a = 1, \ldots, N_f, \quad (3.3)$$

can be coupled to N_f chemical potentials $\mu_{a=1,\ldots,N_f}$ similarly to Eq. (2.36). The resulting action has then a sign problem as in the QCD case. On the lattice, a discretized version of the Schwinger model can be obtained with the ingredients of the previous chapter. We only consider the massless limit, employing the staggered discretization for the fermionic part, and the $U(1)$ plaquette action for the gauge term, obtaining the partition function[1]

$$\mathcal{Z}_{S.M.} = \prod_{n \in \Lambda} \prod_a \int d\bar{\chi}^a(n) d\chi^a(n) \prod_{(n,\mu)} \mathcal{D}U_{n,\mu} \, \exp\left(+\frac{\beta}{2} \sum_p \left(\mathrm{Tr} U_p + \mathrm{Tr} U_p^\dagger \right) - S_F[\bar{\chi}^a, \chi^a, U] \right),$$

(3.4)

$$S_F[\bar{\chi}^a, \chi^a, U] = \sum_{n,\mu} \sum_{a=1}^{N_f} \bar{\chi}^a(n) \left[\eta_\mu(n) e^{\hat{\mu}_a \delta_{\mu,0}} U_{n,\mu} \chi(n + \hat{\mu}) - \eta_\mu(n - \hat{\mu}) e^{-\hat{\mu}_a \delta_{\mu,0}} U_{n-\mu,\mu}^\dagger \chi^a(n - \hat{\mu}) \right].$$

(3.5)

The two-dimensional staggered phases $\eta_\mu(n)$ are given by

$$\eta_0(n) = 1, \qquad \eta_1(n) = (-1)^{n_0}, \tag{3.6}$$

$\hat{\mu}_a$ are the dimensionless lattice chemical potentials, and $U_{n,\mu} \equiv e^{i\phi_{n,\mu}} \in U(1)$ are the Abelian gauge links. The trace in the plaquette action is trivial in the Abelian case since the gauge links are complex numbers, and we have

$$\mathrm{Tr}\, U_{p=(n,\mu,\nu)} = U_{p=(n,\mu,\nu)} \equiv e^{i\phi_p} = e^{i(\phi_{n,\mu} + \phi_{n+\hat{\mu},\nu} - \phi_{n+\hat{\nu},\mu} - \phi_{n,\nu})}. \tag{3.7}$$

On a lattice with periodic boundary conditions, the net flux of the electric field is always zero, and the Gauss law implies global electric neutrality. Therefore only configurations with zero total electric charge can be generated. As a consequence, chemical potentials

$$\mu_a = \mu_Q, \qquad \forall\, a = 1, \ldots N_f, \tag{3.8}$$

which couple to the electric charge operator, do not produce any measurable effects, thus one needs at least $N_f = 2$. Other choices of the chemical potentials generate instead a non-trivial dependence in thermodynamic quantities, and the corresponding phase diagram has a rich structure [54].

---

[1]Ignoring the two tastes produced by each flavor of staggered quarks.

Before starting with the dualization process, we can get rid of the staggered phases which can be absorbed with a redefinition of the gauge links

$$U_{n,\mu} \to \eta_\mu(n) U_{n,\mu} \,. \tag{3.9}$$

This transformation does not change the Haar measure because the staggered phases are elements of the $U(1)$ gauge group. As the product of the staggered phases around a plaquette is always

$$\eta_\mu(n)\eta_\nu(n+\hat{\mu})\eta_\mu(n+\hat{\nu})\eta_\nu(n) = -1 \,, \tag{3.10}$$

this has only the effect of changing β to $-\beta$. This statement holds true for every $\mathrm{U}(N)$ or $\mathrm{SU}(2N)$ gauge theory. To obtain a dual representation, we start expanding in Taylor series[2] the Boltzmann factors corresponding to the plaquette term (expansion in $\beta/2$), and to the fermionic action (hopping expansion)

$$\exp\left(-\frac{\beta}{2}\sum_p \mathrm{Tr}U_p + \mathrm{Tr}U_p^\dagger\right) = \sum_{\{n_p,\bar{n}_p\}} \prod_p \frac{(-\beta/2)^{n_p+\bar{n}_p}}{n_p!\bar{n}_p!}(\mathrm{Tr}U_p)^{n_p}(\mathrm{Tr}U_p^\dagger)^{\bar{n}_p}\,, \tag{3.11}$$

$$\exp\left(-S_F[\bar{\chi}^a,\chi^a,U]\right) = \sum_{\{d^a_{n,\mu},\bar{d}^a_{n,\mu}\}} \prod_{(n,\mu)} \prod_{a=1}^{N_f} \left(W^a_{n,\mu}\right)^{d^a_{n,\mu}} \left(\overline{W}^a_{n,\mu}\right)^{\bar{d}^a_{n,\mu}}\,, \tag{3.12}$$

where we introduced the dual variables $n_p, \bar{n}_p \in \mathbb{N}$ and $d^a_{n,\mu}, \bar{d}^a_{n,\mu} \in \{0,1\}$. The positive ($W$) and negative ($\overline{W}$) *hopping weights* are given by

$$W^a_{n,\mu} = -\bar{\chi}^a(n)\,e^{\hat{\mu}_a\delta_{\mu,0}}\,U_{n,\mu}\,\chi^a(n+\hat{\mu})\,, \tag{3.13}$$

$$\overline{W}^a_{n,\mu} = +\bar{\chi}^a(n+\hat{\mu})\,e^{-\hat{\mu}_a\delta_{\mu,0}}\,U_{n,\mu}^\dagger\,\chi^a(n)\,. \tag{3.14}$$

The dual variables n_p and $\bar{n}_p$ are called respectively the plaquette and antiplaquette occupation numbers, and clearly live on the lattice plaquettes. The $d_{n,\mu}$ and $\bar{d}_{n,\mu}$ are instead defined on the lattice link (n,μ). In the following, to identify lattice links we will oftentimes use the notation $(n,\pm\mu)$, meaning

$$(n,+\mu) \equiv (n,\mu), \qquad (n,-\mu) \equiv (n-\hat{\mu},\mu). \tag{3.15}$$

---

[2]Historically the dual representation of the Schwinger model was derived from a character expansion [7]. In view of the generalization to non-Abelian gauge theories, we will perform a Taylor expansion showing at the end of the section the simple connection between the two representations.

For later convenience, we also introduce the *dimer numbers* $k_{n,\mu}^a$ and the *fermion fluxes* $f_{n,\mu}^a$ via

$$k_{n,\mu}^a = \min\left\{ d_{n,\mu}^a, \bar{d}_{n,\mu}^a \right\} \in \{0,1\}, \qquad f_{n,\mu}^a = d_{n,\mu}^a - \bar{d}_{n,\mu}^a \in \{-1,0,1\}, \tag{3.16}$$

which can be used as dual variables in place of $d_{n,\mu}$ and $\bar{d}_{n,\mu}$. In this way Eq. (3.12) can be rewritten as

$$\exp\left(-S_F[\bar{\chi}^a, \chi^a, U]\right) = \sum_{\{k_{n,\mu}^a, f_{n,\mu}^a\}} \prod_{(n,\mu)} \prod_{a=1}^{N_f} \left(W_{D;n,\mu}^a\right)^{k_{n,\mu}^a} W_{F;n,\mu}^a(f_{n,\mu}^a), \tag{3.17}$$

where the new dimer and flux weights W_D and W_F are given by

$$W_{D;n,\mu}^a = \bar{\chi}^a(n)\chi^a(n)\bar{\chi}^a(n+\hat{\mu})\chi^a(n+\hat{\mu}), \tag{3.18}$$

$$W_{F;n,\mu}^a(f_{n,\mu}^a) = \delta_{f_{n,\mu}^a,1}\, W_{n,\mu}^a + \delta_{f_{n,\mu}^a,-1}\, \bar{W}_{n,\mu}^a + \delta_{f_{n,\mu}^a,0}. \tag{3.19}$$

The dimer weight $W_{D;n,\mu}$ does not depend explicitly on the gauge link and describes two fermion-antifermion pairs at site n and $n+\hat{\mu}$. The flux weight $W_{F;n,\mu}$ describes instead a fermion-antifermion hopping between the two sites, and contains a forward or backward gauge link depending on the sign of $f_{n,\mu}$.

3.2.2 Grassmann and gauge integration

The Grassmann and gauge integrals can now be performed. We will start integrating out the fermionic field. Given the properties of Grassmann integration, to get a non-vanishing integral, at each lattice site n and for each flavor a, exactly one fermion $\chi^a(n)$ and antifermion $\bar{\chi}^a(n)$ must be present in the product in Eq. (3.17). When this happens we say that the Grassmann measure has been *saturated*. To fulfill this condition at each site n, we have two possibilities for each flavor a: we can either place a dimer on one link $(n, \pm\mu)$, i.e. $k_{n,\pm\mu}^a = 1$, or insert two fermion fluxes on two different links $(n, \pm\hat{\mu}), (n, \pm\hat{\nu})$. The two possibilities are mutually exclusive. In the first case, the Grassmann measure is saturated at site $(n \pm \hat{\mu})$ as well, and the corresponding integrals simply give

$$\int d\bar{\chi}^a(n)d\chi^a(n)d\bar{\chi}^a(n\pm\hat{\mu})d\chi^a(n\pm\hat{\mu})\bar{\chi}^a(n)\chi^a(n)\bar{\chi}^a(n\pm\hat{\mu})\chi^a(n\pm\hat{\mu}) = 1. \tag{3.20}$$

In the second case, to obtain a non-zero result from Grassmann integration, the fermion fluxes $f_{n,\pm\mu}^a$ and $f_{n,\pm\nu}^a$, must be chosen such that a fermion ($\chi^a(n)$) or antifermion ($\bar{\chi}^a(n)$) "excess" generated by one flux is always compensated by an antifermion or fermion from

the second flux. This condition can be written as

$$\sum_{\mu=0,1} f^a_{n,+\mu} - f^a_{n,-\mu} = 0, \qquad \forall\, a = 1, \ldots, N_f, \tag{3.21}$$

which expresses a conservation law for the net flux. As a consequence, fermion fluxes of any flavor a must always form oriented self-avoiding loops, including loops that wind around the periodic boundaries of the lattice. These loops can never cross a site attached to a dimer of the same flavor. The Grassmann integral for all sites belonging to one loop ℓ^a, can be performed and gives a total contribution of

$$W_{\ell^a}[U] = (-1)^{L(\ell^a)/2 + w(\ell^a) + 1} \prod_{(n,\mu)\in\ell^a} e^{f^a_{n,\mu}\,\hat{\mu}_a\,\delta_{\mu,0}}\; U^{f^a_{x,\mu}}_{n,\mu}, \tag{3.22}$$

where $L(\ell^a)$ is the number of links inside the loop (i.e. its length) and $w(\ell^a)$ is the winding number around the temporal direction. In fact, inspecting Eqs. (3.19), (3.13) and (3.14), we get a factor $U^{\pm 1}_{n,\mu} e^{\pm\hat{\mu}_a\delta_{\mu,0}}$ from each positive $(+)$ or negative $(-)$ hopping term (for unitary groups $U^{-1}_{n,\mu} = U^\dagger_{n,\mu}$). Moreover we get a minus sign from each positive hopping (which are $L(\ell^a)/2$ in total[3]), and an additional minus sign every time a fermion flux crosses the temporal boundary due to the antiperiodic conditions for fermionic fields. In addition, as explained in Sec. 2.1, the Grassmann variables must be put in canonical ordering before performing the integrals using Eq. (2.13). To do this, the first and last variable appearing in the product of the hopping terms must be commuted, which accounts for the last minus sign in the sign factor Eq. (3.22).

Thus, each lattice site is either attached to a dimer or crossed by a fermion flux. The (Grassmann-) constraint on $\{k^a_{n,\mu}, f^a_{n,\mu}\}$ is

$$\sum_{\pm\mu} k^a_{n,\mu} + \frac{|f^a_{n,\mu}|}{2} = 1, \qquad \forall\, n \in \Lambda, \qquad \forall\, a = 1, \ldots, N_f, \tag{3.23}$$

along with the flux conservation law Eq. (3.21). After Grassmann integration, the partition function takes the form

$$\mathcal{Z}_{\text{S.M.}} = \sum_{\substack{\{n_p,\bar{n}_p\} \\ \{k_{n,\mu}, f_{n,\mu}\}}} \prod_{(n,\mu)} \mathcal{D}U_{n,\mu} \left[\prod_{a=1}^{N_f} \prod_{\ell^a} W_{\ell^a}[U] \right] \prod_p \frac{(-\beta/2)^{n_p+\bar{n}_p}}{n_p!\,\bar{n}_p!} (\mathrm{Tr}U_p)^{n_p}(\mathrm{Tr}U^\dagger_p)^{\bar{n}_p}, \tag{3.24}$$

---

[3]For loops with a non-zero winding number this is not true, but Eq. (3.22) still holds if the number of sites in each direction is a multiple of 4.

Having integrated out the Grassmann variables, to complete the dualization process we need to integrate out the gauge fields. The U(1) Haar measure takes the trivial form

$$\int \mathcal{D}U_{n,\mu} = \frac{1}{2} \int_0^{2\pi} d\phi_{n,\mu} , \qquad (3.25)$$

hence any polynomial integral over the gauge link $U_{n,\mu}$ gives simply

$$\int \mathcal{D}U_{n,\mu} \left(U_{n,\mu}\right)^a \left(U_{n,\mu}^\dagger\right)^b = \delta^{a,b} . \qquad (3.26)$$

The integration over the gauge measure in the U(1) case, acts simply as a constraint on the allowed set of dual variables $\{n_p, \bar{n}_p, f_{n,\mu}\}$, which must be chosen such that the gauge integrals are non-vanishing. As the dimer weight $W_{D;n,\mu}$ does not depend on the gauge links, this condition does not constrain further the dimer numbers $k_{n,\mu}$. A non-zero weight is thus obtained only when at each link the same number of forward $U_{n,\mu}$ and backward $U_{n,\mu}^\dagger$ gauge links are present. If this condition is satisfied, the integral in Eq. (3.24) gives simply one. This (gauge-) constraint can be stated in terms of dual variables as

$$\sum_{\nu > \mu} \left(\delta n_{n,\mu,\nu} - \delta n_{n-\hat{\nu},\mu,\nu}\right) + \sum_{\nu < \mu} \left(\delta n_{n-\hat{\nu},\nu,\mu} - \delta n_{n,\nu,\mu}\right) + \sum_{a=1}^{N_f} f_{n,\mu}^a = 0, \qquad \forall (n,\mu), \qquad (3.27)$$

where $\delta n_p = n_p - \bar{n}_p$. Indeed, every unit of n_p and $\bar{n}_p$ produces, on each of the four links that make the plaquette p, a forward or a backward gauge link depending on the relative orientation of the plaquette with respect to the link. An excess of gauge links in one direction, generated by the plaquettes, must be compensated by oppositely oriented fermion fluxes.

3.2.3   The dual partition function

The fully dualized partition function can be thus expressed as a sum over configurations $\mathcal{C}$ made of fermion loops ℓ^a, dimers $k_{n,\mu}^a$, and plaquette occupation numbers $\{n_p, \bar{n}_p\}$ via

$$\mathcal{Z}_{\text{S.M.}} = \sum_{\substack{\{n_p, \bar{n}_p\} \\ \{k_{n,\mu}^a, \ell^a\}}} \sigma\left(\mathcal{C}\right) \prod_{\ell^a} e^{\hat{\mu}_a N_t w(\ell^a)} \prod_p \frac{(\beta/2)^{n_p + \bar{n}_p}}{n_p! \bar{n}_p!} , \qquad (3.28)$$

where N_t is the temporal extent of the lattice, and the dual variables must fulfill the constraints Eqs. (3.21), (3.23) and (3.27). A graphical representation of an allowed configuration is shown in Fig. 3.1. Notice that the dependence on the chemical potential is only carried by fermion loops with non-zero winding number in temporal direction. For other types of loop instead, the number of positive and negative temporal hoppings is the same, and the
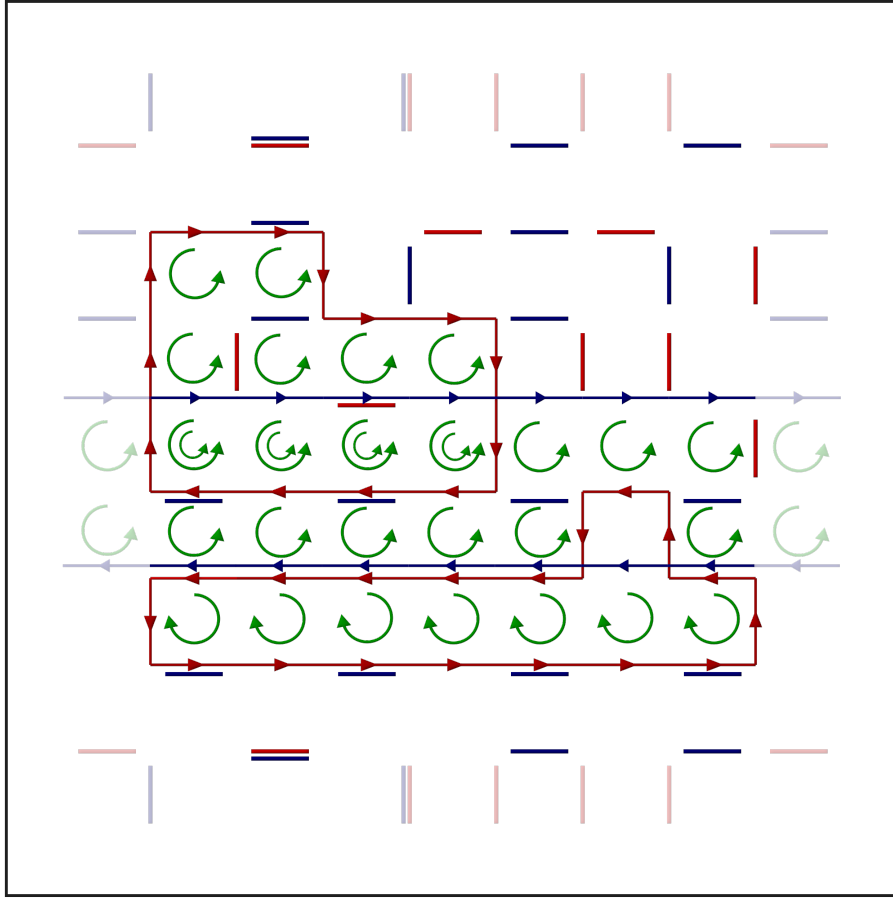
FIGURE 3.1: An allowed configuration on a 8×8 lattice with periodic boundary conditions for $N_f = 2$. Unoriented and oriented lines represent respectively dimers and fermion fluxes. Different colors refer to different flavors. Every clockwise or anti-clockwise green arrow corresponds respectively to a positive or negative unit of $\delta n_p = n_p - \bar{n}_p$.

chemical potential dependence cancels. The overall sign $\sigma\left(\mathcal{C}\right)$ in Eq. (3.28) is

$$\sigma\left(\mathcal{C}\right) = \left(-1\right)^{\sum_p \delta n_p + \sum_{\ell^a}\left(L(\ell^a)/2 + w(\ell^a) + 1\right)}, \tag{3.29}$$

thus it might look like we did not solve the sign problem after all. Remarkably, it can be shown (see [7] for a detailed proof) that for all sets of allowed dual variables, the minus signs always combine to produce $\sigma\left(\mathcal{C}\right) = 1$, and the sign problem is absent in this representation. The dual variables can be sampled using a generalization of the Prokofiev-Svistunov Worm algorithm [55] that includes an update of the plaquette occupation numbers. This has been discussed in [56] to which we refer for further readings about simulation strategies.

At finite fermion masses $\hat{m}_a$, a sign problem is instead present. We can understand this
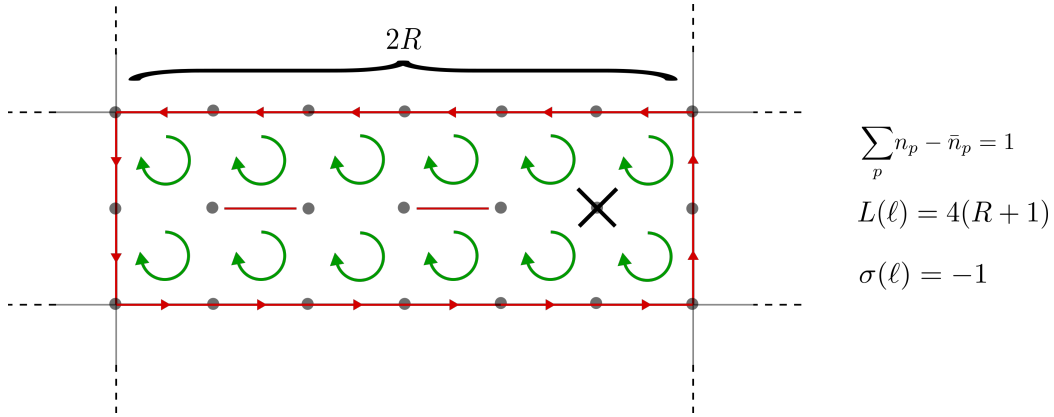
FIGURE 3.2: A negative configuration generated by a $2R \times 2$ fermion loop for $N_f = 1$. The Grassmann constraint within the loop cannot be fulfilled by placing dimers only, and it is forbidden in the chiral limit.

effect diagrammatically: rectangular $2R \times 2$ fermion loops are forbidden in the chiral limit $\hat{m}_a = 0$ since the Grassmann constraint Eq. (3.55) cannot be fulfilled at lattice sites within the loops using dimers only. Given that they carry a negative sign (see Fig. 3.2), the appearance of the sign problem can be explained as a proliferation of these kind of loop geometries at non-zero fermion masses, since now the Grassmann integrals within the loop can be saturated by terms of the form

$$\exp\left(-\sum_a \hat{m}_a \, \bar{\chi}^a(n)\chi^a(n)\right) = \sum_{m_n^a=0,1} (-\hat{m}_a)^{m_n^a} \left(\bar{\chi}^a(n)\chi^a(n)\right)^{m_n^a} . \tag{3.30}$$

One last remark concerns the connection between the Taylor and character expansions. The gauge constraint Eq. (3.27), only involves the difference $n_p - \bar{n}_p$ between plaquette and antiplaquette occupation numbers. This means that a resummation of n_p and $\bar{n}_p$ is possible, and the partition function can be expressed only in terms of their difference δn_p with modified weights given by

$$\frac{(\beta/2)^{n_p+\bar{n}_p}}{n_p!\bar{n}_p!} \rightarrow \sum_{\bar{n}_p=0}^{+\infty} \frac{(\beta/2)^{2\bar{n}_p+\delta n_p}}{\bar{n}_p!(\bar{n}_p+\delta n_p)!} = I_{\delta n_p}(\beta), \tag{3.31}$$

where $I_\alpha(x)$ are the modified Bessel functions of the first kind. As the modified Bessel functions are the expansion coefficients in the character expansion of the plaquette action

$$\exp\left(\frac{\beta}{2}\sum_p \mathrm{Tr}U_p + \mathrm{Tr}U_p^\dagger\right) = \sum_{\nu=-\infty}^{+\infty} I_\nu(\beta)\hat{\chi}_\nu(U_p), \quad \hat{\chi}_\nu(U_p) = e^{i\nu\phi_p}, \tag{3.32}$$

this resummation connects the Taylor and character expansion based, dual representations. For the latter the dual partition function is simply

$$\mathcal{Z}_{\text{S.M.}}(\beta, \hat{\mu}_a) = \sum_{\{\delta n_p, k^a_{n,\mu}, \ell^a\}} \prod_{\ell^a} e^{\hat{\mu}_a N_t w(\ell^a)} \prod_p I_{\delta n_p}(\beta) \,. \tag{3.33}$$

In the case of non-Abelian gauge theories, including QCD, such a simple correspondence does not exist, and the resulting representations can have in general different properties (see the discussion in Sec. 5.2.4).

The sign problem in other Abelian models, such as in the gauge-Higgs model and in the charged scalar ϕ^4 theory, can be solved using strategies similar to the one we just discussed [6, 57]. For non-Abelian systems, the corresponding dual representations will have in general a residual sign problem. As we will show in the next subsection, this does not always represent a failure of the method. The magnitude of the sign problem can be drastically reduced in the dual representation, and reweighting techniques be applied.

3.3 Lattice QCD at strong coupling

In this subsection we continue the overview on dual methods analyzing a second model: lattice QCD in the strong coupling limit. This model corresponds to a one-parameter deformation of the full theory, since it is obtained setting the bare lattice coupling β to zero. Despite its crudeness, it has some interesting properties. For example the realization of chiral symmetry at strong coupling happens in a similar way as in the continuum limit $\beta \to \infty$: it is spontaneously broken by the vacuum, and restored at some finite temperature T_c. The system also possesses pion-like and baryon-like modes, and the phase structure at finite temperature and density can provide qualitative indications about the corresponding structure in the continuum limit. Finally, it corresponds to the zeroth-order term in the strong coupling expansion; thus performing the dualization of this theory allows to introduce some of the ingredients needed for the understanding of the following chapters, where the problem of a systematic inclusion of the β corrections will be tackled.

3.3.1 The dual formulation

We start directly from the partition function on the lattice, employing one flavor of staggered fermions[4]. To keep the discussion as general as possible, we consider the case of a SU(N) or

---

[4]We remind the reader that in the continuum limit, for $D + 1 = 4$, the action describes four degenerate quark flavors.

U(N) theory in $D + 1$ spacetime dimensions. The strong coupling partition function is

$$\mathcal{Z}_{\text{s.c.}} = \prod_n d\bar{\chi}(n) d\chi(n) \prod_{(n,\mu)} \int_G \mathcal{D}U_{n,\mu} \exp\left(-S_F[\bar{\chi}, \chi, U]\right), \qquad U_{n,\mu} \in G, \qquad (3.34)$$

$$S_F[\bar{\chi}, \chi, U] = \sum_n \left(-\sum_\mu \left[\text{Tr}\, \mathcal{M}_{n,\mu}^\dagger U_{n,\mu} + \text{Tr}\, U_{n,\mu}^\dagger \mathcal{M}_{n,\mu}\right] + 2\hat{m}_q \bar{\chi}(n)\chi(n)\right), \qquad (3.35)$$

where $G = \text{SU}(N)$, $\text{U}(N)$, and $\hat{m}_q$ is the dimensionless quark mass. The staggered fields $\bar{\chi}(n)$ and $\chi(n)$ are now $N-$component vectors

$$\bar{\chi}(n) \equiv (\bar{\chi}_1(n), \ldots, \bar{\chi}_N(n)), \qquad \chi(n) \equiv \begin{pmatrix} \chi_1(n) \\ \vdots \\ \chi_N(n) \end{pmatrix}. \qquad (3.36)$$

The plaquette action is of course absent in the strong coupling limit since $\beta = 0$. To simplify the notation, we have defined the staggered action in term of the fermion matrices $\mathcal{M}$ and $\mathcal{M}^\dagger$, which are given by

$$(\mathcal{M}_{n,\mu})_{i,j} = \eta_\mu(n) e^{-\hat{\mu}_q \delta_{\mu,0}} \bar{\chi}_i(n + \hat{\mu})\chi_j(n), \qquad (3.37)$$

$$(\mathcal{M}_{n,\mu}^\dagger)_{i,j} = -\eta_\mu(n) e^{\hat{\mu}_q \delta_{\mu,0}} \bar{\chi}_i(n)\chi_j(n + \hat{\mu}). \qquad (3.38)$$

The color indices i, j run from 1 to N, and $\hat{\mu}_q$ is the dimensionless quark chemical potential. The trace in Eq. (3.35) is intended over color indices. Given the anticommutation rules for Grassmann variables, the fermion matrices satisfy the properties

$$\text{Tr}\left[\left(\mathcal{M}_{n,\mu}\mathcal{M}_{n,\mu}^\dagger\right)^i\right] = (-1)^{i+1}\left(M_n M_{n+\hat{\mu}}\right)^i, \qquad M_n \equiv \sum_{i=1}^N \bar{\chi}_i(n)\chi_i(n), \qquad (3.39)$$

$$\left(\mathcal{M}_{n,\mu}\right)^{N+1} = \left(\mathcal{M}_{n,\mu}^\dagger\right)^{N+1} = 0 \qquad (3.40)$$

To obtain a dual representation, we start performing the integral over the gauge links $U_{n,\mu}$. As there are no plaquette terms, the functional integral in Eq. (3.34) factorizes into one-link contributions of the form

$$\mathcal{I}_G(\mathcal{M}, \mathcal{M}^\dagger) = \int_G \mathcal{D}U \exp\left(\text{Tr}\,\mathcal{M}^\dagger U + \text{Tr}\,\mathcal{M}U^\dagger\right), \qquad (3.41)$$

which can be computed independently. The quantity $\mathcal{I}_G(A, A^\dagger)$, for a generic complex $N \times N$ matrix A, is the Brézin-Gross-Witten integral and it is known, for unitary groups G of sufficiently small rank, as a power series in terms of the invariants of A, $A^\dagger$ [58]. For example

in the case of $\mathrm{SU}(3)$ the invariants are:

$$\det[A], \quad \det[A^\dagger], \quad \mathrm{Tr}[(AA^\dagger)], \quad \mathrm{Tr}[(AA^\dagger)^2], \tag{3.42}$$

while for $G = \mathrm{U}(N), \mathrm{SU}(N)$ the power series contains higher order traces $\mathrm{Tr}[(AA^\dagger)^k]$ with $k < N$. In our case the fermion matrices satisfy the properties Eqs. (3.39) and (3.40); hence the power series is finite and it can be obtained for any unitary group. The result is[5]

$$\mathcal{I}_G(\mathcal{M}_{n,\mu}, \mathcal{M}_{n,\mu}^\dagger) = \sum_{k_{n,\mu}=0}^{N} \frac{(N-k_{n,\mu})!}{N! k_{n,\mu}!} \left(M_n M_{n+\hat{\mu}}\right)^{k_{n,\mu}} + z\left((-1)^N \alpha_{n,\mu} \bar{B}_n B_{n+\hat{\mu}} + \alpha_{n,\mu}^{-1} \bar{B}_{n+\hat{\mu}} B_n\right) \tag{3.43}$$

$$B_n \equiv \frac{1}{N!} \epsilon_{i_1,\dots,i_N} \chi_{i_1}(n) \dots \chi_{i_N}(n), \quad \bar{B}_n \equiv \frac{1}{N!} \epsilon_{i_1,\dots,i_N} \bar{\chi}_{i_1}(n) \dots \bar{\chi}_{i_N}(n). \tag{3.44}$$

z is 1 for $\mathrm{SU}(N)$ and 0 for $\mathrm{U}(N)$, while

$$\alpha_{n,\mu} = \left(\eta_\mu(n)\right)^N e^{N \hat{\mu}_q \delta_{\mu,0}}, \quad \alpha_{n,\mu}^{-1} = \left(\eta_\mu(n)\right)^N e^{-N \hat{\mu}_q \delta_{\mu,0}}. \tag{3.45}$$

Similarly to what we did for the Schwinger model, we can introduce dual variables associated to the various terms in Eq. (3.43). The integers $k_{n,\mu} \in \{0,\dots,N\}$ are the dimer numbers, while the second and third term represent respectively a $N-$quark flux ($f_{n,\mu} = N$) and an $N-$antiquark flux ($f_{n,\mu} = -N$). In the context of strong coupling lattice QCD, the latter two are usually referred to as a baryon flux and an antibaryon flux. This definition of dimers and quark fluxes exactly coincides with the one given for the Schwinger model as the various pieces in Eq. (3.43) originate respectively from the following expansion terms of the staggered action:

$$\left(\mathrm{Tr}\,\mathcal{M}_{n,\mu}^\dagger U_{n,\mu}\right)^{k_{n,\mu}} \left(\mathrm{Tr}\,\mathcal{M}_{n,\mu} U_{n,\mu}^\dagger\right)^{k_{n,\mu}}, \quad \left(\mathrm{Tr}\,\mathcal{M}_{n,\mu}^\dagger U_{n,\mu}\right)^N, \quad \left(\mathrm{Tr}\,\mathcal{M}_{n,\mu} U_{n,\mu}^\dagger\right)^N. \tag{3.46}$$

An exact derivation of Eq. (3.43), starting directly from the Taylor expansion of $S_F[\bar{\chi}, \chi]$, will be given in the next chapter.

Before performing the Grassmann integral, it is convenient to expand also the mass term in Eq. (3.35) as

$$e^{-2\hat{m}_q \bar{\chi}(n)\chi(n)} = \sum_{m_n=0}^{N} \frac{(-2\hat{m}_q)^{m_n}}{m_n!} M_n^{m_n}. \tag{3.47}$$

---

[5] For a derivation of this equation see [59] or Ch. 4 where it will be obtained using a different formalism.

The associated dual variables $m_n \in \{0,\ldots,N\}$ are called *monomers*. Putting together Eqs. (3.47) and (3.43) the strong coupling partition function assumes the dual form

$$\mathcal{Z}_{\text{s.c.}} = \sum_{\{m_n,k_{n,\mu},f_{n,\mu}\}} \prod_n \mathcal{D}[\bar{\chi}(n),\chi(n)] \frac{(-2\hat{m}_q)^{m_n}}{m_n!} M_n^{m_n} \prod_{(n,\mu)} W_{D;n,\mu}(k_{n,\mu}) W_{B;n,\mu}(f_{n,\mu}) \qquad (3.48)$$

with the dimer and baryon weights given by

$$W_{D;n,\mu}(k_{n,\mu}) = \frac{(N-k_{n,\mu})!}{N!k_{n,\mu}!} \left(M_n M_{n+\hat{\mu}} \right)^{k_{n,\mu}}, \qquad k_{n,\mu} \in \{0,\ldots,N\}, \qquad (3.49)$$

$$W_{B;n,\mu}(f_{n,\mu}) = z \left((-1)^N \alpha_{n,\mu} \bar{B}_n B_{n+\hat{\mu}} \, \delta_{f_{n,\mu},N} + \alpha_{n,\mu}^{-1} \bar{B}_{n+\hat{\mu}} B_n \, \delta_{f_{n,\mu},-N} \right) + \delta_{f_{n,\mu},0}, \qquad (3.50)$$

$$f_{n,\mu} \in \{-N,0,N\}. \qquad (3.51)$$

We can now proceed integrating out the staggered fields. The Grassmann measure can be saturated in a similar way as in the Schwinger model. Since the staggered fields have N components, at each site n exactly one quark-antiquark pair $\bar{\chi}_i(n)\chi_i(n)$, for each quark color $i \in \{1,\ldots,N\}$, must be present in order to get a non-zero result. The first possibility for saturating the Grassmann measure at site n consists in activating dimers $k_{n,\pm\mu}$ and monomers m_n. Given the Grassmann integral

$$\int d\bar{\chi}(n) \, d\chi(n) \, (M_n)^K = N! \, \delta_{K,N}, \qquad (3.52)$$

this produces an allowed configuration only if the dimer and monomer numbers satisfy the (Grassmann-) constraint

$$m_n + \sum_{\pm\mu} k_{n,\pm\mu} = N, \qquad \forall \, N; \qquad (3.53)$$

then the integration simply produces an additional factor $N!$. The second possibility is to activate a baryon flux ($f_{n,\pm\mu} = \pm N$) on a link ($n,\pm\mu$). As each factor B_n, $\bar{B}_n$ carries respectively N quarks and antiquarks with different colors, the excess of quarks or antiquarks produced at site n can only be compensated by a second baryon flux in another direction. Therefore, baryon fluxes can only form oriented self-avoiding loops that never cross a site attached to dimers or occupied by monomers. This condition can be stated, as in the case of the Schwinger model, as a local conservation law for the baryon flux

$$\sum_{\mu=0}^{D} f_{n,+\mu} - f_{n,-\mu} = 0, \qquad (3.54)$$

and Eq. (3.53) can be generalized in order to account for baryon fluxes as well via

$$m_n + \sum_{\pm\mu} k_{n,\pm\mu} + \frac{|f_{n,\pm\mu}|}{2} = N. \tag{3.55}$$

Of course in the U(N) case since $z = 0$ there are no baryon fluxes, and the system is described only by dimers and monomers. The Grassmann integral along a baryon loop ℓ can be performed and gives a total contribution of

$$N!^{L(\ell)} W_\ell \equiv \sigma(\ell) \prod_{(n,\mu)\in\ell} e^{f_{n,\mu} \hat{\mu}_q \delta_{\mu,0}} = \sigma(\ell) \exp\left(N N_t \hat{\mu}_q w(\ell)\right), \tag{3.56}$$

$$\sigma(\ell) = \begin{cases} (-1)^{N_+(\ell)+w(\ell)+1} \prod_{(n,\mu)\in\ell} \eta_\mu(n) & N \text{ odd} \\ 1 & N \text{ even.} \end{cases} \tag{3.57}$$

$N_+(\ell)$ and $w(\ell)$ are respectively the total number of positive baryon segments and the temporal winding number, while N_t is the temporal extent of the lattice. Indeed, similarly to the fermion loops in the Schwinger model, we get from the weights W_B in Eq. (3.48), a factor $e^{N \hat{\mu}_q} (e^{-N \hat{\mu}_q})$ for each baryon (antibaryon) flux in temporal direction, a factor $(-1)^N$ from each (positive) baryon flux (which are $N_+(\ell)$ in total), and a factor $(\eta_\mu(n))^N$ for every link (n, μ) traversed by the loop. The remaining part of the sign factor $\sigma(\ell)$ is determined by the antiperiodic boundary condition in temporal directions $((-1)^{w(\ell)})$ and from commuting the first and last term $\bar{B}_n, B_n$ in the product of the factors W_B around the loop. Notice that when B_n and $\bar{B}_n$ are made of an even number of quarks and antiquarks (the case of even N), since baryons are bosons in this case, we do not get any minus sign when commuting B_n with $\bar{B}_n$ or when crossing the temporal boundary.

Putting it all together, the final partition function assumes the form[6]

$$\mathcal{Z}_{s.c.} = \sum_{\{m_n, k_{n,\mu}, \ell\}} \prod_n \frac{N!}{\hat{m}_q!} (2\hat{m}_q)^{m_n} \prod_{(n,\mu)} \frac{(N - k_{n,\mu})!}{N! k_{n,\mu}!} \prod_\ell W_\ell; \tag{3.58}$$

hence it is a sum over configurations made of monomers, dimers and baryon loops, subject to the constraints Eqs. (3.54) and (3.55). The first determination of Eq. (3.58) was obtained in [60] by P. Rossi and U. Wolff. An example of an admissible configuration is shown in Fig. 3.3. Unlike the massless Schwinger model, the partition function contains negative configuations because the minus signs from baryon loops do not always cancel. Indeed in the U(1) case, because of the gauge constraint Eq. (3.27), fermion fluxes can only exist in combination with plaquette terms which counterbalance the gauge links appearing in the

---

[6]Since on an even lattice the total number of monomers $\sum_n m_n$ is even, we neglected the factor $(-1)^{m_n}$ from the monomer weight.
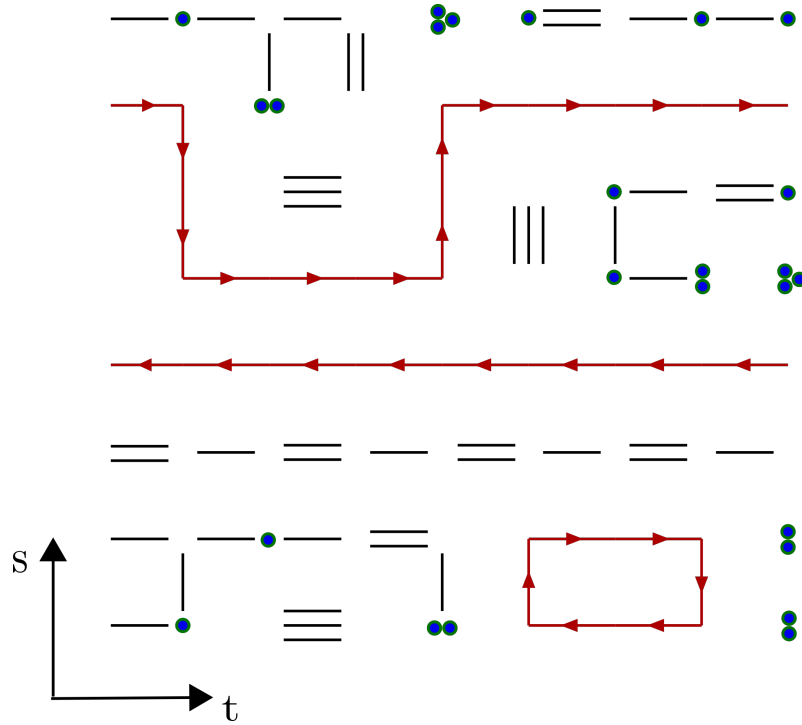
FIGURE 3.3: Graphical representation of an allowed configuration for SU(3) on a 8×8 lattice with periodic boundary conditions. At each lattice site the monomer number m_n is given by the number of blue circles, while on each link every black line represents a dimer, i.e. one unit of $k_{n,\mu}$. Oriented red lines are instead baryon fluxes ($f_{n,\mu} = \pm 3$) and always form closed loops. The Grassmann constraint Eqs. (3.54) and (3.55) is always satisfied.

flux weights $W_F[U]$ (see Eq. (3.19)). As a consequence, not all fermion loop geometries are allowed, and in particular those providing negative weights are forbidden in the massless limit. In the case of a SU(N) theory, baryon fluxes can exist even without the plaquettes, and loops of arbitrary shape can be generated, producing a sign problem[7]. The question whether numerical simulations are still feasible depends on its severity, and will be discussed in the next subsection.

3.3.2 Analysis of the sign problem and the finite density phase diagram

To discuss the sign problem in the dual representation, we need a quantitative definition of its magnitude. It is a common practice to do this on the basis of a reweighting criterion: given a generic partition function $\mathcal{Z} = \sum_\alpha P_\alpha$, the sign problem is said to be *mild* if the average sign $\langle \sigma \rangle$ satisfies

$$\langle \sigma \rangle \equiv \langle \frac{P}{|P|} \rangle_{\text{p.q.}} = \frac{\sum_\alpha P_\alpha}{\sum_\alpha |P_\alpha|} = \exp\left(-(f - f_{\text{p.q.}})\frac{V}{T}\right) \approx \mathcal{O}(1), \qquad (3.59)$$

---

[7]In the dual representation negative configurations are present even at zero chemical potential. However in this limit the sign problem can be solved exploiting the Karsch-Mutter trick [61] which resums baryon loops and dimer chains into so-called polymers.

where $\langle\,.\,\rangle_{\text{p.q.}}$ means average over the *phase quenched* distribution $|P_\alpha|$ obtained by taking the norm of the statistical weights P_α. As we already discussed in Sec. 2.3, f and $f_{\text{p.q.}}$ are the free energy densities of the real and reweighted system. Conversely, when $\langle\sigma\rangle \approx 0$ the sign problem is said to be *severe*. Clearly $0 \leq \langle\sigma\rangle \leq 1$. In a nutshell, this definition tells us how expensive it is in terms of machine time to get a fixed statistical accuracy on the observables if we perform a Monte Carlo sampling according to the phase quenched distribution $|P_\alpha|$. Of course, increasing the spatial volume V will always correspond to an exponential deterioration of the signal, but for practical purposes if the mildness condition Eq. (3.59) holds true for a volume V large enough such that finite size effects are under control, we can say that the sign problem is effectively solved. Notice that the mildness condition depends on the lattice parameters, like quark mass $\hat{m}_q$, chemical potential $\hat{\mu}_q$ and temperature T.

The dual strong coupling partition function can be simulated using the Prokofiev-Svistunov Worm algorithm. The algorithmic details are unimportant for the following discussion, hence we refer to [62] for a detailed presentation. However, one important point concerning finite temperature simulations, is realizing that since we are limited to $\beta = 0$, the lattice spacing a of our system cannot be changed[8]. As a consequence, the temperature T can only be varied by changing the temporal extent N_t of the lattice, since $T = \frac{1}{aN_t}$. This is a problem: the highest lattice temperature aT that can be reached is $aT_{\text{max.}} = \frac{1}{2}$ since staggered fermions require an even lattice in all directions. A solution to this problem requires the introduction of *anisotropic* lattices. The idea in this case is to introduce in the Dirac operator a bare anistropy γ that favors the coupling in temporal direction, via

$$\mathcal{M}_{n,\mu} \to \gamma^{\delta_{\mu,0}} \mathcal{M}_{n,\mu}, \quad \mathcal{M}_{n,\mu}^\dagger \to \gamma^{\delta_{\mu,0}} \mathcal{M}_{n,\mu}^\dagger, \quad \gamma \in \mathbb{R}^+. \tag{3.60}$$

This modification triggers a physical anistropy ξ between the spatial (a) and temporal (a_t) lattice spacing

$$\xi(\gamma) \equiv \frac{a}{a_t}, \tag{3.61}$$

and the lattice temperature can now be varied continuously by changing γ, since now

$$aT = \frac{\xi(\gamma)}{N_t}. \tag{3.62}$$

The relation between γ and ξ is of non-perturbative nature and must be determined via the

---

[8]Strictly speaking the lattice spacing cannot be even defined since we are very far from the continuum limit. Setting the scale using an operator $\mathcal{O}$ with length dimension δ via $\mathcal{O}_{\text{phys.}} = a^\delta \hat{\mathcal{O}}_{\text{latt.}}$, produces very different determinations of a depending on what is $\mathcal{O}$ [63].

so-called *calibration procedure* [64]. This has been done so far for the most relevant cases of U(3) and SU(3), and the result is

$$\frac{\xi(\gamma)}{\gamma^2} = \kappa + \frac{1}{1 + \frac{\kappa}{1-\kappa}\gamma^4}\,, \qquad \kappa = \begin{cases} 0.7795(4), & \text{U}(3) \\ 0.7810(8), & \text{SU}(3) \end{cases} \tag{3.63}$$

In the dual partition function, the introduction of a bare anistropy γ only requires a simple modification of the dimer and loop weights, which can be summarized with reference to Eq. (3.58) as

$$\frac{(N - k_{n,\mu})!}{N!k_{n,\mu}!} \to \gamma^{2k_{n,\mu}}\frac{(N - k_{n,\mu})!}{N!k_{n,\mu}!}\,, \qquad W_\ell \to \gamma^{N_0(\ell)}W_\ell\,, \tag{3.64}$$

where $N_0(\ell)$ is the number of temporal lattice links contained in the loop ℓ.

With these ingredients, the magnitude of the sign problem in the dual representation can be analyzed. In Fig. 3.4, we show the average sign $\langle\sigma\rangle$ for SU(3) as obtained from Monte Carlo simulations on a $16^3 \times 4$ lattice as a function of the chemical potential $\hat{\mu}_q$ and temperature aT, in the chiral limit $\hat{m}_q = 0$. The sign problem is very mild for a broad range of temperatures and chemical potentials (essentially because baryons are heavy) and for the purposes of determining the finite density phase diagram, the sign problem can be considered as solved. In the region of the $aT - \hat{\mu}_q$ plane relevant for the determination of the transition line that separates the chirally broken from the chirally restored phase, the average sign $\langle\sigma\rangle$ is sufficiently close to one that sign reweighting can be used. In Fig. 3.5 we show a determination of the phase diagram in the chiral limit. The transition temperature is determined, for each value of the chemical potential, from a finite size scaling analysis of the lattice chiral susceptibility[9]

$$\chi_{\bar{\psi}\psi} = \frac{1}{L^3 N_t}\frac{\partial^2 \log \mathcal{Z}}{\partial^2 (2\hat{m}_q)}\,, \tag{3.65}$$

as shown in Fig. 3.6. At zero chemical potential the chiral transition is of second order with associated O(2) critical exponents[10]. When switching on a chemical potential, the transition temperature decreases keeping its second order nature until a tricritical point at

$$aT_c^{(\text{tric.})} = 0.80(2)\,, \quad (a\mu_q)^{(\text{tric.})} \equiv (\xi(\gamma)\hat{\mu}_q)^{(\text{tric.})} = 0.52(1)\,, \tag{3.66}$$

is reached. A line of first order phase transition is then present for larger values of the

---

[9]See [65, 66, 67] for a review on finite size scaling at phase transitions.

[10]We remind the reader that the staggered Lagrangian has a O(2) $\cong$ U(1) $\subset$ SU(4) chiral symmetry.
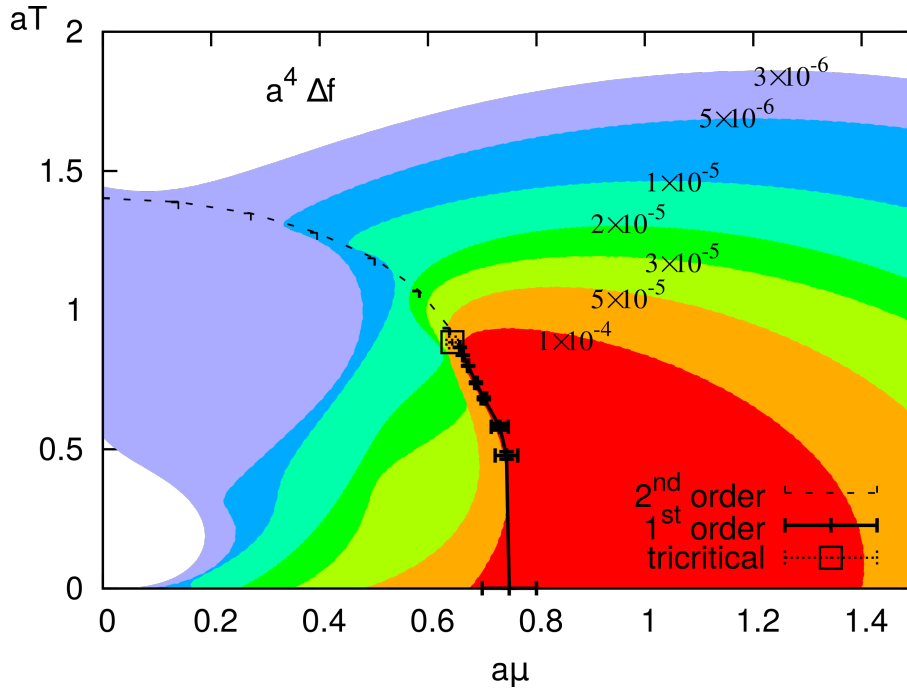
FIGURE 3.4: The dimensionless free energy difference $a^4 \Delta f = -\frac{1}{N_t N_s^3} \log \langle \sigma \rangle$ (Eq. (3.59)) in the $aT - \hat{\mu}_q$ plane for SU(3) in the chiral limit. The temperature aT and the chemical potential $a\mu = \xi(\gamma)\hat{\mu}_q$ were rescaled using the mean field coefficient $\kappa_{mf} = 1$; hence the tricritical point is located at a slightly larger value of the chemical potential with respect to Fig 3.5. Courtesy of Wolfgang Unger.

chemical potential. For finite quark mass instead, the second order line turns into an analytic crossover, while the tricritical point becomes a critical endpoint, hence described by the universality class of the three-dimensional Ising model. The phase diagram resembles the one expected for continuum QCD (see Fig. 1.1). Of course the position of the strong coupling critical endpoint has nothing to do with the continuum one, if any. An artifact of the strong coupling limit is instead related to the nuclear transition: at low temperature, chiral symmetry restoration occurs via the condensation of static baryon fluxes ($f_{n,0} = \pm N$). When $\langle \bar{\psi}\psi \rangle = 0$, the system is in a crystalline phase where every site is occupied by a static baryon, and the nuclear and chiral transition are thus degenerate. In the continuum limit it is expected that this degeneracy gets removed, with a nuclear-liquid phase forming before chiral restoration. To try to determine the fate of the critical endpoint in the continuum limit, and the splitting of the chiral and nuclear transition, it is fundamental to study how the phase diagram gets modified by the gauge corrections. The next two chapters will be devoted to the development of a strategy capable to attack this problem systematically in a strong coupling expansion in the β parameter.
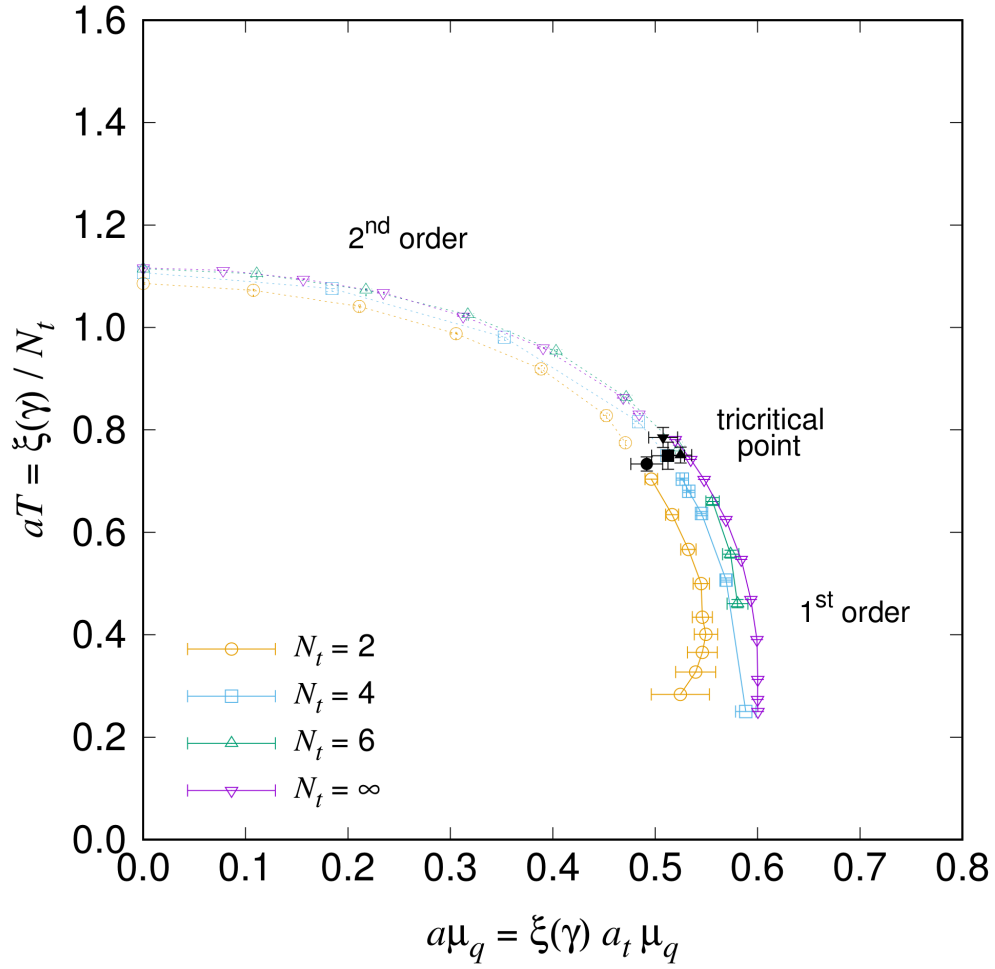
FIGURE 3.5: The phase diagram of strong coupling QCD ($G = SU(3)$) in the chiral limit $\hat{m}_q = 0$. The line of second order critical points ends in a tricritical point at $aT_c^{(\text{tric.})} = 0.80(2)$ and $(a\mu_q)^{(\text{tric.})} = 0.52(1)$. Different lines refer to simulations at different values of the lattice temporal extent N_t. Taken from [64].
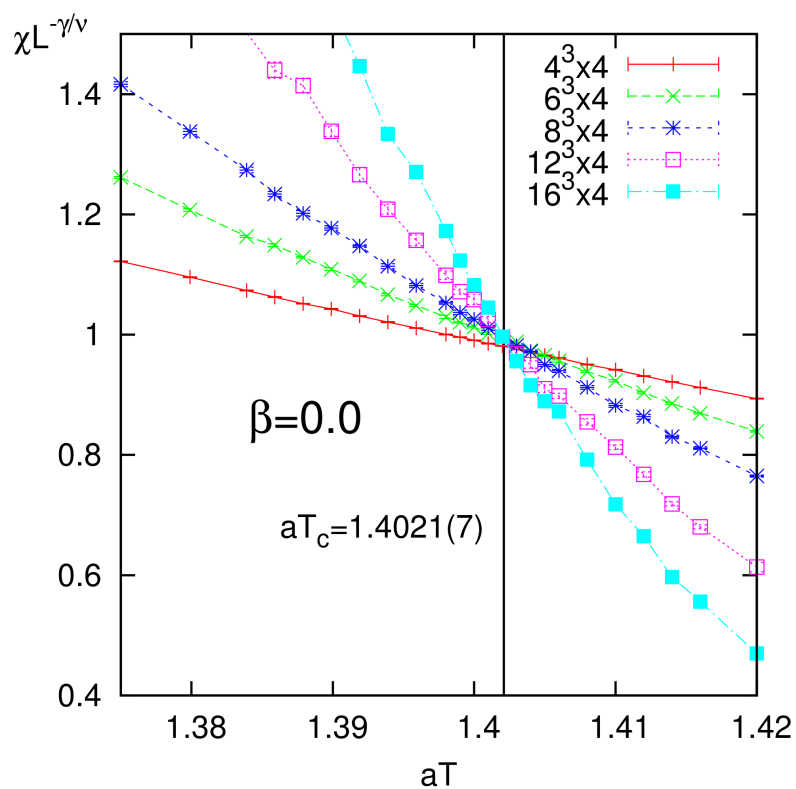
FIGURE 3.6: Example of the procedure followed to determine the critical temperature. For different values of the spatial lattice length L, the combination $\chi_{\bar{\psi}\psi}L^{-\gamma/\nu}$ is plotted as a function of the lattice temperature aT. The critical temperature aT_c is determined as the crossing point of the various curves. In the figure, the mean field temperature $aT = \gamma^2/N_t$, has been used. For O(2) critical behavior in three dimensions $\nu = 0.67155(27)$ and $\gamma = 1.3177(5)$ [68]. At the tricritical point instead $\nu = 1/2$ and $\gamma = 1$. From [69].

Chapter 4

Gauge integration

At $\beta > 0$, the plaquette terms in a non-Abelian gauge theory do not allow for a direct dual-ization since the integrals over gauge links are all coupled together and no longer factorize as in the strong coupling limit. A one-step evaluation of the integrals is not possible, and even if so the resulting partition function would be a non-local function of the dual vari-ables, hence not suited for Monte Carlo simulations. The solution to this problem requires the introduction of *auxiliary* variables, which allow to write down the result of gauge inte-gration, at fixed value of the dual variables, as a sum over local weights, i.e. as a sum of products of scalar quantities distributed over lattice sites, links and plaquettes. The auxil-iary variables can be then promoted to degrees of freedom and evaluated stochastically. The introduction of auxiliary variables can be however problematic: local weights carrying neg-ative signs can represent an additional source for the sign problem which strongly depends on the specific way they are introduced. In the past years, two main strategies have been put forward: in [70, 71, 72] starting from a character expansion of the plaquette action it was possible to dualize two colors QCD using a *spin-foam* representation of the partition func-tion where the role of auxiliary variables is played by the intertwiner labels. Simulations in pure $SU(2)$ Yang-Mills theory, on small to moderate four-dimensional volumes were car-ried out, but the appearance of a sign problem starting at about $\beta \approx 1.8$ prevented them from reaching the weak coupling branch $\beta \to \infty$. In [73, 74] instead, the authors introduced the concept of Abelian color cycles (ACC), i.e. loops of color indices around the plaquettes which are then treated as dynamical degrees of freedom. Basically, at fixed values of the ACC, the dual partition function resembles the one of an Abelian model, and the full parti-tion function can be thought as a collection of Abelian-like systems. However, a severe sign problem was present, and this approach was not further developed.[1] Here we investigate a novel strategy: starting from the Taylor expansion of the plaquette action, we introduce a set of auxiliary variables which we called *decoupling operator indices* (DOI). The DOI arise from our solution of the $SU(N)$ polynomial one-link integral and its decomposition in terms of

---

[1]Although the ACC dualization solved the sign problem of the $SU(2)$ principal chiral model at finite den-sity [75].

decoupling operators. This chapter is concerned with the formal derivation of these results, while their application to the dualization of full QCD will be presented in Ch. 5.

4.1 Beyond strong coupling: the polynomial one-link integral

Including the Wilson plaquette action, the full partition function Eq. (2.87) for one flavor of staggered quarks can be expanded as

$$
\mathcal{Z}(\beta, \hat{m}_q) = \sum_{\substack{\{n_p, \bar{n}_p\} \\ \{d_\ell, \bar{d}_\ell, m_n\}}} \prod_p \frac{\tilde{\beta}^{n_p + \bar{n}_p}}{n_p! \bar{n}_p!} \prod_\ell \frac{1}{d_\ell! \bar{d}_\ell!} \prod_n \frac{(2\hat{m}_q)^{m_n}}{m_n!} \int d\bar{\chi}(n) d\chi(n) \, (\bar{\chi}(n)\chi(n))^{m_n} \, \mathcal{G}_{n_p, \bar{n}_p, d_\ell, \bar{d}_\ell} \, ,
$$

$$(4.1)$$

$$
\mathcal{G}_{n_p, \bar{n}_p, d_\ell, \bar{d}_\ell} = \prod_\ell \int \mathcal{D}U_\ell \operatorname{Tr}[U_\ell \mathcal{M}_\ell^\dagger]^{d_\ell} \operatorname{Tr}[U_\ell^\dagger \mathcal{M}_\ell]^{\bar{d}_\ell} \prod_p \operatorname{Tr}[U_p]^{n_p} \operatorname{Tr}[U_p^\dagger]^{\bar{n}_p} \, , \tag{4.2}
$$

where $\tilde{\beta} \equiv \beta/2N$, and to render the notation more compact we labeled the lattice links with $\ell \equiv (n, \mu)$. The dual variables $\{n_p, \bar{n}_p, d_\ell, \bar{d}_\ell, m_n\}$ are again respectively the plaquette occupation numbers, the hopping expansion coefficients and the monomers. As in the Schwinger model d_ℓ and $\bar{d}_\ell$ are related to dimers and quark fluxes via

$$
k_\ell \equiv \min \{d_\ell, \bar{d}_\ell\} \, , \qquad f_\ell \equiv d_\ell - \bar{d}_\ell \, . \tag{4.3}
$$

We continue keeping the discussion general considering a gauge group $G = \mathrm{U}(N), \mathrm{SU}(N)$. The quantity $\mathcal{G}$ contains the non-local part of the computation, and it is given by a gauge integral over the whole lattice. To obtain a dual representation valid to all order in the β expansion, we split the computation of $\mathcal{G}$ in two parts:

1) The traces appearing in Eq. (4.2) are written explicitly: we do not perform the matrix multiplication, leaving the color indices uncontracted. As a consequence, the gauge integral $\prod_\ell \int \mathcal{D}U_\ell$, becomes a disjoint product of polynomial integrals with open color indices and we integrate out every gauge link independently.

2) After gauge integration, some of the open color indices need to be contracted between links that share a common site such that the plaquette terms are recovered. The remaining indices are contracted with the fermion matrices $M_\ell, M_\ell^\dagger$. We postpone the description of this second step to Ch. 5.

If the matrix multiplications are not performed, the gauge integrals to compute assume the following general form

$$
\mathcal{I}_{ij,kl}^{a,b} \equiv \int_G DU \, U_{i_1}^{j_1} \cdots U_{i_a}^{j_a} U_{k_1}^{\dagger l_1} \cdots U_{k_b}^{\dagger l_b} \, , \tag{4.4}
$$

where the values a, b for a given link ℓ are determined counting the number of forward and backward gauge links U_ℓ and $U_\ell^\dagger$ appearing in the hopping and plaquette terms of Eq. (4.2). We also make use of the multi-index notation

$$
\begin{aligned}
i &= (i_1, i_2, \ldots, i_a), & j &= (j_1, j_2, \ldots, j_a), \\
k &= (k_1, k_2, \ldots, k_b), & l &= (l_1, l_2, \ldots, l_b).
\end{aligned}
\tag{4.5}
$$

Integrals over the invariant Haar measure were studied extensively in the past decades [76, 77, 78, 79, 80, 58, 81, 82, 83, 84, 85, 86, 87, 88]. Although a closed expression for polynomial integrals of the form Eq. (4.4) was available for $G =$ U(N), the solution for SU(N) was unknown. We filled this gap obtaining a closed expression for the most general case.

4.1.1 Solution of the polynomial one-link integral

The integral Eq. (4.4) can be obtained from the generating functional

$$
Z^{a,b}[K, J] = \int_G \mathcal{D}U \, \text{Tr}[UK]^a \, \text{Tr}[U^\dagger J]^b,
\tag{4.6}
$$

by taking successive derivatives with respect to the sources $J, K \in GL(N, \mathbb{C})$, according to the following equation:

$$
\mathcal{I}_{ij,kl}^{a,b} = \frac{1}{a!b!} \frac{\partial^{(a+b)} Z^{a,b}[K, J]}{\partial K_{j_1}^{i_1} \cdots \partial K_{j_a}^{i_a} \partial J_{\ell_1}^{k_1} \cdots \partial J_{\ell_b}^{k_b}} \bigg|_{J=K=0}.
\tag{4.7}
$$

The explicit expression for the Haar measure on G is not important for this computation. The two main properties which we make use of are:

1) *Orthogonality of characters*: given two irreducible representations[2] $R_r(U)$ and $R_s(U)$ of the group G and their irreducible characters $\hat{\chi}_{r,s}(U) \equiv \text{Tr} \, R_{r,s}(U)$

$$
\int_G \mathcal{D}U \, \hat{\chi}_s(UV) \hat{\chi}_r(U^\dagger W) = \frac{\delta_{r,s}}{D_{r,N}} \hat{\chi}_r(VW) \quad \forall \, V, W \in G,
\tag{4.8}
$$

where $D_{r,N}$ is the dimension of the matrices $R_r(U)$.

2) *Center group invariance condition*: if $c\mathbb{1} \in G$ with $c \in \mathbb{C}$ then for all monomial functions $f(U)$

$$
\int_G \mathcal{D}U \, f(U) \neq 0 \implies f(U) = f(cU).
\tag{4.9}
$$

---

[2]A group representation is an homomorphism $R \to \rho(U)$ between the group G and the general linear group $GL(n, V)$ over a field V. In our case $V = \mathbb{C}$, i.e. $R(U)$ is an invertible $n \times n$ complex matrix. A group representation is then said to be irreducible if it cannot be written as a direct sum of other representations.

In the case of the generating functional this property implies

$$
Z^{a,b}\,[K,J] \neq 0 \implies
\begin{cases}
a = b & \mathrm{U}(N) \\
a - b \bmod N = 0 & \mathrm{SU}(N)
\end{cases}
\tag{4.10}
$$

Given Eq. (4.10) we set without loss of generality $a = qN + p$, $b = p$ with $p, q \in \mathbb{N}^+$ and $q = 0$ if $G = \mathrm{U}(N)$. The generating functional is now a function of q and p, and we define $\tilde{Z}^{q,p}\,[K,J] \equiv Z^{qN+p,p}\,[K,J]$. To evaluate it, we first convert the integral in Eq. (4.6) for $G = \mathrm{SU}(N)$ into an $\mathrm{U}(N)$ integral, using

$$
\frac{1}{\det K^q} \int_{\mathrm{SU}(N)} DU \mathrm{Tr}[UK]^{qN+p}\,\mathrm{Tr}[U^\dagger J]^p = \int_{\mathrm{U}(N)} DU \frac{1}{\det[UK]^q} \mathrm{Tr}[UK]^{qN+p}\,\mathrm{Tr}[U^\dagger J]^p, \quad (4.11)
$$

and assuming for the moment $J, K \in \mathrm{U}(N)$. The equality holds because the last integrand is invariant under multiplication of the U matrix by a complex phase. As a consequence, it gives the same result when integrated using the $\mathrm{SU}(N)$ or the $\mathrm{U}(N)$ Haar measure, and for $\mathrm{SU}(N)\det U = 1$. Exploiting this trick, we can make use of the $\mathrm{U}(N)$ character expansion to compute the quantity in the r.h.s. Before doing this we list some of the properties of the irreducible representations (irreps) of the $\mathrm{U}(N)$ group[3] highlighting the connections with the symmetric group S_n:

1) Every irrep of $\mathrm{U}(N)$ is indexed by a N-tuple of integers $\{\lambda_1 \geq \lambda_2 \geq ... \geq \lambda_N\}$ ($\lambda_N \geq 0$ or < 0)). We will denote with R_λ the irrep associated to $\{\lambda_1 \geq \lambda_2 \geq ... \geq \lambda_N\}$. If $\lambda_N \geq 0$ the irrep is called *polynomial*, thus polynomial irreps can be associated to integer partitions $\lambda \vdash n$ with $n = \sum_{i=1}^{N} \lambda_i$ (see Fig. 4.1).

2) For $\mathrm{U}(N)$ it exists a one-dimensional irrep called determinantal representation $R_{\det}$

$$
R_{\det} : U \to \det[U]
\tag{4.12}
$$

and its "inverse" $\overline{R}_{\det} : U \to \det[U^\dagger]$. Every irrep of $\mathrm{U}(N)$ can be obtained as the tensor product of a polynomial irrep with powers of $\overline{R}_{\det}$ since the following holds true:

$$
R_\lambda \otimes (\overline{R}_{det})^{\otimes n} \cong R_{\lambda-n} \implies \chi_\lambda(U)\det[U]^{-n} = \chi_{\lambda-n}(U),
\tag{4.13}
$$

$$
R_\lambda \otimes (R_{det})^{\otimes n} \cong R_{\lambda+n} \implies \chi_\lambda(U)\det[U]^{n} = \chi_{\lambda+n}(U),
\tag{4.14}
$$

where $\lambda \pm n \equiv \{\lambda_1 \pm n, ..., \lambda_N \pm n\}$.

---

[3]Further details and references can be found e.g. in [77].

$$\lambda \vdash 9 = (4, 2, 2, 1)$$

$$\text{len}(\lambda) = 4 \left\{ \begin{array}{l} \\ \\ \\ \\ \end{array} \right. \quad \begin{array}{l} \lambda_1 = 4 \\ \lambda_2 = 2 \\ \lambda_3 = 2 \\ \lambda_4 = 1 \end{array}$$

FIGURE 4.1: Graphical representation of a partition $\lambda \vdash 9$. The length of the partition $\text{len}(\lambda)$ is the number of rows.

3) The symmetric group S_n is the group of permutation of n objects. Its irreps are in one-to-one correspondence with the integer partitions $\lambda \vdash n$. Its irreducible characters are denoted with $\chi_\lambda(\pi)$, where π is a permutation, and the dimension of a given irrep is denoted with f_λ. As for any irreducible character, its value only depends on the conjugacy class of the group element g since $\text{Tr}\, R(g) = \text{Tr}\, R(g'gg'^{-1})$. In the case of the symmetric group, its conjugacy classes are also in one-to-one correspondence with partitions $\rho \vdash n$, therefore we define $\chi_\lambda^\rho \equiv \chi_\lambda(\pi)$ where π is any permutation in the conjugacy class ρ, and we denote by h_ρ the total number of permutations within this class.

4) The irreducible characters $\hat{\chi}_\lambda(U)$ of the polynomial irreps can be expanded in traces of powers of U (Frobenius relation)

$$\hat{\chi}_{\lambda \vdash n}(U) = \frac{1}{n!} \sum_{\rho \vdash n} h_\rho \, \chi_\lambda^\rho \, t_\rho(U), \qquad t_\rho(U) = \prod_{i=1}^{N} \text{tr}[U^{\rho_i}]. \tag{4.15}$$

where the sum is over all partitions $\rho \vdash n$. Similarly, powers of traces of U can be expanded in irreducible characters of the polynomial irreps

$$\text{Tr}[U]^n = \sum_{\substack{\lambda \vdash n \\ \text{len}(\lambda) \le N}} f_\lambda \, \hat{\chi}_\lambda(U), \tag{4.16}$$

where $\text{len}(\lambda)$ is the *partition length*, i.e. the number of non-zero rows in λ.

Making use of these results an explicit expression for the generating functional is readily obtained. We first expand in characters the traces in the r.h.s. of Eq. (4.11) using Eq. (4.16), then we use the relations Eqs. (4.13) and (4.14), and finally the orthogonality of characters

Eq. (4.8) and the Frobenius relation

$$
\begin{aligned}
\frac{\tilde{Z}^{q,p}[K,J]}{\det[K]^q} &= \int_{U(N)} \mathcal{D}U \, \frac{1}{\det[UK]^q} \, \mathrm{Tr}[UK]^{qN+p} \, \mathrm{Tr}[U^\dagger J]^p \\
&= \int_{U(N)} \mathcal{D}U \sum_{\substack{\lambda \vdash qN+p \\ \mathrm{len}(\lambda) \le N}} f_\lambda \, \hat{\chi}_{\lambda-q}(UK) \sum_{\substack{\lambda' \vdash p \\ \mathrm{len}(\lambda') \le N}} f_{\lambda'} \, \hat{\chi}_{\lambda'}(U^\dagger J) \\
&= \sum_{\substack{\lambda \vdash p \\ \mathrm{len}(\lambda) \le N}} f_{\lambda+q} f_\lambda \, \frac{\hat{\chi}_\lambda(JK)}{D_{\lambda,N}} = \frac{(qN+p)!}{p!} \prod_{i=0}^{N-1} \frac{i!}{(i+q)!} \sum_{\substack{\lambda \vdash p \\ \mathrm{len}(\lambda) \le N}} \frac{(f_\lambda)^2}{D_{\lambda,N+q}} \hat{\chi}_\lambda(JK) \\
&= \frac{(qN+p)!}{p!^2} \prod_{i=0}^{N-1} \frac{i!}{(i+q)!} \sum_{\substack{\lambda \vdash p \\ \mathrm{len}(\lambda) \le N}} \frac{(f_\lambda)^2}{D_{\lambda,N+q}} \sum_{\rho \vdash p} h_\rho \, \hat{\chi}^\lambda(\rho) \, t_\rho(JK) \\
&= (qN+p)! \prod_{i=0}^{N-1} \frac{i!}{(i+q)!} \sum_{\rho \vdash p} h_\rho \, \tilde{\mathrm{Wg}}_N^{q,p}(\rho) \, t_\rho(JK) \,.
\end{aligned}
\tag{4.17}
$$

The fourth equality follows from the combinatorial identity

$$
\frac{f_{\lambda+q}}{D_{\lambda,N}} = \frac{(qN+p)!}{p!} \prod_{i=0}^{N-1} \left[\frac{i!}{(i+q)!} \right] \frac{f_\lambda}{D_{\lambda,N+q}} \,,
\tag{4.18}
$$

valid for $\mathrm{len}(\lambda) \le N$, and which will be demonstrated in App. A. The last line is just a rearrangement of terms. We called the functions $\tilde{\mathrm{Wg}}_N^{q,p}$ *generalized Weingarten functions*

$$
\tilde{\mathrm{Wg}}_N^{q,p}(\rho) = \frac{1}{(p!)^2} \sum_{\substack{\lambda \vdash p \\ \mathrm{len}(\lambda) \le N}} \frac{(f_\lambda)^2}{D_{\lambda,N+q}} \chi_\lambda^\rho \,.
\tag{4.19}
$$

They are class functions of the symmetric group and therefore only depend on the conjugacy class of a given permutation. In the limiting case $q = 0$ one recovers the ordinary Weingarten functions introduced in [76]. The properties of the generalized Weingarten functions will be discussed in the next section. Summing up, the $SU(N)$ generating functional is

$$
\boxed{\tilde{Z}^{q,p}[K,J] = (qN+p)! \prod_{i=0}^{N-1} \frac{i!}{(i+q)!} \, \det[K]^q \sum_{\rho \vdash p} h_\rho \, \tilde{\mathrm{Wg}}_N^{q,p}(\rho) t_\rho(JK) \,,}
\tag{4.20}
$$

and given the polynomial nature of the expression, it can be extended to any $K, J \in GL(N, \mathbb{C})$. In the limits $q = 0$, $q = 1$, and $p = 0$ the known results [77, 88] are recovered. Given the expression Eq. (4.20), the polynomial one-link integral Eq. (4.4) is obtained by taking derivatives with respect to the sources K, J, setting them to zero at the end of the calculation. This may seem like hard task; luckily we do not need to do this explicitly. Indeed, it is sufficient to know the result in the cases $p = 0$ and $q = 0$ and then make use of the Leibiniz formula for the derivative of a product. The two special cases $p = 0$, $q = 0$ have already been solved

respectively by Creutz [78] and Collins [83, 84], and the result is

$$\mathcal{I}^{qN,0}_{ij,kl} = \frac{1}{(qN)!} \frac{\partial^{(qN)} \tilde{Z}^{q,0}[K]}{\partial K_{j_1,i_1} \cdots \partial K_{j_{qN},i_{qN}}} \Bigg|_{J=K=0} = \left[\prod_{r=1}^{N-1} \frac{r!}{(r+q)!} \right] \sum_{\{\alpha\}} \epsilon^{\otimes q}_{i_{\{\alpha\}}} \, \epsilon^{\otimes q, j_{\{\alpha\}}}, \tag{4.21}$$

$$\mathcal{I}^{p,p}_{ij,kl} = \frac{1}{p!^2} \frac{\partial^{(2p)} \tilde{Z}^{0,p}[K,J]}{\partial K_{j_1,i_1} \partial J_{l_1,k_1} \cdots \partial K_{j_p,i_p} \partial J_{l_p,k_p}} \Bigg|_{J=K=0} = \sum_{\pi,\sigma \in S_p} \delta^{l_\pi}_i \, \tilde{\mathrm{Wg}}^{0,p}_N(\pi \circ \sigma^{-1}) \delta^j_{k_\sigma}. \tag{4.22}$$

The integral $\mathcal{I}^{qN,0}$ is written as a sum of $q-$fold epsilon tensors, with

$$\epsilon^{\otimes q}_{i_{\{\alpha\}}} \equiv \epsilon_{i_{\alpha_1},\dots,i_{\alpha_N}} \, \epsilon_{i_{\alpha_{N+1}},\dots,\alpha_{2N}} \cdots \epsilon_{i_{\alpha_{(q-1)N+1}},\dots,i_{\alpha_{qN}}}. \tag{4.23}$$

The sum is over all possible ways of partitioning the qN indices i and j, into the q different epsilon tensors, and partitions that can be obtained from one another by permuting the epsilon tensors are considered equivalent. We labeled them with $\{\alpha\}$. The genuine $U(N)$ integral $\mathcal{I}^{p,p}$ is instead written as a double sum over permutations $\pi, \sigma \in S_p$. Every element of the sum is a product of two Kronecker delta functions with permuted indices

$$\delta^{l_\pi}_i \equiv \delta^{l_{\pi(1)}}_{i_1} \cdots \delta^{l_{\pi(p)}}_{i_p}, \qquad \delta^j_{k_\sigma} \equiv \delta^{j_1}_{k_{\sigma(1)}} \cdots \delta^{j_p}_{k_{\sigma(p)}}, \tag{4.24}$$

weighted by the Weingarten function $\tilde{\mathrm{Wg}}^{0,p}_N(\pi \circ \sigma^{-1})$. To get the general $\mathcal{I}$-integral it is sufficient to exploit the fact that the generating functional (4.20) can be decomposed, apart from a trivial combinatorial factor, as a product of $\tilde{Z}^{q,0}$ and a term that resembles the generating functional $Z^{0,p}$. The only difference is in the coefficients $\tilde{\mathrm{Wg}}^{0,p}_N$ that must be substituted with $\tilde{\mathrm{Wg}}^{q,p}_N$. Therefore, by looking at Eq. (4.7), when qN derivatives w.r.t. K act on $\det[K]^q$, they reproduce $I^{qN,0}$. Similarly, when p derivatives w.r.t. K and p derivatives w.r.t. J act on the second term, they reproduce $I^{p,p}$ with the substitution $\tilde{\mathrm{Wg}}^{0,p}_N \to \tilde{\mathrm{Wg}}^{q,p}_N$. Any other combination of derivatives gives zero. Making use of the Leibniz formula, we can thus write down the expression of the $\mathcal{I}$-integral as

$$\boxed{\mathcal{I}^{qN+p,p}_{ij,kl} = \left[\prod_{r=1}^{N-1} \frac{r!}{(r+q)!} \right] \sum_{\{\alpha,\beta\}} \sum_{\pi,\sigma \in S_p} \epsilon^{\otimes q}_{i_{\{\alpha\}}} \delta^{l_\pi}_{i_{\{\beta\}}} \tilde{\mathrm{Wg}}^{q,p}_N(\pi \circ \sigma^{-1}) \, \epsilon^{\otimes q, j_{\{\alpha\}}} \delta^{j_{\{\beta\}}}_{k_\sigma}.} \tag{4.25}$$

The leftmost sum now runs over all the ways (α, β) of partitioning the i and j indices into the Kronecker deltas and into the q epsilon tensors. This "multiplicity" stems from the fact that we need to take into account every possible way of acting with the K derivatives on the determinant and on the traces $\mathrm{tr}_\rho(JK)$, and from the previous result for $\mathcal{I}^{qN,0}$ in Eq. (4.21). This result was obtained independently by us [89] and by Borisenko et al. [90]. For the

SU(N) integral $\mathcal{I}^{N+1,1}$, one for instance gets

$$\mathcal{I}^{N+1,1}_{ij,kl} = \frac{1}{N!} \tilde{\text{Wg}}_N^{1,1}(\mathbb{1}) \sum_{a=1}^{N+1} \epsilon_{i_1...i_{a-1}i_{a+1}...i_{N+1}} \epsilon^{j_1...j_{a-1}j_{a+1}...j_{N+1}} \delta^{l_1}_{i_a} \delta^{j_a}_{k_1} \tag{4.26}$$

$$= \frac{1}{N!(N+1)} \sum_{a=1}^{N+1} \epsilon_{i_1...i_{a-1}i_{a+1}...i_{N+1}} \epsilon^{j_1...j_{a-1}j_{a+1}...j_{N+1}} \delta^{l_1}_{i_a} \delta^{j_a}_{k_1}. \tag{4.27}$$

Since $p = 1$ for this integral, the "mesonic" part is trivial (i.e. $\lambda \vdash 1$) while there are $N+1$ partitions (α, β) depending on the values i_a, j_a that enter the delta functions.

4.1.2 Properties of the Weingarten functions

The computation of the Weingarten functions can be automatized evaluating their character expansion

$$\tilde{\text{Wg}}_N^{q,p}(\rho) = \frac{1}{(p!)^2} \sum_{\substack{\lambda \vdash p \\ \text{len}(\lambda) \leq N}} \frac{(f_\lambda)^2}{D_{\lambda,N+q}} \chi^\rho_\lambda. \tag{4.28}$$

The partitions $\lambda \vdash p$ can be efficiently generated with simple algorithms [91], while the symmetric group characters χ^ρ_λ are computed recursively implementing the Murnaghan–Nakayama rule [92, 93, 94]. The dimensions $f_\lambda, D_{\lambda,N}$ of the irreps of S_p and U(N), are instead computed via

$$f_\lambda = \frac{p!}{\prod_{(i,j)\in\lambda} h_\lambda(i,j)}, \qquad D_{\lambda,N} = \frac{\prod_{(i,j)\in\lambda}(N+i-j)}{\prod_{(i,j)\in\lambda} h_\lambda(i,j)}, \tag{4.29}$$

where the product $\prod_{(i,j)\in\lambda}$ runs over all boxes of λ with coordinates (i,j), and $h_\lambda(i,j)$ is the *hook* of the box (i,j), i.e. the number of boxes having coordinates (i',j') with $i' = i, j' \geq j$ or $j = j', i' \geq i$. For the symmetric group S_3, the complete list of generalized Weingarten functions is

$$\tilde{\text{Wg}}_N^{q,3}(\{1,1,1\}) = \begin{cases} \frac{(N+q)^2-2}{(N+q)((N+q)^2-1)((N+q)^2-4)} & N \geq 3 \\ \frac{5q+17}{6(q+2)(q+4)((q+2)^2-1)} & N = 2 \end{cases} \tag{4.30}$$

$$\tilde{\text{Wg}}_N^{q,3}(\{2,1\}) = \begin{cases} -\frac{1}{((N+q)^2-1)((N+q)^2-4)} & N \geq 3 \\ \frac{1}{6(q+2)(q+3)(q+4)} & N = 2 \end{cases} \tag{4.31}$$

$$\tilde{\text{Wg}}_N^{q,3}(\{3\}) = \begin{cases} \frac{2}{(N+q)((N+q)^2-1)((N+q)^2-4)} & N \geq 3 \\ -\frac{q+7}{6(q+2)(q+4)((q+2)^2-1)} & N = 2 \end{cases} \tag{4.32}$$

For $N \geq p$ the functions $\tilde{W}g$ are rational functions of $N + q$. Notice that the restriction on the partition length ($\mathrm{len}(\lambda) \leq N$) always prevents the appearance of poles (due to the zeros of $D_{\lambda,N}$), and the Weingarten functions are always finite. A complete list for S_4 will be given in App. B. As can be seen already in the case of S_3, the $\tilde{W}g$ are not always positive. In particular one can show that for $N \geq p$

$$\mathrm{sgn}\left[\tilde{W}g_N^{q,p}(\lambda)\right] \stackrel{N \geq p}{=} \prod_{i=1}^{\mathrm{len}(\lambda)} (-1)^{\lambda_i + 1}. \tag{4.33}$$

These sign oscillations make the representation of the $\mathcal{I}-$integral in Eq. (4.25) not particularly useful. Having in mind the dualization of the full theory, one can think of using as auxiliary variables the permutations π, σ and the partitions (α, β). Then one proceed to the contraction of the color indices considering single terms in the sum in Eq. (4.25). Since the sum over the auxiliary variables must be then sampled via Monte Carlo, the negative signs from the Weingarten functions would completely hinder this approach. A possible way out to this problem requires a reparameterization of the integrals. This will be done introducing the decoupling operators.

4.2 The decoupling operators and the DOI

4.2.1 The irreducible matrix elements

To find a different parameterization of the $\mathcal{I}$-integral we start to make explicit the definition of the irreducible characters of the symmetric group

$$\chi_\lambda(\pi) \equiv \mathrm{Tr}\, M_\lambda(\pi) \implies \chi_\lambda(\pi \circ \sigma^{-1}) = \sum_{a,b=1}^{f_\lambda} \left(M_\lambda(\pi)\right)_{a,b} \left(M_\lambda(\sigma^{-1})\right)_{b,a}. \tag{4.34}$$

The choice of the matrix representation M_λ is not unique since the traces are invariant under conjugation

$$M_\lambda(\pi) \to S\, M_\lambda(\pi)\, S^{-1}, \qquad \forall\, \pi \in S_n, \; S \in GL(f_\lambda, \mathbb{C}). \tag{4.35}$$

Two popular basis choices are the so-called Young's orthogonal form and the natural representation [95]. In these two basis the matrices M_λ satisfy the properties

$$(\text{Orthogonal basis}) \qquad M_\lambda(\pi)^{-1} = (M_\lambda(\pi))^T, \quad (M_\lambda(\pi))_{a,b} \in \mathbb{R}, \tag{4.36}$$

$$(\text{Natural basis}) \qquad (M_\lambda(\pi))_{a,b} \in \mathbb{Z}. \tag{4.37}$$

FIGURE 4.2: The five standard Young tableaux associated to the partition $\lambda \vdash 5 = \{2, 2, 1\}$. The SYT are canonically ordered, from left to right, according to the value of their Yamanouchi symbols.

The computation of the matrix elements in both basis have been automatized. In the case of the orthogonal basis, to compute $M_\lambda(\pi)$, we first decompose π as a product of adjacent transpositions via

$$\pi = \tau^{k_1} \circ \tau^{k_2} \circ \ldots \circ \tau^{k_r}, \qquad \tau^k \equiv (k, k+1), \tag{4.38}$$

so that τ^k only swaps the consecutive numbers k and $k+1$. The matrices $M_\lambda(\tau^k)$ can be then obtained associating to each row (a) and column (b) of the matrices M_λ a *standard Young tableaux* (SYT) T_a, i.e. a filling of the partition $\lambda \vdash n$ with the positive integers $\{1, \ldots, n\}$ such that in every row and column the numbers are in ascending order when reading them respectively from left to right and from top to bottom. An illustrative example of SYT is provided in Fig. 4.2. The number of SYT of a given *shape* $\lambda \vdash n$ is exactly f_λ, therefore every row and column can be uniquely associated to a SYT. To do so, we define an ordering between the tableaux of the same shape via the *Yamanouchi symbols $M(T)$*

$$M(T) \equiv \{m_1, \ldots, m_n\}, \tag{4.39}$$

where m_i is the row of T containing the number i. One can then impose lexicographic ordering on the Yamanouchi symbols M so that

$$T_{a_1} \leq T_{a_2} \Leftrightarrow M(T_{a_1}) \leq M(T_{a_2}). \tag{4.40}$$

Having defined an ordering, we associate the row and column a of M_λ to T_a. The matrix $M_\lambda(\tau^k)$ is obtained in terms of the *axial distance $L_a(k, k+1)$* between the numbers k and $k+1$ in T_a

$$L_a(k, k+1) \equiv (x_{k+1} - x_k) - (y_{k+1} - y_k), \tag{4.41}$$

where (x_k, y_k) are the coordinates of the number k in $\mathcal{T}_a$. The final formula is

$$\left(M_\lambda(\tau^k)\right)_{a,b} = \frac{1}{L_a(k,k+1)}\delta_{a,b} + \sqrt{1 - \left(\frac{1}{L_a(k,k+1)}\right)^2}\,\delta_{T_b,T_a^k}\,, \qquad (4.42)$$

where T_a^k is the possibly nonstandard Young tableaux obtained swapping k and $k+1$ in T_a. Notice that the matrices $M_\lambda(\tau^k)$ are orthogonal since the square sum of the matrix elements on a given row is clearly 1 if T_a^k is a SYT, and a nonstandard Young Tableaux can only be obtained if k and $k+1$ appear consecutively in a given row or column. In this case however $L_a(k,k+1) = \pm 1$. For instance, the matrix associated to the adjacent transpositions τ^1, τ^2 of S_5 in the irrep λ corresponding to the partition in Fig. 4.2 are

$$M_\lambda(\tau^1) = \begin{pmatrix} 1 & 0 & 0 & 0 & 0 \\ 0 & 1 & 0 & 0 & 0 \\ 0 & 0 & -1 & 0 & 0 \\ 0 & 0 & 0 & -1 & 0 \\ 0 & 0 & 0 & 0 & -1 \end{pmatrix}, \qquad M_\lambda(\tau^2) = \begin{pmatrix} -\frac{1}{2} & 0 & \frac{\sqrt{3}}{2} & 0 & 0 \\ 0 & -\frac{1}{2} & 0 & \frac{\sqrt{3}}{2} & 0 \\ \frac{\sqrt{3}}{2} & 0 & \frac{1}{2} & 0 & 0 \\ 0 & \frac{\sqrt{3}}{2} & 0 & \frac{1}{2} & 0 \\ 0 & 0 & 0 & 0 & -1 \end{pmatrix}. \qquad (4.43)$$

Swapping 1 and 2 in the SYT in Fig. 4.2 always produce a nonstandard Young tableaux, hence $M_\lambda(\tau^1)$ is a diagonal matrix.

In the case of the natural representation the description is a bit more involved and requires the introduction of a number of concepts which are not particularly relevant for the discussion. Hence we refer to [96] for definitions and basic properties of the matrix elements in this basis, and to [95] where the relation between the orthogonal and the natural representation is discussed, and a method to obtain the matrix elements from one another is presented. Before ending this subsection we want to highlight one important property of the matrix elements in the orthogonal represention. It is the so-called *great orthogonality theorem* [97], which states a very general orthogonality relation between the matrix elements of the irreps, and that in the case of the symmetric group reads

$$\frac{1}{n!}\sum_{\pi \in S_n} (M_\lambda(\pi))_{a,b}\,(M_{\lambda'}(\pi)))_{c,d} = \frac{1}{f_\lambda}\delta_{\lambda,\lambda'}\,\delta_{a,c}\,\delta_{b,d}\,. \qquad (4.44)$$

This theorem will play an important role in the following chapter to prove some of the properties of the Boltzmann weights in the dual representation.

4.2.2 Final form of the polynomial $1-$link integral

Making use of the the irreducible matrix elements, the Weingarten functions can be cast in the following form

$$\tilde{\mathrm{Wg}}_N^{q,p}(\pi \circ \sigma^{-1}) = \sum_{\substack{\lambda \vdash p \\ \mathrm{len}(\lambda) \leq N}} \frac{1}{(p!)^2} \frac{f_\lambda^2}{D_{\lambda,N+q}} \chi_\lambda(\pi \circ \sigma^{-1}) \tag{4.45}$$

$$= \sum_{\lambda_{a,b}} \left(\frac{1}{p!} \frac{f_\lambda}{\sqrt{D_{\lambda,N+q}}} M_{\lambda;ab}(\pi) \right) \left(\frac{1}{p!} \frac{f_\lambda}{\sqrt{D_{\lambda,N+q}}} M_{\lambda;ab}(\sigma) \right), \tag{4.46}$$

$$\sum_{\lambda_{ab}} \equiv \sum_{\substack{\lambda \vdash p \\ \mathrm{len}(\lambda) \leq N}} \sum_{a,b=1}^{f_\lambda}, \qquad M_{\lambda;ab}(\pi) \equiv \left(M_\lambda(\pi) \right)_{a,b}, \tag{4.47}$$

and we made use of the orthogonal basis for which $M_{\lambda;ba}(\sigma^{-1}) = M_{\lambda;ab}(\sigma)$. Substituting this expression into Eq. (4.25), we obtain

$$\mathcal{I}_{i\,j,k}^{qN+p,p}{}_l \propto \sum_{\{\alpha,\beta\}} \sum_{\lambda_{a,b}} \left(\sum_{\pi \in S_p} \frac{f_\lambda/p!}{\sqrt{D_{\lambda,N+q}}} M_{\lambda;ab}(\pi) \epsilon_{i_{\{\alpha\}}}^{\otimes q} \delta_{i_{\{\beta\}}}^{\ell_\pi} \right) \left(\sum_{\sigma \in S_p} \frac{f_\lambda/p!}{\sqrt{D_{\lambda,N+q}}} M_{\lambda;ab}(\sigma) \epsilon^{\otimes q, j_{\{\alpha\}}} \delta_{k_\sigma}^{j_{\{\beta\}}} \right). \tag{4.48}$$

We see that by introducing explicitly the irreducible matrix elements, we can perform a resummation of the permutations π and σ. The quantities in brackets

$$\left(P^{(\alpha,\beta),\lambda_{ab}} \right)_i^l \equiv \sqrt{\prod_{r=1}^{N-1} \frac{r!}{(r+q)!}} \sum_{\pi \in S_p} \frac{f_\lambda/p!}{\sqrt{D_{\lambda,N+q}}} M_{\lambda;ab}(\pi) \epsilon_{i_{\{\alpha\}}}^{\otimes q} \delta_{i_{\{\beta\}}}^{\ell_\pi}, \tag{4.49}$$

$$\left(P^{(\alpha,\beta),\lambda_{ab}} \right)_k^j \equiv \sqrt{\prod_{r=1}^{N-1} \frac{r!}{(r+q)!}} \sum_{\sigma \in S_p} \frac{f_\lambda/p!}{\sqrt{D_{\lambda,N+q}}} M_{\lambda;ab}(\sigma) \epsilon^{\otimes q, j_{\{\alpha\}}} \delta_{k_\sigma}^{j_{\{\beta\}}}, \tag{4.50}$$

are the decoupling operators. They are functions of the partitions (α, β) and of the two SYT T_a, T_b of shape λ, associated to the row a and column b of the matrix representation M_λ. In terms of the multi-index

$$\rho \equiv \{ (\alpha, \beta), (T_a, T_b) \}, \tag{4.51}$$

the $\mathcal{I}-$integral can be written in compact form as

$$\boxed{\mathcal{I}_{i\,j,k}^{qN+p,p}{}_l = \sum_\rho \left(P^\rho \right)_i^l \left(P^\rho \right)_k^j.} \tag{4.52}$$

The reason for calling the operators P^ρ decoupling operators, stems from the fact that at fixed value of ρ the indices $\{i,l\}$ and $\{k,j\}$ are decoupled in the expression of the $\mathcal{I}$-integral. This property is crucial to obtain a dual formulation in terms of local weights, as we will show in the next chapter. The multi-index ρ, which uniquely identifies a given operator P^ρ, is what we called the *decoupling operator index* (DOI), and will correspond to the auxiliary variable which we will use to write down the partition function at finite β. Even if ρ is a multi-index, a one-to-one mapping between $\{(\alpha,\beta),\,(T_a,T_b)\}$ and positive integers can be easily found (see App. C). From now on we will assume this mapping and refer to the ρ as integer variables. Finally, the number of DOI for given values of (q,p) is

$$N_\rho = N_{\text{part.}} \cdot (N_{\text{SYT}})^2 = \frac{(qN+p)!}{q!N!^q p!} \cdot \sum_{\substack{\lambda \vdash p \\ \text{len}(\lambda) \leq N}} f_\lambda^2. \tag{4.53}$$

4.2.3   Recovering the strong coupling one-link integral

The result for $\mathcal{I}_G[\mathcal{M}, \mathcal{M}^\dagger]$ in Eq. (3.43) can be obtained using the generating functional $\tilde{Z}^{q,p}$ or the formalism of the decoupling operators. As an application of this formalism we will use the P^ρ . The idea is to expand as usual the integrand in a Taylor series, retaining only the orders that are compatible with the nilpotency of the fermionic matrices Eq. (3.40) and with the gauge constraint Eq. (4.10)

$$\mathcal{I}_G[\mathcal{M}_{n,\mu}, \mathcal{M}_{n,\mu}^\dagger] = \int_G \mathcal{D}U \exp\left(\text{Tr}\,[\mathcal{M}_{n,\mu}^\dagger U] + \text{Tr}\,[\mathcal{M}_{n,\mu} U^\dagger] \right) \tag{4.54}$$

$$= \sum_{\kappa=1}^{N} \frac{1}{\kappa!^2} \int_G \mathcal{D}U \, \text{Tr}[\mathcal{M}_{n,\mu}^\dagger U]^\kappa \text{Tr}[\mathcal{M}_{n,\mu} U^\dagger]^\kappa$$

$$+ \frac{z}{N!} \int_G \mathcal{D}U \left(\text{Tr}[\mathcal{M}_{n,\mu}^\dagger U]^N + \text{Tr}[\mathcal{M}_{n,\mu} U^\dagger]^N \right), \tag{4.55}$$

where again $z=1$ for $\text{SU}(N)$ and $z=0$ for $\text{U}(N)$ because of the gauge constraint. The result for $\mathcal{I}_G$ can be then obtained integrating term by term the r.h.s. of the previous equation. The last two terms are

$$\int_{\text{SU}(N)} \mathcal{D}U \, \text{Tr}[\mathcal{M}_{n,\mu}^\dagger U]^N = (-1)^N \alpha_{n,\mu} \sum_\rho \left(P^\rho\right)_i \left(P^\rho\right)^j \bar{\chi}_i(n)\,\chi_j(n+\hat{\mu})\,, \tag{4.56}$$

$$\int_{\text{SU}(N)} \mathcal{D}U \, \text{Tr}[\mathcal{M}_{n,\mu} U^\dagger]^N = \alpha_{n,\mu}^{-1} \sum_\rho \left(P^\rho\right)^l \left(P^\rho\right)_k \chi_l(n)\,\bar{\chi}_k(n+\hat{\mu})\,, \tag{4.57}$$

and the operators P^ρ carry only one type of color indices, since in Eqs. (4.56) and (4.57) only gauge links in one direction are present. We also used the shorthand notation

$$\chi_i(n) = \chi_{i_1}(n)\chi_{i_2}(n)\ldots\chi_{i_N}(n)\,, \qquad \bar{\chi}_j(n) \equiv \bar{\chi}_{j_1}(n)\bar{\chi}_{j_2}(n)\ldots\bar{\chi}_{j_N}(n)\,. \tag{4.58}$$

These integrals are somewhat trivial since there is only one DOI ρ which corresponds to the epsilon tensor

$$(P^\rho)_i = \frac{1}{\sqrt{N!}} \, \epsilon_{i_1 \dots i_N} \, , \qquad (P^\rho)^j = \frac{1}{\sqrt{N!}} \, \epsilon^{j_1 \dots j_N} \, , \tag{4.59}$$

$$(P^\rho)_k = \frac{1}{\sqrt{N!}} \, \epsilon_{k_1 \dots k_N} \, , \qquad (P^\rho)^l = \frac{1}{\sqrt{N!}} \, \epsilon^{l_1 \dots l_N} \, ; \tag{4.60}$$

hence we immediately obtain

$$\int_G \mathcal{D}U \frac{z}{N!} \left(\mathrm{Tr}[\mathcal{M}_{n,\mu}^\dagger U]^N + \mathrm{Tr}[\mathcal{M}_{n,\mu} U^\dagger]^N \right) = z \left((-1)^N \alpha_{n,\mu} \bar{B}_n B_{n+\hat{\mu}} + \alpha_{n,\mu}^{-1} \bar{B}_{n+\hat{\mu}} B_n \right) \, , \tag{4.61}$$

$$B_n \equiv \frac{1}{N!} \epsilon_{i_1, \dots, i_N} \chi_{i_1}(n) \dots \chi_{i_N}(n) \, , \quad \bar{B}_n \equiv \frac{1}{N!} \epsilon_{i_1, \dots, i_N} \bar{\chi}_{i_1}(n) \dots \bar{\chi}_{i_N}(n) \, , \tag{4.62}$$

as in Eq. (3.43). Concerning the first term, the expression in terms of the decoupling operators is

$$\int_G \mathcal{D}U \frac{1}{\kappa!^2} \mathrm{Tr}[\mathcal{M}_{n,\mu}^\dagger U]^\kappa \mathrm{Tr}[\mathcal{M}_{n,\mu} U^\dagger]^\kappa = \sum_\rho \left(P^\rho \right)_i^l \left(P^\rho \right)_k^j \, \bar{\chi}_i(n) \chi_l(n) \, \bar{\chi}_k(n+\hat{\mu}) \chi_j(n+\hat{\mu}) \, . \tag{4.63}$$

where

$$\bar{\chi}_i(n) \chi_l(n) \equiv \bar{\chi}_{i_1}(n) \chi_{l_1}(n) \dots \bar{\chi}_{i_\kappa}(n) \chi_{l_\kappa}(n) \, , \tag{4.64}$$

and similarly for $\bar{\chi}_k(n+\hat{\mu}) \chi_j(n+\hat{\mu})$. In this case, several DOI corresponding to pairs of SYT of any shape $\lambda \vdash \kappa$, are present. Since epsilon tensors are instead absent, there is no multiplicity from the partitions (α, β). The general form of the decoupling operators appearing in the sum over ρ is

$$\left(P^{\rho=\lambda_{ab}} \right)_i^l = \frac{1}{\kappa!} \sum_{\pi \in S_\kappa} \frac{f_\lambda}{\sqrt{D_{\lambda, N}}} M_{\lambda; ab}(\pi) \, \delta_i^{l_\pi} \, , \qquad \left(P^{\rho=\lambda_{ab}} \right)_k^j = \frac{1}{\kappa!} \sum_{\sigma \in S_\kappa} \frac{f_\lambda}{\sqrt{D_{\lambda, N}}} M_{\lambda; ab}(\sigma) \, \delta_{k_\sigma}^j \, . \tag{4.65}$$

The contraction of the color indices between a single delta function with permuted indices and the staggered fields gives

$$\delta_i^{l_\pi} \bar{\chi}_i(n) \chi_l(n) = \mathrm{sgn}(\pi) \, (M_n)^\kappa \, , \qquad M_n \equiv \sum_{i=0}^N \bar{\chi}_i(n) \chi_i(n) \, , \tag{4.66}$$

$$\delta_{k_\sigma}^j \bar{\chi}_k(n+\hat{\mu}) \chi_j(n+\hat{\mu}) = \mathrm{sgn}(\sigma) \, (M_{n+\hat{\mu}})^\kappa \, , \qquad M_{n+\hat{\mu}} \equiv \sum_{i=0}^N \bar{\chi}_i(n+\hat{\mu}) \chi_i(n+\hat{\mu}) \, , \tag{4.67}$$

where $\mathrm{sgn}(\pi)$ is the parity of the permutation π, i.e. $\mathrm{sgn}(\pi) = (-1)^{N_\pi}$ if π can be written as a composition of N_π transpositions. The homomorphism $\pi \to \mathrm{sgn}(\pi)$, defines a one-dimensional irreducible representation called the completely antisymmetric irrep, which is associated to the partition

$$\lambda \vdash \kappa = \{\underbrace{1,1,\ldots,1}_{\kappa \text{ times}}\}, \tag{4.68}$$

and we will refer to this particular irrep with $\mathbb{1}^\kappa$. Hence, we can make use of the great orthogonality theorem (Eq. (4.44)), obtaining

$$\left(P^{\rho=\lambda_{ab}}\right)_i^l \bar{\chi}_i(n)\chi_l(n) = \frac{(M_n)^\kappa}{\kappa!} \sum_{\pi \in S_\kappa} \frac{f_\lambda}{\sqrt{D_{\lambda,N}}} M_{\lambda;ab}(\pi)\,\mathrm{sgn}(\pi) = \frac{(M_n)^\kappa}{\sqrt{D_{\lambda,N}}} \delta_{\lambda,\mathbb{1}^\kappa}, \tag{4.69}$$

$$\left(P^{\rho=\lambda_{ab}}\right)_k^j \bar{\chi}_k(n+\hat{\mu})\chi_j(n+\hat{\mu}) = \frac{(M_n)^\kappa}{\kappa!} \sum_{\sigma \in S_\kappa} \frac{f_\lambda}{\sqrt{D_{\lambda,N}}} M_{\lambda;ab}(\sigma)\,\mathrm{sgn}(\sigma) = \frac{(M_n)^\kappa}{\sqrt{D_{\lambda,N}}} \delta_{\lambda,\mathbb{1}^\kappa}. \tag{4.70}$$

Hence, the only decoupling operator that contributes is the one associated to the partition $\mathbb{1}^\kappa$. Clearly in this case $a = b = 1$ since the irrep is one-dimensional. The final form of the $\mathcal{I}_G$ integral is thus

$$\mathcal{I}_G[\mathcal{M}_{n,\mu}, \mathcal{M}_{n,\mu}^\dagger] = \sum_{\kappa=0}^{N} \frac{1}{(\kappa!)^2 D_{\lambda_{\mathbb{1}^\kappa},N}} \left(M_n M_{n+\hat{\mu}}\right)^\kappa + z\left((-1)^N \alpha_{n,\mu}\bar{B}_n B_{n+\hat{\mu}} + \alpha_{n,\mu}^{-1}\bar{B}_{n+\hat{\mu}}B_n\right), \tag{4.71}$$

and Eq. (3.43) is recovered since from Eq. (4.29) we get

$$\frac{1}{(\kappa!)^2 D_{\mathbb{1}^\kappa,N}} = \frac{1}{(\kappa!)^2} \frac{\kappa!}{N(N-1)\ldots(N-\kappa+1)} = \frac{(N-\kappa)!}{\kappa!N!}. \tag{4.72}$$

Chapter 5

The dual representation at finite β

In this chapter we present our results concerning the dualization of $SU(N)$ lattice gauge theories with staggered fermions. It contains most of the results we recently published in [98]. In the dualization process, the DOI already introduced in the previous chapter, will play the role of auxiliary dual variables, and will allow us to write down the full series expansion in the lattice coupling β, as a product of local weights. To illustrate how the dualization process must be carried out, we start considering the pure Yang-Mills theory, i.e. we neglect the quark fields. The partition function will be organized as a power series in term of the occupation numbers plus the DOI. The statistical weight of any given configuration, which is now identified by assigning a specific value to both DOI and occupation numbers, will be simply the product of local site weights that are obtained contracting the color indices of the decoupling operators attached to a given site, and can be computed numerically. When including the staggered quark fields, the dualization is essentially the same. The only difference is that now color contraction can also take place between decoupling operators and Grassmann fields. This modification does not introduce any overhead in the algorithm. We will show how to write down the full partition function in a compact form, and how to compute the Boltzmann weights in the dual representation. In particular, a combinatorial form of the partition function at order $\mathcal{O}(\beta)$ and $\mathcal{O}(\beta^2)$ will be explicitly given. For the higher orders, since a classification of all weights would be too lengthy, an analytic resummation in small two-dimensional volumes will be performed and the result cross checked against standard hybrid Monte Carlo (HMC) simulations. A preliminary analysis of the magnitude of the sign problem when including the higher order β corrections will be finally presented.

5.1 Dualization in Yang-Mills theory

For a pure gauge theory, the Taylor expansion of the Wilson action reads

$$\mathcal{Z}_{\text{Y.M.}} = \int_G \prod_{(n,\mu)} \mathcal{D}U_{n,\mu} \exp\left(\frac{\beta}{2N}\sum_p \text{Tr}U_p + \text{Tr}U_p^\dagger\right) \tag{5.1}$$

$$= \sum_{\{n_p,\bar{n}_p\}} \frac{\left(\frac{\beta}{2N}\right)^{n_p+\bar{n}_p}}{n_p!\bar{n}_p!} \int_G \prod_{(n,\mu)} \mathcal{D}U_{n,\mu} \prod_p \text{Tr}[U_p]^{n_p}\,\text{Tr}[U_p^\dagger]^{\bar{n}_p}\,. \tag{5.2}$$

Depending on the gauge group G, the occupation numbers are subject to a (gauge-) constraint: they must be chosen such that all link integrals over the Haar measure are non-vanishing. As we have shown in Eq. (4.10), this means that the number of gauge links in forward ($U_{n,\mu}$) and backward ($U_{n,\mu}^\dagger$) direction contained in the product over the plaquettes must be the same for $G = \text{U}(N)$, or differ by a multiple of N for $\text{SU}(N)$. This requirement can be written in compact notation as

$$\sum_{\nu>\mu}\left[\delta n_{n,\mu,\nu} - \delta n_{n-\hat{\nu},\mu,\nu}\right] - \sum_{\nu<\mu}\left[\delta n_{n,\nu,\mu} - \delta n_{n-\hat{\mu},\nu,\mu}\right] = \begin{cases} 0 & \text{U}(N) \\ 0\,\text{mod}\,N & \text{SU}(N) \end{cases} \quad \forall\,(n,\mu)\,, \tag{5.3}$$

where $\delta n_p \equiv n_p - \bar{n}_p$. Assuming that this constraint is satisfied by some choice of the occupation numbers, the integral can be decomposed as a product of local weights making use of the DOI. The idea is to select for each lattice link $\ell \equiv (n,\mu)$ a DOI ρ_μ^n, which thus identifies a given decoupling operator $P^{\rho_\mu^n}$ in the decomposition of the $\mathcal{I}$−integral

$$\mathcal{I}_{ij,kl}^{q_\ell N+p_\ell,p_\ell} = \sum_{\rho_\mu^n} \left(P^{\rho_\mu^n}\right)_i^l \left(P^{\rho_\mu^n}\right)_k^j\,. \tag{5.4}$$

The values of q_ℓ and p_ℓ are determined, as mentioned in the previous chapter, from the plaquette occupation numbers. When a given DOI ρ_μ^n is selected for each link $\ell = (n,\mu)$, the contraction of the color indices that brings from the $\mathcal{I}$−integrals to the traces appearing in Eq. (5.2), can be done *locally* at each lattice site. In order to show this feature, for every link $\ell = (n,\mu)$ we associate the decoupling operator $P^{\rho_\mu^n}$ carrying color indices $\{i,l\}$ to site n, and the second operator $P^{\rho_\mu^n}$ with color indices $\{k,j\}$ to site $n+\hat{\mu}$ (see Fig. 5.1). In the following we will also make use of the notation $\rho_{-\mu}^n \equiv \rho_\mu^{n-\hat{\mu}}$. As depicted in Fig. 5.2, the color indices relative to the decoupling operator associated to n are *always* contracted with the color indices of decoupling operators on different links but associated to the same site n.
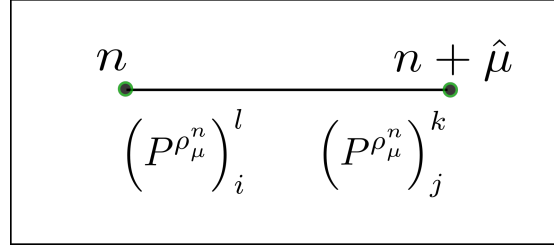
FIGURE 5.1: The decoupling operator $\left(P^{\rho_\mu^n}\right)_i^l$ is associated to the site n, while $\left(P^{\rho_\mu^n}\right)_k^j$ to $n+\hat{\mu}$.

This follows from the definition of plaquette and antiplaquette

$$\text{Tr}\, U_p = (U_1)_{i1}^{j1} (U_2)_{i2}^{j2} (U_3^\dagger)_{k3}^{l3} (U_4^\dagger)_{k4}^{l4} \, \delta_{j1}^{i2} \delta_{j2}^{k3} \delta_{l3}^{k4} \delta_{l4}^{i1} \, , \tag{5.5}$$

$$\text{Tr}\, U_p^\dagger = (U_1^\dagger)_{k1}^{l1} (U_2^\dagger)_{k2}^{l2} (U_3)_{i3}^{j3} (U_4)_{i4}^{j4} \, \delta_{l2}^{k1} \delta_{j3}^{k2} \delta_{j4}^{i3} \delta_{l1}^{i4} \, , \tag{5.6}$$

where $U_1,\dots,U_4$ are the four links that make up the plaquette, and a summation over repeating indices is implied. Indeed, as is also shown in Fig. 5.3 in the case of a single pla-quette, the structure of the delta functions in Eqs. (5.5) and (5.6) is such that the indices i,l of a gauge link $U_{n,\mu}$ are always contracted with the color indices of the gauge links attached to site n, while the indices k,j are contracted with the color indices of the gauge links at-tached to site $n+\hat{\mu}$. Therefore, at fixed value of the DOI, the contraction of color indices for decoupling operators associated to different lattice sites is completely *independent*. This is the crucial observation to obtain a dual form in terms of local weights. The result of the contraction at a given site n, is a scalar number that in $D+1$ spacetime dimensions only depends on the $2(D+1)$ DOI $\rho_{\pm\mu}^n$, and on the plaquette occupation numbers $n_p, \bar{n}_p$ relative to the plaquettes p surrounding n (which are $2D(D+1)$ in total). In particular the plaquette occupation numbers determine the *contraction rules* of the decoupling operators, i.e. how the color indices of the different $P^{\rho_{\pm\mu}^n}$ must be paired when performing the contraction. If two links $(n,\pm\mu), (n,\pm\mu')$ span a given plaquette p, then all the color indices in $P^{\rho_{\pm\mu}^n}$ and $P^{\rho_{\pm\mu'}^n}$ stemming from the decomposition of $\text{Tr}[U_p]^{n_p}$ and $\text{Tr}[U_p^\dagger]^{\bar{n}_p}$ into matrix elements of the gauge links $U_{n,\pm\mu}$ and $U_{n,\pm\mu'}$, must be saturated accordingly. When doing so for all pairs of decoupling operators associated to the same lattice site, every color index will be contracted and the result is just a scalar number. Formally, we can write down this result as

$$T_n^{\rho_{-D}^n\cdots\rho_D^n}(\{n_p,\bar{n}_p\}) \equiv \text{Tr}_{\{n_p,\bar{n}_p\}}\left[\prod_{\pm\mu} P^{\rho_{\pm\mu}^n}\right] \in \mathbb{R} \tag{5.7}$$

where the symbol $\text{Tr}_{\{n_p,\bar{n}_p\}}$ means that the contraction is performed according to the afore-mentioned rules. The computation of the site weights T_n^ρ has been automatized. We de-veloped a code, that for a given set of DOI $\{\rho_\mu^n\}$ builds up the decoupling operators and
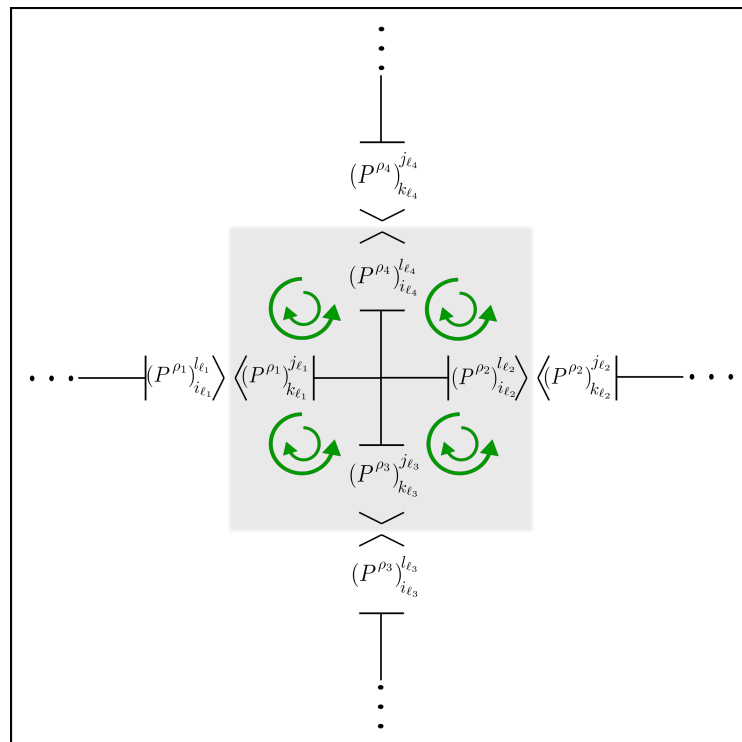
FIGURE 5.2: Illustration of the decoupling in two dimensions: on each of the four links attached to the central lattice site, the DOI have been fixed. Decoupling operators on the same link undergo a disjoint contraction at different lattice sites. The bra-ket notation has been introduced to display this feature. At the central site, the color indices of the four decoupling operators attached to it are completely saturated. The contraction rule of the color indices are defined by the plaquette occupation numbers n_p and $\bar{n}_p$ relative to the four plaquettes (in two dimensions) attached to this site (green arrows). The result of the contraction is a scalar quantity which only depends on the value of the DOI and on the plaquette occupation numbers around the site.

$$\operatorname{Tr} U_p = \operatorname{Tr} U_1 U_2 U_3^\dagger U_4^\dagger$$

$$\operatorname{Tr} U_p^\dagger = \operatorname{Tr} U_4 U_3 U_2^\dagger U_1^\dagger$$
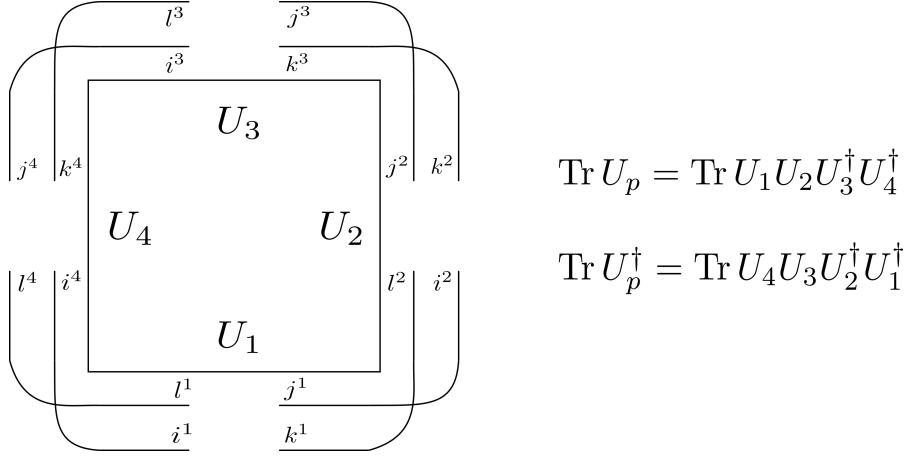
FIGURE 5.3: The contraction of color indices that produces a plaquette. For every gauge link the indices $\{i, l\}$ and $\{k, j\}$ undergo a disjoined contraction at different lattice sites. Given the structure of the decoupling operators, this means that $\left(P^{\rho_\mu^n}\right)_i^l$ and $\left(P^{\rho_\mu^n}\right)_k^j$ contract respectively with the decoupling operators associated to site n and $n + \hat{\mu}$.

performs automatically the color contraction as specified by the plaquette occupation numbers in the background. In terms of the site weights in Eq. (5.7), the Yang-Mills partition function can be written simply as

$$\mathcal{Z}_{\text{Y.M.}} = \sum_{\{n_p, \bar{n}_p\}} \sum_{\{\rho_\mu^n\}} \prod_p \frac{\left(\frac{\beta}{2N}\right)^{n_p + \bar{n}_p}}{n_p! \bar{n}_p!} \prod_n T_n^{\rho_{-D}^n \cdots \rho_D^n}(\{n_p, \bar{n}_p\}) . \tag{5.8}$$

Having postponed the sum over the DOI, one can think of promoting them to dual variables to be sampled along with the plaquette occupation numbers. In this case the weight of a configuration, which is now identified by the plaquette occupation numbers and by the DOI, is the product of scalar site weights, and a fully local dual form is obtained. In this formulation, neighboring lattice sites communicate only through the common DOI on the shared bond since $\rho_\mu^n = \rho_{-\mu}^{n+\hat{\mu}}$ by construction.

Performing directly simulations at large β is however very time consuming, and this approach will never be competitive when compared for instance with the Cabibbo-Marinari pseudo heat-bath algorithm [99]. There are several reasons for this: first of all the computation of the site weights T_n^ρ gets more and more time consuming as the plaquette occupation numbers get larger. Secondly, the site weights T_n^ρ are not all positive definite and one should expect a sign problem even if the conventional formulation in term of gauge links does not have one. Nevertheless the fact that the weights are, at least in principle, known for every value of $n_p, \bar{n}_p$, can play an important role in the regime where conventional simulations are not possible, e.g. in finite density QCD. As we are going to show, the partition function Eq. (5.8) can be extended, without making any approximation, to include staggered

fermions. In this case, the dual formalism will allow to obtain the higher-order β-corrections to strong coupling and will provide an important tool to generate the statistical weights to be used in Monte Carlo simulations.

5.2 Dualization including staggered fermions

5.2.1 Formulation and main properties

When including staggered fermions, as outlined in Ch. 4, the Taylor expansion in terms of dual variables is

$$
\mathcal{Z}(\beta, \hat{m}_q, \hat{\mu}_q) = \sum_{\substack{\{n_p, \bar{n}_p\} \\ \{d_\ell, \bar{d}_\ell, m_n\}}} \prod_p \frac{\tilde{\beta}^{n_p + \bar{n}_p}}{n_p! \bar{n}_p!} \prod_\ell \frac{1}{d_\ell! \bar{d}_\ell!} \prod_n \frac{(2\hat{m}_q)^{m_n}}{m_n!} \int d\bar{\chi}(n) d\chi(n) \left(\bar{\chi}(n)\chi(n)\right)^{m_n} \mathcal{G}_{n_p, \bar{n}_p, d_\ell, \bar{d}_\ell},
$$

(5.9)

$$
\mathcal{G}_{n_p, \bar{n}_p, d_\ell, \bar{d}_\ell} = \prod_\ell \int \mathcal{D}U_\ell \, \text{Tr}[U_\ell \mathcal{M}_\ell^\dagger]^{d_\ell} \, \text{Tr}[U_\ell^\dagger \mathcal{M}_\ell]^{\bar{d}_\ell} \prod_p \text{Tr}[U_p]^{n_p} \, \text{Tr}[U_p^\dagger]^{\bar{n}_p},
$$

(5.10)

with $\tilde{\beta} = \beta/2N$. In addition to the plaquette occupation numbers, we now have the monomers m_n, and the hopping coefficients d_ℓ and $\bar{d}_\ell$ which are related to dimers and quark fluxes via

$$
k_\ell \equiv \min\{d_\ell, \bar{d}_\ell\}, \qquad f_\ell \equiv d_\ell - \bar{d}_\ell.
$$

(5.11)

Before going through the evaluation of $\mathcal{G}$, we want to analyze how the strong coupling constraints on the dual variables get modified at finite β. The Grassmann constraint is clearly blind to the presence of the plaquettes, and therefore takes the same form as in the strong coupling limit

$$
m_n + \sum_{\pm\mu} k_{n,\pm\mu} + \frac{|f_{n,\pm\mu}|}{2} = N, \qquad \sum_{\mu=0}^{D} f_{n,+\mu} - f_{n,-\mu} = 0.
$$

(5.12)

The (gauge-) constraint Eq. (5.3) is instead modified by the presence of quark fluxes. Every unit of $f_{n,\mu}$ in Eq. (5.10) contains a forward ($U_{n,\mu}$) or backward ($U_{n,\mu}^\dagger$) gauge link depending on its sign. As a consequence, the requirement that every integral $\int \mathcal{D}U_{n,\mu}$ be non-zero is translated in term of dual variables into

$$
f_{n,\mu} + \sum_{\nu > \mu} \left[\delta n_{n,\mu,\nu} - \delta n_{n-\hat{\nu},\mu,\nu}\right] - \sum_{\nu < \mu} \left[\delta n_{n,\nu,\mu} - \delta n_{n-\hat{\mu},\nu,\mu}\right] = \begin{cases} 0 & \text{U}(N) \\ 0 \bmod N & \text{SU}(N) \end{cases} \quad \forall\, (n, \mu).
$$

(5.13)
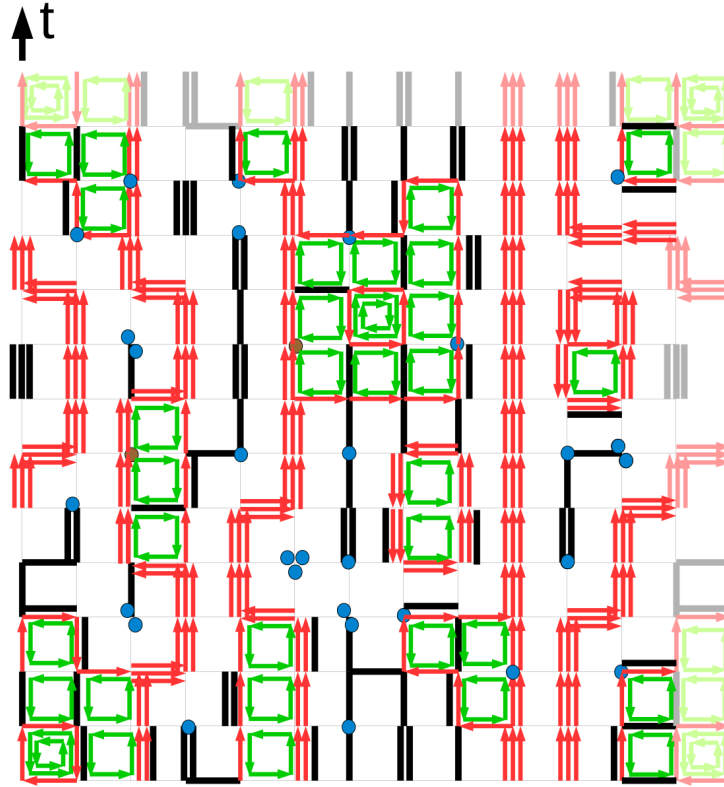
FIGURE 5.4: An allowed configuration in $d = 2$ for SU(3): for each plaquette, a (counter-) clockwise loop corresponds to one unit of (n_p) $\bar{n}_p$. On each site the monomer number m_n is given by the number of circles, while on each link the unoriented black lines represent dimers (n lines for $k_{n,\mu} = n$). Every red arrow represents instead one unit of quark flux $f_{n,\mu}$. The Grassmann constraint, in agreement with Eq. (5.12), is satisfied at each site with the net quark flux being always zero. For every link, the difference between the total flux (gluons + quarks) in positive and negative direction is a multiple of $N = 3$. Periodic boundary conditions are employed.

The dimers $k_{n,\mu}$ are clearly not involved in this constraint as they carry the same number of forward and backward gauge links. The first consequence of this relation is that in contrast to strong coupling, quark fluxes are not required to be integer multiples of N. Moreover, dimers and quark fluxes are not mutually exclusive on a given link, i.e. the constraint allows for a dimer to be superimposed to a quark flux. Lastly, even though the flux conservation law in Eq. (5.12) still holds, quark fluxes can form *intersecting loops* as shown in Fig. 5.4 where we provide an example of an admissible configuration.

When all constraints are satisfied, the goal is to obtain a closed expression for the weight of an allowed configuration. As in the Yang-Mills case, this can be done making use of the DOI. We start by building up, on each gauge link $\ell = (n, \mu)$, the corresponding $\mathcal{I}$-integral. The values of q_ℓ and p_ℓ, are now co-determined by the plaquette occupation numbers on the plaquettes p adjacent to ℓ, and by the number of hopping terms $\text{Tr}[U_\ell \mathcal{M}_\ell^\dagger]$ and $\text{Tr}[U_\ell^\dagger \mathcal{M}_\ell]$. We then select a given decoupling operator $P^{\rho_\mu^n}$ on each link, and consider the color contraction in a fixed background of DOI. The locality property of the contractions still holds. The

main difference is that now the color indices are not only contracted among decoupling operators, but also with the fermionic matrices $\mathcal{M}_\ell$ and $\mathcal{M}_\ell^\dagger$. We thus distinguish two types of color indices: those associated to the hopping terms, and those arising from the expansion of the Wilson gauge action. We will refer to them as *fermionic* and *gluonic* color indices. In the case of the gluonic color indices, the contraction proceeds exactly as in the Yang-Mills case: associating the decoupling operator $\left(P^{\rho_\mu^n}\right)_i^l$ to site n, and $\left(P^{\rho_\mu^n}\right)_k^j$ to site $n + \hat{\mu}$, the gluonic color indices in $\{i, l\}$ and $\{k, j\}$ get contracted respectively with the gluonic color indices of decoupling operators at site n and $n + \hat{\mu}$, according to the rules described in the previous subsection. After having contracted all gluonic color indices, the resulting object is no longer a scalar quantity, but contains the yet uncontracted $2(N - m_n)$ fermionic color indices[1] which in turn must be contracted with the fermionic matrices in order to recover the hopping expansion terms $\text{Tr}[U_\ell \mathcal{M}_\ell^\dagger]$ and $\text{Tr}[U_\ell^\dagger \mathcal{M}_\ell]$. The structure of the fermionic matrices is such that again the contraction at a given site decouples from the rest. Indeed, by definition we have

$$\text{Tr}[U_\ell \mathcal{M}_\ell^\dagger]^{d_\ell} \propto \prod_{a=1}^{d_\ell} \left(U_{n,\mu}\right)_{i_a}^{j_a} \bar{\chi}^{i_a}(n)\chi_{j_a}(n + \hat{\mu}), \tag{5.14}$$

$$\text{Tr}[U_\ell^\dagger \mathcal{M}_\ell]^{\bar{d}_\ell} \propto \prod_{b=1}^{\bar{d}_\ell} \left(U_{n,\mu}^\dagger\right)_{k_b}^{l_b} \bar{\chi}^{k_b}(n + \hat{\mu})\chi_{l_b}(n); \tag{5.15}$$

hence the fermionic color indices in $\{i, l\}$ (resp. $\{k, j\}$) are contracted with the staggered fields $\bar{\chi}(n), \chi(n)$ (resp. $\bar{\chi}(n + \hat{\mu}), \chi(n + \hat{\mu})$). This additional contraction has been implemented in our code: the idea is to collect all Grassmann variables $\bar{\chi}(n)$ and $\chi(n)$ appearing in the definition of $\mathcal{G}$ (Eq. (5.10)), performing symbolically the Grassmann integral via

$$G_{i_1,\dots,i_{N-m_n}}^{j_1,\dots,j_{N-m_n}}(n) = \prod_{i=1}^{N} \int d\bar{\chi}_i(n) d\chi_i(n)\, \chi_{i_1}(n)\dots\chi_{i_{N-m_n}}(n)\bar{\chi}^{j_1}(n)\dots\bar{\chi}^{j_{N-m_n}}(n)\left(\bar{\chi}(n)\chi(n)\right)^{m_n}$$

$$= m_n!\, \tilde{\epsilon}_{i_1,\dots,i_{N-m_n}}^{j_1,\dots,j_{N-m_n}}, \tag{5.16}$$

where

$$\tilde{\epsilon}_{i_1,\dots,i_k}^{j_1,\dots,j_k} = \begin{cases} \text{sgn}(\pi) & \text{if } \forall m, n \; j_m \neq j_n \wedge (j_1,\dots,j_k) = \pi(i_1,\dots,i_k), \;\; \pi \in S_k \\ 0 & \text{otherwise} \end{cases} \tag{5.17}$$

The indices $\{i_1,\dots,i_{N-m_n}\}$ and $\{j_1,\dots,j_{N-m_n}\}$ of the tensor $G(n)$ are in one-to-one correspondence with the fermionic color indices, and one can define an ordering between them, so that every $\chi_i(n)$ and $\bar{\chi}_j(n)$ in Eq. (5.16) is unambiguously associated to a fermionic color

---

[1] The number of Grassmann variables at a given site must be always $2N$ (counting both quarks and antiquarks), and the monomers m_n contribute with a factor $(\bar{\chi}(n)\chi(n))^{m_n}$.

index[2] of a decoupling operator $P^{\rho_\mu^n}$ attached to site n. In this way we can simply take the result of the contraction of the gluonic color indices, which is a tensor containing only the fermionic color indices, and contract it further with the tensor $G(n)$ in Eq. (5.16). The result is again a scalar quantity, which similarly to the Yang-Mills case, can be written as

$$T_n^{\rho_{-D}^n \cdots \rho_{+D}^n}(\mathcal{D}_n) \equiv \mathrm{Tr}_{\mathcal{D}_n}\left[\prod_{\pm\mu} P^{\rho_\mu^n}\, G(n)\right], \qquad \mathcal{D}_n = \{m_n, f_{n,\pm\mu}, k_{n,\pm\mu}, n_{n,\mu\nu}, \bar{n}_{n,\mu\nu}\} \qquad (5.18)$$

where now the symbol $\mathrm{Tr}_{\mathcal{D}_n}$ means that the contraction must be performed not only according to the plaquette occupation numbers (which only determine the contraction rules of the gluonic color indices), but also according to the number of dimers $(k_{n,\pm\mu})$, quark fluxes $(f_{n,\pm\mu})$ and monomers (m_n). Notice that in the definition of $G(n)$ we did not take into account neither the chemical potential dependence nor the staggered phases contained in the fermionic matrices. Since these quantities simply factorize, we will reintroduce them explicitly when writing down the expression of the partition function. In addition, when collecting the staggered fields before performing the Grassmann integration (Eq. (5.16)), a certain number of swaps of Grassmann variables is performed. The relative minus sign must be then taken into account when determining the global sign of a configuration. This (called geometric) sign is already present at strong coupling, where given the simple structure of the quark loops it only contributes with a factor $(-1)^N$ to the sign σ_ℓ in Eq. (3.56). For the moment we disregard the problem of computing the sign of a configuration at finite β, postponing the discussion to the next subsection. Up to a yet undetermined fermionic sign σ_f, the value of the combined Grassmann and gauge integral in Eq. (5.9), is expressed in terms of the DOI ρ_μ^n and of the site weights T_n^ρ as

$$\prod_n \int d\bar{\chi}(n) d\chi(n)\, (\bar{\chi}(n)\chi(n))^{m_n}\, \mathcal{G}_{n_p, \bar{n}_p, k_\ell, f_\ell} = \sigma_f \prod_{(n,\mu)} e^{\hat{\mu}_q\, \delta_{\mu,0}\, f_{n,\mu}} \sum_{\{\rho_\mu^n\}} \prod_n T_n^{\rho_{-D}^n \cdots \rho_{+D}^n}(\mathcal{D}_n) \quad (5.19)$$

$$\equiv \sigma_f \prod_{(n,\mu)} e^{\hat{\mu}_q\, \delta_{\mu,0}\, f_{n,\mu}}\, W\left[n_p, \bar{n}_p, k_\ell, f_\ell, m_n\right], \quad (5.20)$$

and the fully dualized partition function Eq. (5.9) is given by

$$\mathcal{Z}(\beta, \mu_q, \hat{m}_q) = \sum_{\substack{\{n_p, \bar{n}_p\} \\ \{k_\ell, f_\ell, m_n\}}} \sigma_f \sum_{\{\rho_\mu^n\}} \prod_p \frac{\left(\frac{\beta}{2N}\right)^{n_p + \bar{n}_p}}{n_p!\bar{n}_p!} \prod_{\ell=(n,\mu)} \frac{e^{\mu_q \delta_{\mu,0} f_{n,\mu}}}{k_\ell!(k_\ell + |f_\ell|)!} \prod_n \frac{(2\hat{m}_q)^{m_n}}{m_n!} T_n^{\rho_{-D}^n \cdots \rho_{+D}^n}(\mathcal{D}_n),$$

$$(5.21)$$

with the dual variables $\{n_p, \bar{n}_p, k_\ell, f_\ell, m_n\}$ subject to the Grassmann and gauge constraints

---

[2]We follow the convention of associating the color indices of G_n (from left to right) to the fermionic color indices of the decoupling operators $P^{\rho_\mu^n}$ starting from $\mu = -0, +0$ to $\mu = -D, +D$.

Eqs. (5.12) and (5.13). The system is an ensemble of plaquette occupation number, dimers, quark fluxes and monomers. The DOI can be either thought as an auxiliary degree of freedom to be sampled, or as a mathematical tool that allows to obtain the statistical weight of configurations identified only by $\{n_p, \bar{n}_p, k_\ell, f_\ell, m_n\}$. The two possibilities have their advantages and shortcomings. In the latter case, the resummation of the DOI proceeds as follows: at any lattice site one evaluates the *tensor* $T_n^{\rho_{-D} \cdots \rho_{+D}}$, meaning that one computes the site weight for *all* possible combinations of DOI around site n. This defines a *tensor network*. Given the fact that $\rho_\mu^n = \rho_{-\mu}^{n+\mu}$ (because DOI on the same link are equal by construction), the tensor-to-scalar contraction of the tensor network returns the value $W\left[n_p, \bar{n}_p, k_\ell, f_\ell, m_n\right]$ (see Fig. 5.6). The advantage of this method, as compared to the use of the DOI as dynamical variables, is that the sign problem is always milder since we are resumming configurations. At the same time the weight $W\left[n_p, \bar{n}_p, k_\ell, f_\ell, m_n\right]$ is clearly a non-local object and becomes increasingly more expensive to compute for large occupation numbers. Even if so, since we are interested in evaluating the partition function perturbatively in β, non-local effects can be under control if β is not too large, and one can still obtain the weights W reasonably fast. In particular, one can exploit the fact that the weight W always decomposes as a product of a strong coupling part $W_{\text{s.c.}}$, and a term W_β corresponding to the sublattice where non-zero plaquette occupation numbers are present. One can write

$$W = W_{\text{s.c.}} \cdot W_\beta , \qquad W_\beta \equiv \prod_{\text{bubbles } i} W_{\mathcal{B}_i} , \tag{5.22}$$

where a bubble $\mathcal{B}_i$ is any *plaquette-connected* region. The tensors $T_n^{\rho_{-D}^n \cdots \rho_{+D}^n}$ are trivial if some direction $\pm\mu$ corresponds to a nonexcited link $(n, \pm\mu)$, i.e. a link that is not attached to an excited plaquette. Indeed, a nonexcited link can be either traversed by a baryon flux $f_{n,\mu} = \pm N$, or be occupied by dimers (or the link is empty). In the first case, there is only one DOI ρ_μ^n corresponding to the epsilon tensor (see Sec. 4.2.3), and the tensor network is *closed* in this direction. In the case of strong coupling dimers, this property also holds true. As we showed in Sec. 4.2.3, the only DOI that contributes at strong coupling is the one associated to the completely antisymmetric representation $\rho_\mu^n = \mathbb{1}^{k_{n,\mu}}$. This property also extends to the case where the dimers $k_{n,\mu}$ are connected to excited links (Fig. 5.7). In this case, the tensor T_n^ρ factorizes as

$$T_n^{\rho_{-D}^n \cdots \rho_{+D}^n} \propto \left(\prod_{\mu_{\text{sc}}} \delta_{\mathbb{1}^{k_{n,\mu}}}^{\rho_{\mu_{\text{sc}}}^n}\right) \tilde{T}_n^{\rho_{\mu_{\text{exc}}(1)}^n \cdots \rho_{\mu_{\text{exc}}(n_{\text{exc}})}^n} \tag{5.23}$$

where μ_{sc} and $\mu_{\text{exc}}(a)$, $a = 1, \ldots, n_{\text{exc}}$ are respectively the directions of the nonexcited and excited links. Therefore, to evaluate the total weight of a configuration, it is sufficient to use
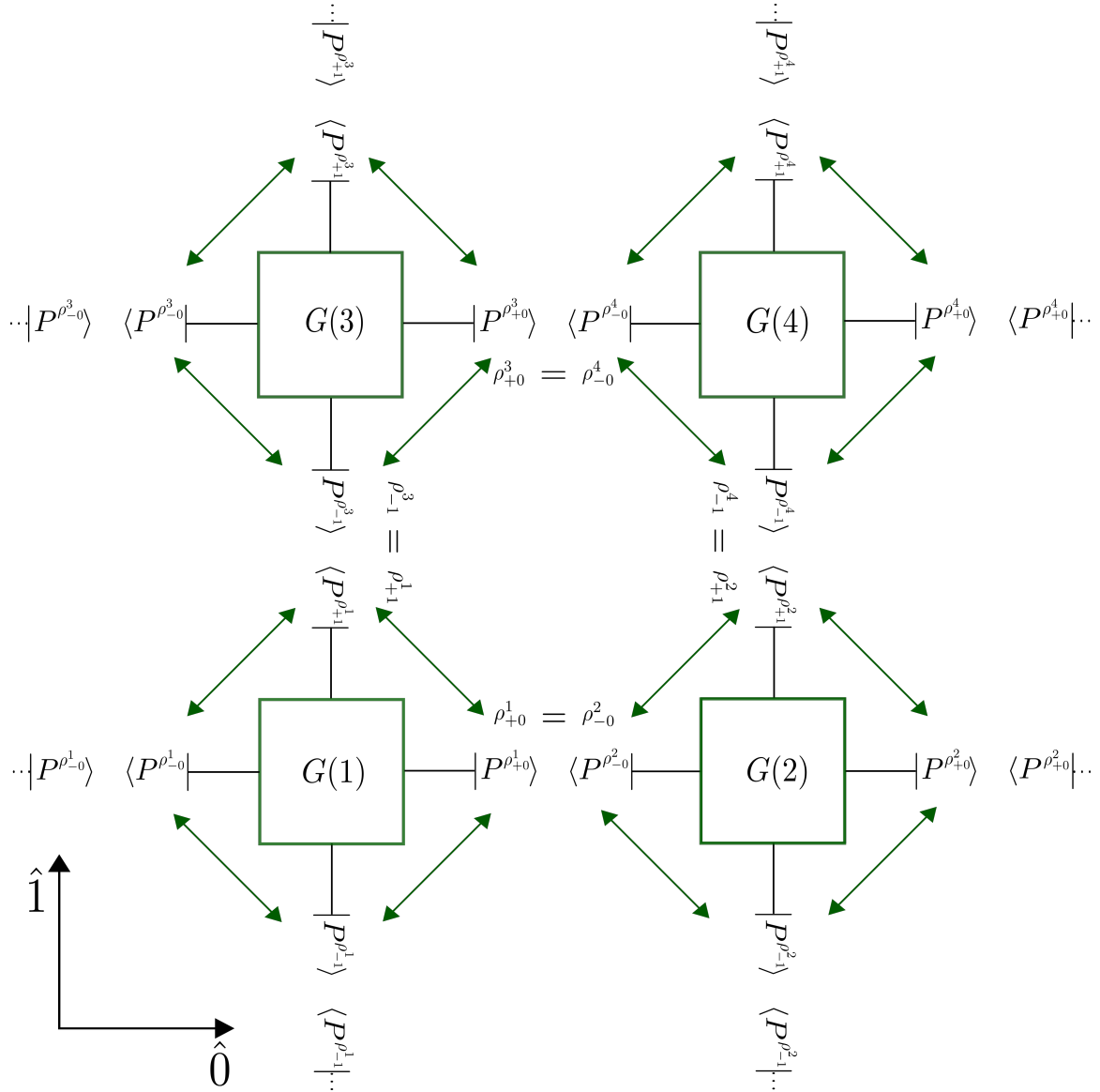
FIGURE 5.5: The decoupling in presence of staggered fermions in two dimensions. At fixed values of the DOI, the statistical weight of a configuration, up to trivial combinatorial factors, is the product of the site weights $T_n^{\rho_{-D}^n \cdots \rho_{+D}^n}$. Every site weight is obtained contracting the color indices of the decoupling operators attached to that site. The gluonic color indices (green arrows), which stem from the expansion of the Wilson gauge action, are contracted among the different operators P^ρ as in the Yang-Mills case. The result of this contraction is a tensorial object containing the fermionic color indices. An additional contraction with $G_{i_1,\ldots,i_{N-m_n}}^{j_1,\ldots,j_{N-m_n}}(n)$ produces the scalar site weight $T_n^{\rho_{-D}^n \cdots \rho_{+D}^n} \in \mathbb{R}$.
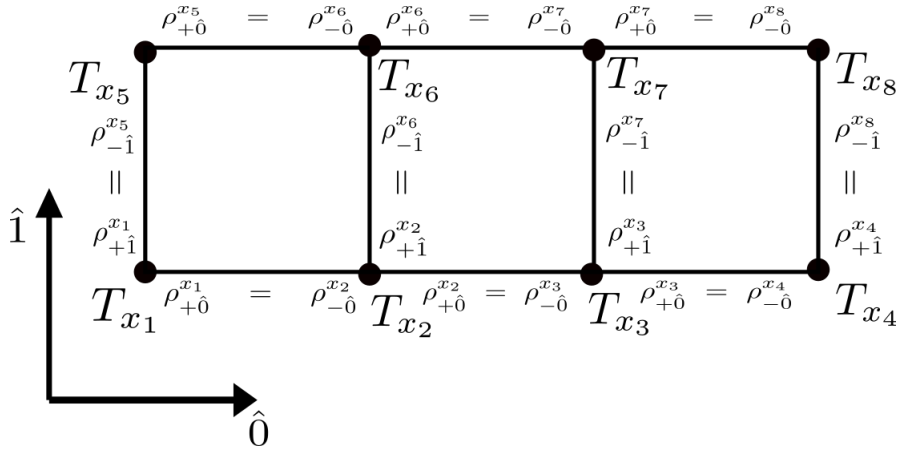
FIGURE 5.6: Example of tensor network contraction. Depending on the dual variables, at any lattice site the tensor T_n is evaluated. Given two neighboring sites n and $n + \hat{\mu}$, the DOI on the common link is contracted ($\rho_\mu^n = \rho_{-\mu}^{n+\hat{\mu}}$). The weight W, is the scalar quantity obtained by contracting all pairs of indices between lattice neighbors. In the figure, the tensor indices have been displaced for visualization purposes.

the more involved structure based on the tensor network contraction only on the sublattice where the plaquette occupation numbers are non-zero, exploiting the factorization of the tensor network for disconnected plaquette contributions. The strong coupling part can be evaluated using the standard combinatorial formulae (e.g. Eq. (3.58)). This is particularly useful since at small values of β, the bubbles $\mathcal{B}_i$ extend over few lattice spacings and the non-local effects from the tensor network are manageable. In Fig. 5.8 we illustrate an example of this factorization, whereas in Tab. 5.1 we report the values of the associated tensor network.

The other possibility, as already outlined, is to promote the DOI to dual variables. In this case, the increasing complexity and the non-localities induced by the tensor network can be overcome by importance sampling. When the DOI are considered dynamical, the former configurations are split into many subconfigurations determined by selecting one tensor element T_n^ρ per lattice site n. When doing so, the weight of such configurations is local and an additional Metropolis acceptance test can be introduced to make sure that the system explores the DOI configuration space during Monte Carlo. For instance, when a bond, an elementary plaquette or a cube containing six plaquettes is updated, we can propose a quasi-local update by randomly choosing new DOI on the bonds involved. The feasibility of this approach depends on the minus signs induced by splitting the former configurations in terms of $\{n_p, \bar{n}_p, k_\ell, f_\ell, m_n\}$ with weights W, into subconfigurations labeled by the DOI. Indeed, the tensor elements are not positive defined, and it could happen that without a full contraction of the network, additional sign fluctuations are introduced. In Sec. 5.3.3, we will provide preliminary evidences, based on an exact enumeration of the partition function on small volumes, that the sign problem does not seem to worsen drastically, and that the DOI can constitute a valid alternative to the bubble diagrams when the evaluation of the

$$\sum_\mu k_{n,\mu} = N \qquad\qquad k_{n,-0} + k_{n,-1} = N-1$$

$$T_n^{\rho_{-1}^n,\rho_{-0}^n,\rho_{+0}^n,\rho_{+1}^n} \propto \prod_{\pm\mu} \delta^{\rho_{\pm\mu}^n}_{\mathbb{1}^{k_{n,\pm\mu}}} \qquad\qquad T_n^{\rho_{-1}^n,\rho_{-0}^n,\rho_{+0}^n,\rho_{+1}^n} \propto \delta^{\rho_{-1}^n}_{\mathbb{1}^{k_{n,-1}}}\,\delta^{\rho_{-0}^n}_{\mathbb{1}^{k_{n,-0}}}\, \tilde{T}_n^{\rho_{+0}^n,\rho_{+1}^n}$$
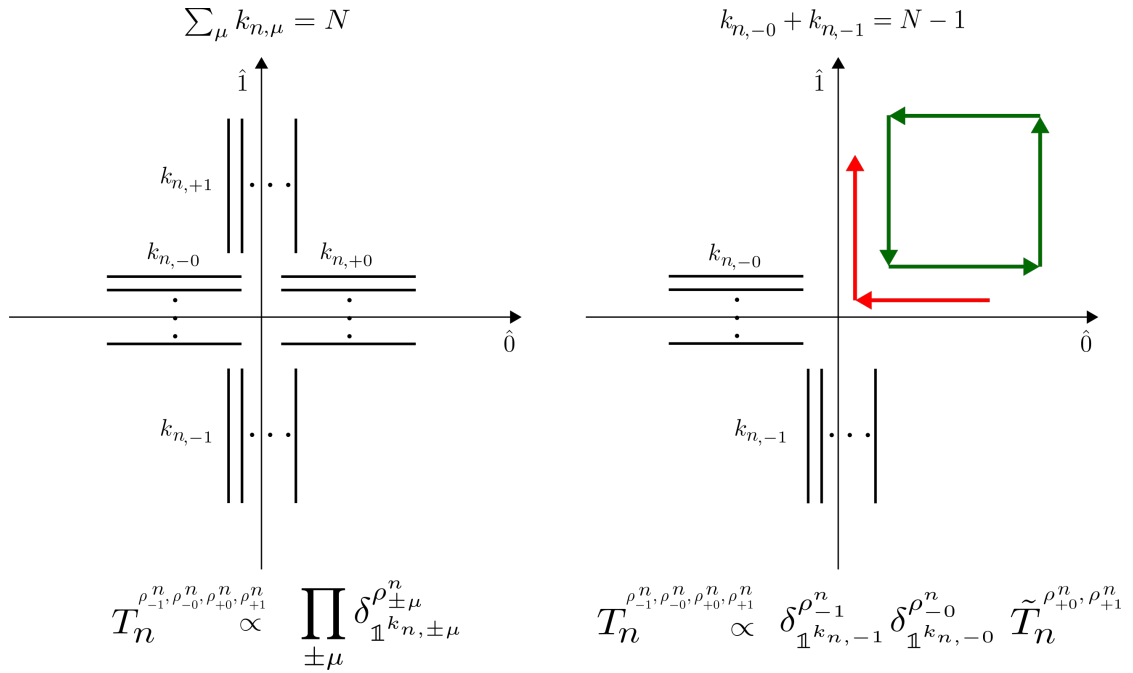
FIGURE 5.7: *Left*: a typical strong coupling configuration where dimers are attached to a given site. The tensor T_n^ρ is trivial as only one combination of DOI (totally antisymmetric irrep on each leg) contributes. *Right*: an $\mathcal{O}(\beta)$ correction. In this case the tensor T_n^ρ decomposes as the product of a tensor carrying the indices from the DOI on the excited links ($\tilde{T}_n^\rho$), and delta functions corresponding to the strong coupling legs which single out the irrep $\mathbb{1}^{k_{n,\mu}}$.

Tensors $\mathcal{B}_1$	(DOI) / value				Tensors $\mathcal{B}_2$	(DOI) / value
T_{n_1}	$(1,1,2,1)$ 2				T_{n_1}	$(1,1,1,2)$ 2.912
T_{n_2}	$(1,2,2,1)$ 1.154				T_{n_2}	$(1,1,1,2)$ 2.912
T_{n_3}	$(1,2,1,1)$ 2				T_{n_3}	$(2,1,2,2)$ 0.816
T_{n_4}	$(1,1,2,1)$ 1.154				T_{n_4}	$(2,2,1,2)$ 0.816
T_{n_5}	$(1,1,1,5)$ 0.384	$(1,2,1,5)$ 0.544	$(1,1,1,6)$ 0.544	$(1,2,1,6)$ -0.384	T_{n_5}	$(2,1,2,1)$ 1.682
T_{n_6}	$(1,1,1,1)$ 1.154				T_{n_6}	$(2,2,1,1)$ 1.682
T_{n_7}	$(1,2,1,1)$ 2					
T_{n_8}	$(6,1,1,1)$ 2					
T_{n_9}	$(1,1,1,1)$ 2					

TABLE 5.1: The tensors T_n^ρ corresponding to the bubble diagrams $\mathcal{B}_1$ and $\mathcal{B}_2$ in Fig. 5.8. The indices in parentheses are respectively the DOI $\rho_{-D}^n, \ldots, \rho_{+D}^n$. Only the non-zero tensor elements have been reported. For small plaquette occupation numbers, contracting the reduced tensor network within the bubbles is straightforward and can be done on the fly during Monte Carlo evolution without any overhead.
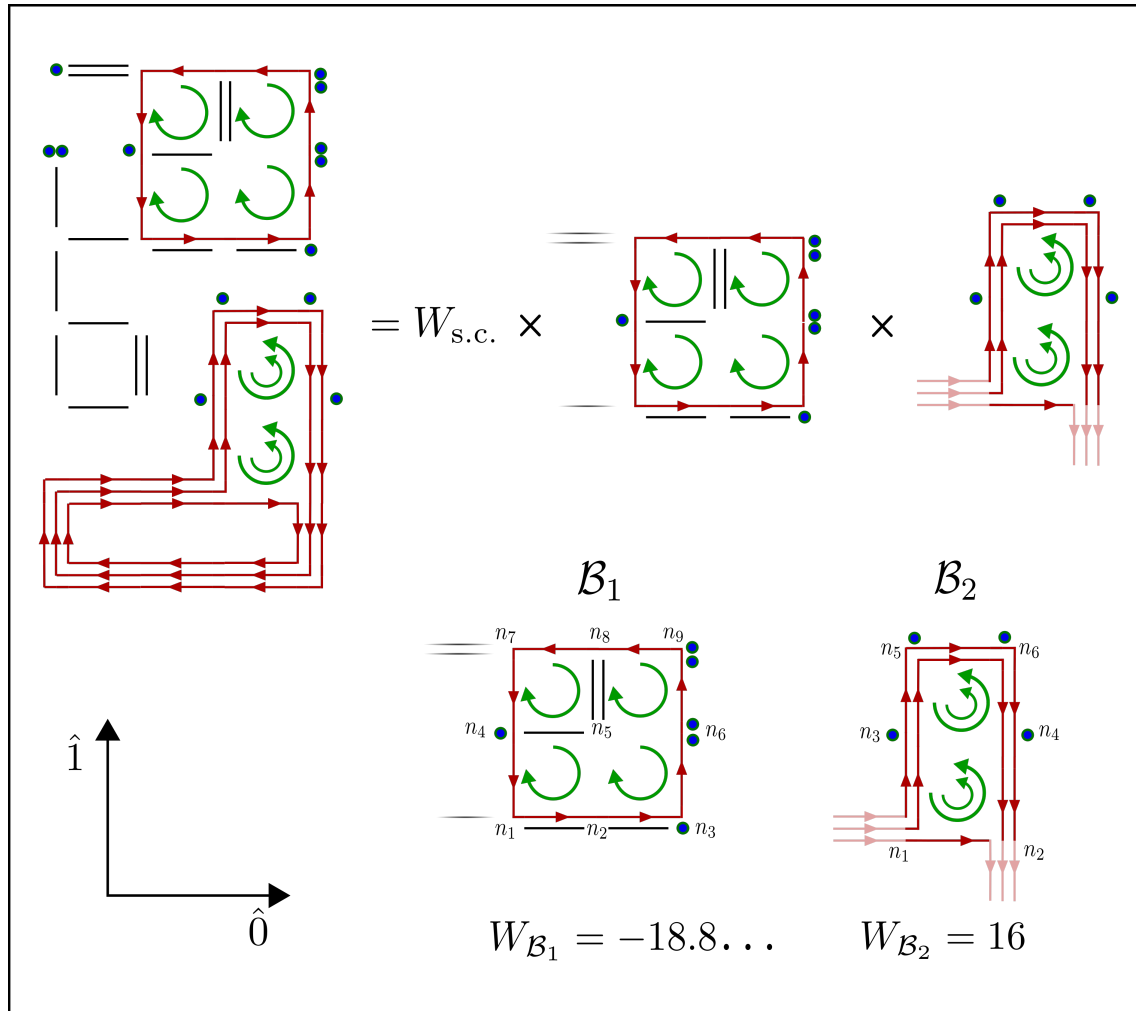
FIGURE 5.8: Example of the factorization of the tensor network for SU(3) in two dimensions. The total weight $W[n_p, \bar{n}_p, k_\ell, f_\ell, m_n]$ is the product of the bubbles weights $W_{\mathcal{B}_1}$ and $W_{\mathcal{B}_2}$, times the weight $W_{\text{s.c.}}$ of the strong coupling background. In $\mathcal{B}_1$ and $\mathcal{B}_2$, the external (strong coupling) legs are *amputated*. This means that for each external leg of a tensor T_n, the correction factors $v_B = \sqrt{N!}$, $v(k) = \sqrt{\frac{N!}{(N-k)!k!}}$ are introduced depending on whether the leg contains a baryon (v_B) or k dimers ($v(k)$). The tensor networks corresponding to $\mathcal{B}_1$ and $\mathcal{B}_2$ are reported in Tab. 5.1.

full tensors T_n^ρ become too expensive to be computed, and the tensor networks within the bubble diagrams become too large to be contracted exactly. However, for small truncation order we will show that most of the DOI can be resummed locally in favor of simple local combinatorial factors, in such a way that the system can be sampled using the standard Worm algorithm already used for simulations in the strong coupling limit.

5.2.2 The fermionic sign

We now turn into the computation of σ_f in the dual representation. In general, the fermionic sign $\sigma_f(\mathcal{C})$ of a configuration $\mathcal{C}$ is determined by the staggered phases, the antiperiodic boundary condition for fermion fields in temporal direction, and by the so-called geometric sign σ_g. The latter, as already outlined, stems from the reordering of the Grassmann variables $\bar{\chi}(n), \chi(n)$ that must be done before integrating them out at each lattice site n using Eq. (5.16). Similarly to the strong coupling case, a negative fermionic sign σ_f can only arise from quark flux loops, and for every loop ℓ we have

$$\sigma_f(\ell) = \sigma_g(\ell)(-1)^{w(\ell)} \prod_{(n,\mu)\in\ell} \left(\eta_\mu(n)\right)^{f_{n,\mu}} \qquad \sigma_f(\mathcal{C}) = \prod_{\text{loop }\ell} \sigma_f(\ell). \qquad (5.24)$$

In the previous equation, the winding number $w(\ell)$ is the total number of quark fluxes in the loop ℓ that cross the temporal boundary

$$w(\ell) = \sum_{\vec{n}} w_{\vec{n}}, \quad w_{\vec{n}} = \begin{cases} 0 & \text{if } ((N_t - 1, \vec{n}), 0) \notin \ell \\ f_{(N_t-1,\vec{n}),0} & \text{otherwise} \end{cases} \qquad (5.25)$$

where the sum $\sum_{\vec{n}}$ is over all spatial lattice sites. The computation of the geometric sign $\sigma_g(\ell)$ is instead slightly more involved. The main complication is that differently from strong coupling, quark fluxes can have non-trivial geometries in presence of excited plaquettes. This is for instance the case of the loop $\ell_{\mathcal{B}_2}$ to which $\mathcal{B}_2$ belongs to (see Fig. 5.8). For standard loop geometries, where every lattice site n in the loop is traversed by two and only two non-zero $f_{n,\mu}$ (e.g. the one in $\mathcal{B}_1$), it is straightforward to show that the geometric sign is given by

$$\sigma_g(\ell) = \begin{cases} 1 & \text{if } \ell \text{ is an even flux loop} \\ (-1)^{N_+(\ell)+1} & \text{otherwise} \end{cases} \qquad (5.26)$$

where $N_+(\ell)$ is as usual the number of forward links traversed by the loop. Using formulae Eqs. (5.24) and (5.26) one gets for instance $\sigma_f(\ell_{\mathcal{B}_1}) = -1$. Notice that for an even flux loop (i.e. a loop where $f_{n,\mu}$ is even) $\sigma_f(\ell) = 1$, always. However, in the most general case a closed expression for $\sigma_g(\ell)$ cannot be obtained. To determine its value for non-trivial geometries, we only make use of its definition, i.e. we explicitly count the number of swaps of Grassmann variables that need to be performed in order to bring them in canonical ordering at each lattice site. In this way one gets for instance $\sigma_g(\ell_{\mathcal{B}_2}) = -1$, which implies $\sigma_f(\ell_{\mathcal{B}_2}) = 1$.

5.2.3 Observables

Since both the fermion fields and the gauge links have been integrated out, the observables in the dual representation take a different form. The observables defined as derivatives of $\log(\mathcal{Z})$ with respect to external parameters, can be clearly obtained taking the same derivatives in the partition function expressed in terms of dual variables. For instance, the chiral condensate $\langle \bar{\psi}\psi \rangle$, the net quark number[3] $\langle n_q \rangle$, and the average plaquette $\langle P \rangle$ are obtained as the following expectation values

$$\langle \bar{\psi}\psi \rangle = \frac{1}{L^D N_t} \frac{\partial \log \mathcal{Z}}{\partial (2\hat{m}_q)} = \frac{1}{L^D N_t} \frac{\sum_n \langle m_n \rangle}{2\hat{m}_q}, \tag{5.27}$$

$$\langle n_q \rangle = \frac{1}{L^D N_t} \frac{\partial \log \mathcal{Z}}{\partial \hat{\mu}_q} = \frac{1}{L^D N_t} \sum_n \langle f_{n,0} \rangle, \tag{5.28}$$

$$\langle P \rangle = \frac{1}{L^D N_t} \frac{\partial \log \mathcal{Z}}{\partial \beta} = \frac{1}{L^D N_t} \frac{\sum_p \langle n_p + \bar{n}_p \rangle}{\beta}, \tag{5.29}$$

where L and N_t are the spatial and temporal extent of the lattice. Notice that the r.h.s. of Eq. (5.29) implies that for any truncation of the maximally allowed plaquette occupation numbers $\lim_{\beta \to \infty} \langle P(\beta) \rangle = 0$. This is clearly an artifact: at large β values the contribution of large n_p and $\bar{n}_p$ cannot be neglected because excited plaquettes come with a factor of $\beta^{n_p + \bar{n}_p}$. Therefore at fixed truncation order, by increasing β, the average plaquette will always reach a maximum and then drop to zero.

Analogous expressions for the susceptibilities of the observables in Eqs. (5.27), (5.28) and (5.29) are readily obtained

$$\chi_{\bar{\psi}\psi} \equiv = \frac{1}{L^D N_t} \frac{\partial^2 \log \mathcal{Z}}{\partial (2\hat{m}_q)^2} = \frac{1}{L^D N_t (2\hat{m}_q)^2} \left[\sum_{n,n'} (\langle m_n m_{n'} \rangle - \langle m_n \rangle \langle m_{n'} \rangle) - \sum_n \langle m_n \rangle \right], \tag{5.30}$$

$$\chi_{n_q} \equiv = \frac{1}{L^D N_t} \frac{\partial^2 \log \mathcal{Z}}{\partial \hat{\mu}_q^2} = \frac{1}{L^D N_t} \sum_{n,n'} \left[\langle f_{n,0} f_{n',0} \rangle - \langle f_{n,0} \rangle \langle f_{n',0} \rangle \right], \tag{5.31}$$

$$\chi_P \equiv = \frac{1}{L^D N_t} \frac{\partial^2 \log \mathcal{Z}}{\partial \beta^2} = \frac{1}{L^D N_t \beta^2} \left[\sum_{p,p'} (\langle r_p r_{p'} \rangle - \langle r_p \rangle \langle r_{p'} \rangle) - \sum_p \langle r_p \rangle \right], \quad r_p \equiv n_p + \bar{n}_p. \tag{5.32}$$

Concerning non-derivative observables, their expression in the dual representation is less trivial, and cannot always be obtained. Unfortunately this is the case of the Polyakov loop $\langle L \rangle$. Formally it can be written as a ratio of partition functions via

$$\langle L \rangle = \frac{1}{L^D} \sum_{\vec{n}} \frac{1}{N} \left\langle \text{Tr} \prod_{\tau=0}^{N_t-1} U_{(\tau,\vec{n}),0} \right\rangle_0 = \frac{1}{NL^D} \sum_{\vec{n}} \frac{\mathcal{Z}_{L_{\vec{n}}}}{\mathcal{Z}}, \tag{5.33}$$

---

[3] the quark number n_q is related to the net baryon number n_B via $n_B = n_q/N$.

where $\langle\rangle_0$ means taking the average in the conventional formulation in terms of gauge links, and $\mathcal{Z}_{L_{\vec{n}}}$ is the partition function with a Polyakov loop insertion at $\vec{n}$. $\mathcal{Z}_{L_{\vec{n}}}$ admits a dual representation similar to $\mathcal{Z}$. The main difference is that on the lattice links $(n, 0)$ crossed by the Polyakov loop, the gauge constraint Eq. (5.13) gets replaced by

$$f_{n,\mu} + \sum_{\nu > \mu} \left[\delta n_{n,\mu,\nu} - \delta n_{n-\hat{\nu},\mu,\nu} \right] - \sum_{\nu < \mu} \left[\delta n_{n,\nu,\mu} - \delta n_{n-\hat{\mu},\nu,\mu} \right] - 1 = \begin{cases} 0 & \text{U}(N) \\ 0 \bmod N & \text{SU}(N) \end{cases},$$

(5.34)

while the site weights T_n^ρ, with $n = (\tau, \vec{n})$, are now different because the two decoupling operators $P^{\rho_{-0}^n}$ and $P^{\rho_{+0}^n}$, carry the additional color index of the Polyakov loop which must be contracted in order to obtain $\text{Tr} \prod_{\tau=0}^{N_\tau - 1} U_{(\tau,\vec{n}),0}$. Hence, the modified contraction rules of the decoupling operators $P^{\rho_\mu^n}$ produce modified site weights $\tilde{T}_n^\rho$ which are computed numerically similarly to the standard T_n^ρ. However, the main (unsolved) problem is to connect the valid configurations in the two ensembles $\mathcal{Z}$ and $\mathcal{Z}_{L_{\vec{n}}}$. One indeed wishes to obtain a local mapping between the valid configurations $\{\mathcal{C}\}$ of $\mathcal{Z}$, and $\{\mathcal{C}_L\}$ of $\mathcal{Z}_{L_{\vec{n}}}$, such that after the stochastic generation of a valid configuration $\mathcal{C}$ of $\mathcal{Z}$, one can reweight to a subset of configurations $\{\mathcal{C}_L | \mathcal{C}\}$ of $Z_{L_{\vec{n}}}$ via

$$\langle L_{\vec{x}} \rangle = \frac{\sum_{\{\mathcal{C}_L\}} W(\mathcal{C}_L)}{\sum_{\{\mathcal{C}\}} W(\mathcal{C})} = \frac{\sum_{\{\mathcal{C}\}} W(\mathcal{C}) \sum_{\{\mathcal{C}_L | \mathcal{C}\}} \frac{W(\mathcal{C}_L)}{W(\mathcal{C})} P_{\mathcal{C}_L, \mathcal{C}}}{\sum_{\{\mathcal{C}\}} W(\mathcal{C})}, \qquad \sum_{\{\mathcal{C}\}} P_{\mathcal{C}_L, \mathcal{C}} = 1 \;\; \forall \mathcal{C}_L, \qquad (5.35)$$

where $P_{\mathcal{C}_L, \mathcal{C}}$ is the proposal probability from a configuration $\mathcal{C}$ to $\mathcal{C}_L$, and $\frac{W(\mathcal{C}_L)}{W(\mathcal{C})}$ the acceptance probability. The problem is that the modified gauge constraint on the lattice links $(n, 0)$ produce configurations $\mathcal{C}_L$ that differ from the standard configurations $\mathcal{C}$ globally, and the ratio $\frac{W(\mathcal{C}_L)}{W(\mathcal{C})}$ in Eq. (5.35) depends in general exponentially on the lattice volume, causing bad sampling. Indeed, the presence of the Polyakov loop modifies the allowed values of the plaquette occupation numbers on the temporal plaquettes crossed by the Polyakov loop, and this "flux defect" propagates to the entire lattice.

5.2.4 Improving the Taylor expansion

The dualization that we discussed in the previous subsections, although exact, cannot be used as it stands to generate the statistical weights for arbitrary values of the dual variables as they get more and more expensive to compute for large occupation numbers. Continuum physics is expected to emerge above $\beta/2N \approx 1$, where the contributions of large plaquette occupation numbers cannot be neglected. To try to make contact with the continuum limit as much as possible, one wishes to find an expansion of the Wilson plaquette action of the

form

$$\prod_p \exp\left(\frac{\beta}{2N}\left(\operatorname{Tr} U_p + \operatorname{Tr} U_p^\dagger\right)\right) = \prod_p \sum_i a_i(\beta) F_i(U_p),\tag{5.36}$$

such that with a small number of coefficients a_i one captures larger β effects. This is achieved with a character expansion. Since the r.h.s. of Eq. (5.36) is a class function[4] of G, it can be expanded in the irreducible characters $\hat\chi_\lambda(U_p)$ of G. Considering for definiteness the case of $G = \mathrm{SU}(N)$, its irreducible representations R_λ are similar to the $\mathrm{U}(N)$ ones (see Sec. 4.1.1) with the additional constraint $\lambda_N = 0$. Any irrep can be thus associated to a partition λ with length at most $N - 1$. The formula in Eq. (4.29) is still valid for computing the dimension $D_{\lambda,N}$ of the irrep λ. Clearly in this case tensoring an irrep λ with a determinantal irrep does not have any effect since $\det U = 1$. The character expansion of the $\mathrm{SU}(N)$ Wilson action is [77]

$$\prod_p \exp\left(\frac{\beta}{2N}\left(\operatorname{Tr} U_p + \operatorname{Tr} U_p^\dagger\right)\right) = \prod_p \sum_\lambda u_\lambda(\beta/N)\,\hat\chi_\lambda(U_p),\tag{5.37}$$

$$u_\lambda(x) = \sum_{n=-\infty}^{+\infty} \det I_{\lambda_j - j + i + n}(x),\tag{5.38}$$

where $I_\alpha(x)$ are the modified Bessel functions of the first kind already introduced in the discussion of the Schwinger model, and $u_\lambda(\beta/N)$ the character coefficients. The character expansion has better convergency properties as compared to the Taylor expansion. The main reason why we did not make use of it from the beginning is that we could not obtain an analytic expression similar to Eq. (4.25) in the case where U_i^j and U_k^l are substituted by the matrix elements of the irreps $R_\lambda(U)$[5]. Moreover, it is not easy to get a posteriori a character-based dual representation from the one obtained with a Taylor expansion, as we did for the Schwinger model. This difficulty arises from the necessity of introducing the auxiliary variables: their form is indeed very specific to the expansion adopted, and switching from one to the other is no longer possible. Despite this fact, we can still try to use the character expansion in Eq. (5.37) to improve the coefficients $(\beta/2N)^{n_p + \bar n_p}$ of the Taylor expansion. To do so, we start writing the characters $\hat\chi_\lambda(U_p)$ in terms of power of traces of $U_p, U_p^\dagger$ and their powers. As explained in [77] this can be done systematically. For the low-lying representations

---

[4]A class function $f(g) \in \mathbb{C}, g \in G$ is a function that is invariant under group conjugation, i.e. $f(g) = f(g'gg'^{-1}), \forall g' \in G$.

[5]Although for $\mathrm{SU}(2)$ Cherrington et. al in [70, 71, 72] proposed an interesting dual form based on a character expansion supplied by the invariant intertwiners.

of $SU(N)$ one gets for instance

$$
\begin{aligned}
\hat{\chi}_{\{0,\dots\}}(U_p) &= 1\,, & D_{\lambda,N} &= 1\,, \\
\hat{\chi}_{\{1,0,\dots\}}(U_p) &= \mathrm{Tr}U_p\,, & D_{\lambda,N} &= N\,, \\
\hat{\chi}_{\underbrace{\{1,\dots,1,0\}}_{N}}(U_p) &= \mathrm{Tr}U_p^\dagger\,, & D_{\lambda,N} &= N\,,
\end{aligned}
$$

$$
\begin{aligned}
\hat{\chi}_{\{1,1,0,\dots\}}(U_p) &= \frac{\mathrm{Tr}[U_p]^2 - \mathrm{Tr}[U_p^2]}{2}\,, & D_{\lambda,N} &= \frac{N(N-1)}{2}\,, \\
\hat{\chi}_{\underbrace{\{1,\dots,1,0\}}_{N-1}}(U_p) &= \frac{\mathrm{Tr}[U_p^\dagger]^2 - \mathrm{Tr}[U_p^{\dagger 2}]}{2}\,, & D_{\lambda,N} &= \frac{N(N-1)}{2}\,, \\
\hat{\chi}_{\{2,0,\dots\}}(U_p) &= \frac{\mathrm{Tr}[U_p]^2 + \mathrm{Tr}[U_p^2]}{2}\,, & D_{\lambda,N} &= \frac{N(N+1)}{2}\,, \\
\hat{\chi}_{\underbrace{\{2,\dots,2,0\}}_{N}}(U_p) &= \frac{\mathrm{Tr}[U_p^\dagger]^2 + \mathrm{Tr}[U_p^{\dagger 2}]}{2}\,, & D_{\lambda,N} &= \frac{N(N+1)}{2}\,, \\
\hat{\chi}_{\underbrace{\{2,1,\dots,1,0\}}_{N}}(U_p) &= \mathrm{Tr}[U_p]\,\mathrm{Tr}[U_p^\dagger] - 1\,, & D_{\lambda,N} &= N^2 - 1\,. & (5.39)
\end{aligned}
$$

Traces of the form $\mathrm{Tr}[U_p^a]$ and $\mathrm{Tr}[U_p^{\dagger b}]$ can be in turn cast into power of traces of only U_p and $U_p^\dagger$ for both $SU(2)$ and $SU(3)$. This is essentially a consequence of the Cayley-Hamilton theorem. In the most relevant case of $SU(3)$, the characteristic polynomials of U_p and $U_p^\dagger$ are

$$
P_{U_p}(t) = \det\left(U_p - t\mathbb{1}\right) = -t^3 + \mathrm{Tr}[U_p]\,t^2 - \mathrm{Tr}[U_p^\dagger]t + 1\,, \qquad P_{U_p}(U_p) = 0\,, \qquad (5.40)
$$

$$
P_{U_p^\dagger}(t) = \det\left(U_p^\dagger - t\mathbb{1}\right) = -t^3 + \mathrm{Tr}[U_p^\dagger]\,t^2 - \mathrm{Tr}[U_p]t + 1\,, \qquad P_{U_p^\dagger}(U_p^\dagger) = 0\,, \qquad (5.41)
$$

This determines recursion relations between the traces $\mathrm{Tr}[U_p^a]$ and $\mathrm{Tr}[U_p^{\dagger b}]$ of the form

$$
\mathrm{Tr}[U_p^a] = \mathrm{Tr}[U_p]\mathrm{Tr}[U_p^{a-1}] - \mathrm{Tr}[U_p^\dagger]\,\mathrm{Tr}[U_p^{a-2}] + \mathrm{Tr}[U_p^{a-3}]\,, \qquad a \geq 3 \qquad (5.42)
$$

$$
\mathrm{Tr}[U_p^{\dagger b}] = \mathrm{Tr}[U_p^\dagger]\mathrm{Tr}[U_p^{\dagger b-1}] - \mathrm{Tr}[U_p]\,\mathrm{Tr}[U_p^{\dagger b-2}] + \mathrm{Tr}[U_p^{\dagger b-3}]\,, \qquad b \geq 3 \qquad (5.43)
$$

from which it is straightforward to show by induction that one can express traces of power of U_p and $U_p^\dagger$ only in terms of $\mathrm{Tr}[U_p]$ and $\mathrm{Tr}[U_p^\dagger]$. In particular, making use of the three-steps Lucas polynomials $L_n(x, \bar{x})$ defined by

$$
L_n(x, \bar{x}) \equiv \begin{cases} 3 & n = 0 \\ x & n = 1 \\ x^2 - 2\bar{x} & n = 2 \\ xL_{n-1}(x, \bar{x}) - \bar{x}L_{n-2}(x, \bar{x}) + L_{n-3}(x, \bar{x}) & n \geq 3 \end{cases} \qquad (5.44)
$$

we get

$$\text{Tr}[U_p^n] = L_n(L, L^*), \qquad \text{Tr}[U_p^{\dagger n}] = L_n(L^*, L), \qquad L = \text{Tr}[U_p], \tag{5.45}$$

and substituting back this expression into Eq. (5.39), one obtains an equality of the form

$$\hat{\chi}_\lambda(U_p) = \sum_{n_p, \bar{n}_p} c_\lambda(n_p, \bar{n}_p) \, \text{Tr}[U_p]^{n_p} \, \text{Tr}[U_p^\dagger]^{\bar{n}_p} \tag{5.46}$$

The coefficients $c_\lambda(n_p, \bar{n}_p)$ can be easily computed numerically for any λ. We can then truncate the character expansion Eq. (5.37), considering only those characters $\{\lambda\}_r$ for which the Taylor expansion of the corresponding Bessel function determinant starts at $\mathcal{O}(\beta^k)$ with $k \leq r$. For SU(3) this means neglecting all characters with $\lambda_1 > r$ since

$$u_\lambda(x) = a_\lambda x^{\lambda_1} + \mathcal{O}(x^{\lambda_1 + 1}). \tag{5.47}$$

Making use of the formulae in Eq. (5.39) and of the three-steps Lucas polynomials, we can then cast the expansion of the Wilson action into

$$\prod_p \exp\left(\frac{\beta}{6}\left(\text{Tr}\, U_p + \text{Tr}\, U_p^\dagger\right)\right) \approx \prod_p \sum_{n_p, \bar{n}_p} \alpha_{n_p, \bar{n}_p}^r(\beta) \, \text{Tr}[U_p]^{n_p} \, \text{Tr}[U_p^\dagger]^{\bar{n}_p}, \tag{5.48}$$

$$\alpha_{n_p, \bar{n}_p}^r(\beta) = \sum_{\{\lambda\}_r} c_\lambda(n_p, \bar{n}_p) \, u_\lambda(\beta/3). \tag{5.49}$$

The coefficients $\alpha_{n_p, \bar{n}_p}^r(\beta)$ can be used in place of the Taylor coefficients when truncating the expansion of the action. In the limit $r \to \infty$ one has to recover the usual Taylor expansion; hence

$$\lim_{r \to \infty} \alpha_{n_p, \bar{n}_p}^r(\beta) = \frac{1}{n_p! \bar{n}_p!}\left(\frac{\beta}{6}\right)^{n_p + \bar{n}_p}. \tag{5.50}$$

What is expected is that since they involve the character coefficients, the truncation can produce a better agreement with the full result. This will be explicitly shown in Sec. 5.3.3. The expression of the plaquette expectation value is now

$$\langle P \rangle = \frac{1}{L^D N_t} \frac{\partial \log \mathcal{Z}}{\partial \beta} = \frac{1}{L^D N_t} \sum_p \left\langle \frac{\partial_\beta \alpha_{n_p, \bar{n}_p}^r(\beta)}{\alpha_{n_p, \bar{n}_p}^r(\beta)} \right\rangle, \tag{5.51}$$
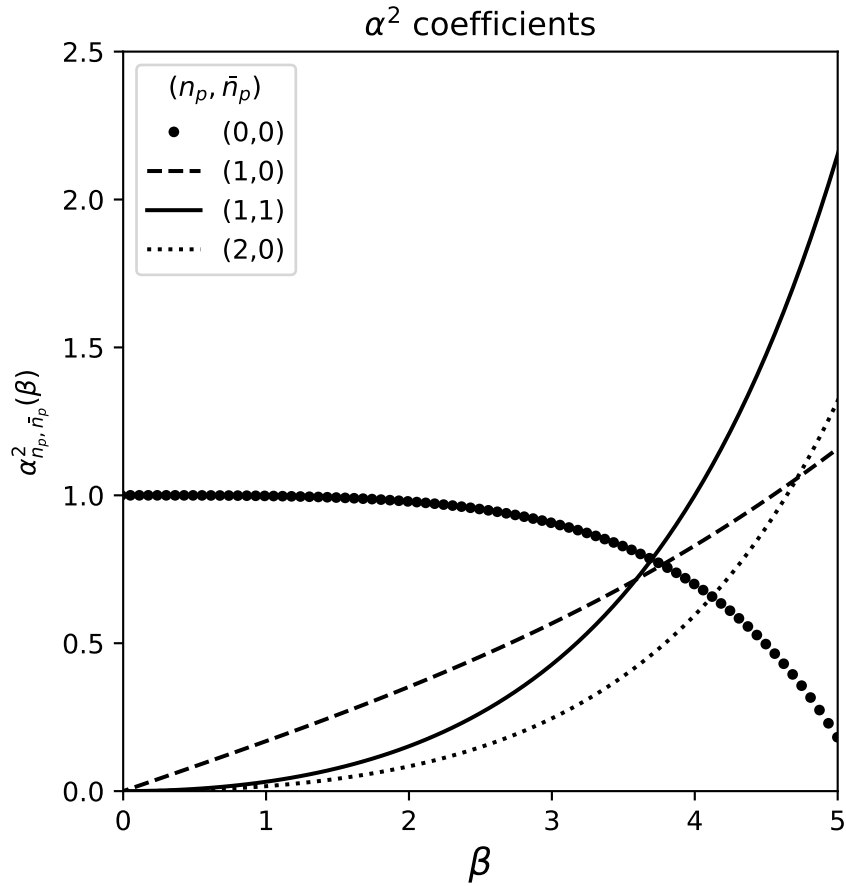
FIGURE 5.9: The behavior of the α^2 coefficients as a function of β. The numbers in round brackets correspond to the values $(n_p, \bar{n}_p)$.

while the α^r coefficients for SU(3) and $r = 2$ are:

$$\alpha^2_{0,0}(\beta) = u_{\{0\}}\left(\frac{\beta}{3}\right) - u_{\{2,1,0\}}\left(\frac{\beta}{3}\right) , \quad \alpha^2_{1,0}(\beta) = \alpha^2_{0,1}(\beta) = u_{\{1,0\}}\left(\frac{\beta}{3}\right) - u_{\{2,0,0\}}\left(\frac{\beta}{3}\right) ,$$

$$(5.52)$$

$$\alpha^2_{1,1}(\beta) = u_{\{2,1,0\}}\left(\frac{\beta}{3}\right) , \qquad\qquad \alpha^2_{2,0}(\beta) = \alpha^2_{0,2}(\beta) = u_{\{2,0,0\}}\left(\frac{\beta}{3}\right) . \qquad (5.53)$$

Some of the coefficients $\alpha^2_{n_p,\bar{n}_p}$ turn negative at some β^*. Therefore when performing simulations, the truncation of the character expansion must be carefully chosen. In Fig. 5.9 we show the behavior of the α^2 coefficients as a function of β.

5.3 Analysis of the β corrections

In this section we present our determination of the bubble diagrams $W_{\mathcal{B}_i}$ contributing to the partition function, for various truncations of the plaquette occupation numbers. The $\mathcal{O}(\beta^k)$

truncation is defined by only allowing bubble diagrams $\mathcal{B}_i$ satisfying $\sum_{p \in \mathcal{B}_i} \left(n_p + \bar{n}_p \right) \leq k$.
Enumerating the various contributions is fundamental to perform simulations at non-zero
β. The code we developed within this Ph.D. project is capable to compute automatically
bubble diagrams of arbitrary shape and truncation order β. A brief description of the al-
gorithm will be presented in App. (C). Here, as a first cross check we compute the $\mathcal{O}(\beta)$
diagrams, reobtaining the partition function used in [100]. We then move to the $\mathcal{O}(\beta^2)$ cor-
rections, where the structure of the tensor network is sufficiently simple that one can rewrite
the partition function in terms of scalar objects depending on the usual dual variables plus
only six DOI. For $\mathcal{O}(\beta^k), k \geq 3$, the bubble computation is still feasible, but the number of
DOI that need to be considered to have a fully local representation grows. So far we were
able to enumerate in four dimensions and for the most relevant case of SU(3), all diagrams
up to order β^4 and all planar bubble contributions up to order β^7. This was done on a single
CPU. For even higher orders, the most time consuming part is represented by the compu-
tation of the tensors T_n^ρ, i.e. the color contraction between the decoupling operators. This
computational barrier can be overcome by either modifying the code for parallel CPU us-
age, or by reaching a better understanding of the group theoretical structure of the tensors
T_n^ρ.

As a cross check of the formalism we developed, bubble contributions of higher order
(up to β^6) will be then resummed on small two dimensional volumes. The resulting partition
function, which is a polynomial in β, quark mass $\hat{m}_q$, and chemical potential $\hat{\mu}_q$, will be
compared with the result of hybrid Monte Carlo simulations, showing how the higher order
diagrams effectively induce a better agreement with the full result. A preliminary analysis
of the sign problem, with and without the DOI as dual degrees of freedom will be finally
presented.

5.3.1 Partition function at $\mathcal{O}\left(\beta\right)$

At $\mathcal{O}(\beta)$, the bubble diagrams are only made up of a single plaquette ($n_p = 1$) or antiplaque-
tte ($\bar{n}_p = 1$). The tensor networks associated to the bubbles are trivial at this order. Indeed,
as we are going to show, for any allowed background of dual variables, all tensors T_n^ρ (except
one) have only one non-zero element. The multiplicity from the bubble diagram containing
the "non-trivial" tensor can be however resummed locally, and one can express the partition
function only in terms of scalar site and link weights depending only on $\{n_p, \bar{n}_p, k_\ell, f_\ell, m_n\}$
without the DOI. To show this feature, we consider all possible tensors T_n^ρ at the corner of
the excited plaquette. For a general SU(N) theory, up to charge conjugation[6], there are two
classes of tensors: those where a single quark flux, oppositely oriented with respect to the

---

[6]i.e. exchanging the direction of all quark fluxes and at the same time swapping n_p and $\bar{n}_p$.
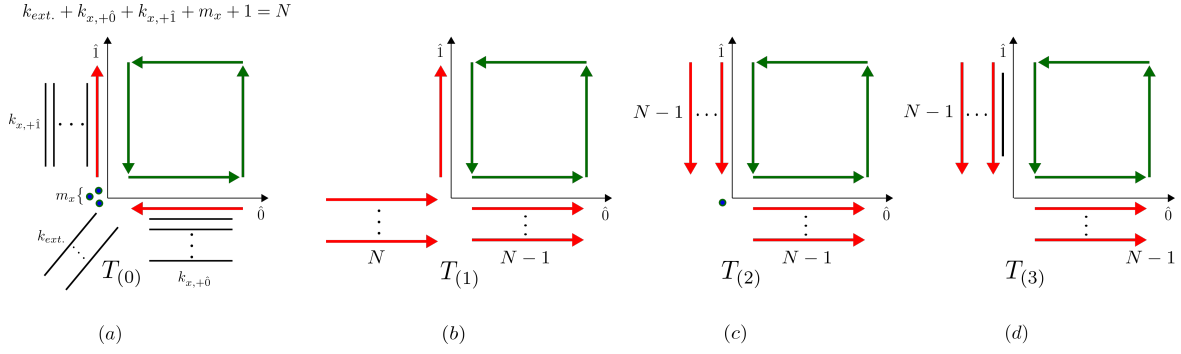
FIGURE 5.10: The four different types of tensor at a corner of the excited plaquette. (a) The U(N) contributions: two excited links are occupied by dimers and a single quark flux. (b) An incoming baryon ($f_\ell = N$) split into a ($N - 1$)-quark flux and a single quark flux. (c) An ($N - 1$)-quark flux travels in the same direction of the gauge flux. An external dimer or a monomer must be present in order to fulfill the Grassmann constraint. (d) As in (c) with a dimer superimposed to one of the two ($N - 1$)-quark fluxes.

plaquette, is superimposed to dimers (Fig. 5.10 (a)), and the ones corresponding to genuine SU(N) contributions (Fig. 5.10 (b)-(d)). The first is a U(N) contribution as the associated $\mathcal{I}$-integrals have $q = 0$. Let us start considering this case:

a) Even though the tensors corresponding to these diagrams can be quite large, the same decoupling that happens at strong coupling takes place in this case. Proceeding in a similar fashion as in Sec. 4.2.3, and with reference to Fig. 5.10 (a), one gets

$$T_{(0)}^{\rho_{-D}^n \cdots \rho_{+D}^n} = N! \left[\prod_{\mu_{\text{s.c.}}} \frac{1}{\sqrt{D_{\mathbb{1}^{k_{n,\mu_{\text{s.c.}}}},N}}} \delta_{\rho_{\mu_{\text{s.c.}}}^n, \mathbb{1}^{k_{n,\mu_{\text{s.c.}}}}} \right] \frac{\delta_{\rho_{+0}^n, \mathbb{1}^{k_{n,+0}+1}}}{\sqrt{D_{\mathbb{1}^{k_{n,+0}+1},N}}} \frac{\delta_{\rho_{+1}^n, \mathbb{1}^{k_{n,+1}+1}}}{\sqrt{D_{\mathbb{1}^{k_{n,+1}+1},N}}} , \tag{5.54}$$

where the first product runs over the external legs ($n, \mu_{\text{s.c.}}$). Thus, as in the strong coupling limit only the tensor element corresponding to the completely antisymmetric DOI is non-zero. The modification of the dimers weight is simply

$$w_\ell^1 (k_\ell) = \frac{1}{k_\ell!(k_\ell + 1)!} \frac{1}{D_{\mathbb{1}^{k_\ell+1},N}} = \frac{1}{k_\ell!(k_\ell + 1)!} \frac{(k_\ell + 1)!}{N(N - 1) \cdots (N - k_\ell)}$$

$$= \frac{(N - k_\ell - 1)!}{N! k_\ell!} , \tag{5.55}$$

which gives the correct link weight to be used when a dimer coexists with a quark flux on an excited link.

The genuine SU(N) contributions are instead of three types:

b) An incoming (strong coupling) baryon splits, at a corner of the excited plaquette, into a single quark flux and a ($N - 1$)-quark flux. Equivalently, a single quark flux and a ($N - 1$)-quark flux can recombine to form an outgoing (strong coupling) baryon (Fig. 5.10 (b)).

c) An incoming $(N-1)$-quark flux exits the site following the gauge flux induced by the plaquette. A monomer or an external dimer is also present in order to fulfill the Grassmann constraint (Fig. 5.10 (c)).

d) As in *c*) with the external dimer or monomer replaced by a dimer on one of the two excited links (Fig. 5.10 (d)).

The first two types of configurations are somewhat trivial as the associated tensors have size one. There is in fact only one DOI associated to the external legs of the two tensors. Their values can be readily computed

$$T_{(1)} = \frac{N!}{\sqrt{N}} \qquad T_{(2)} = (N-1)!. \tag{5.56}$$

In the case of the configurations of type d), the associated tensor has size 2×1. There are indeed two DOI in direction $\hat{1}$, where a dimer is superimposed to a $(N-1)$-quark flux. This tensor is given by[7]

$$T_{(3)}^{1,1} = \frac{N!}{\sqrt{N+1}} \qquad T_{(3)}^{1,2} = \frac{N!}{\sqrt{N(N+1)}}. \tag{5.57}$$

To remove this multiplicity, it is sufficient to exploit the fact that a link carrying a dimer plus a $(N-1)$-quark flux can only recombine with a $(N-1)$-quark flux from another direction because of the Grassmann constraint. The latter involves an $\mathcal{I}$-integral made up of a single decoupling operator, the epsilon tensor. Therefore, we can perform a local resummation of the two DOI by considering the following modified "tensor" of size 1

$$\tilde{T}_{(3)} = \sqrt{\left(T_{(3)}^{1,1}\right)^2 + \left(T_{(3)}^{1,2}\right)^2} = \frac{N!}{\sqrt{N}}. \tag{5.58}$$

In this way all T_n^ρ have been reduced to scalar quantities. It is easy to check that the modified dimer weights (Eq. (5.55)) and the values of $T_{(1)}, T_{(2)}, \tilde{T}_{(3)}$ together with the usual combinatorial factors from the Taylor expansion, are recovered by defining the following link and site weights at the boundary of the excited plaquette

1) If a link ℓ is occupied by $k_\ell \in \{0, \ldots, N-1\}$ dimers and a single quark flux ($f_\ell = \pm 1$), there is an associated factor $w_\ell^1(k_\ell)$.

2) To each $(N-1)$ quark flux superimposed to a dimer corresponds a link weight $v_{N-1,1} = \frac{(N-1)!}{N!} = \frac{1}{N}$.

---

[7]We only show the tensor indices associated to the direction $+0$ and $+1$.
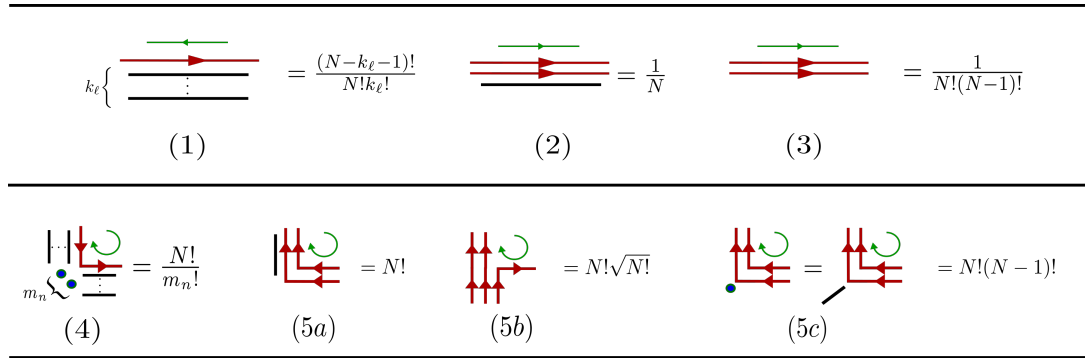
FIGURE 5.11: Modification of the link weights (upper line) and of the site weights (bottom line) induced by an elementary plaquette excitation for $N = 3$. The green arrow shows the direction of the gauge flux.

3) To each $(N - 1)$ quark flux corresponds a link weight $v_{N-1} = \frac{1}{N!(N-1)!}$.

4) At each corner n of the excited plaquette corresponding to a U(N) configuration (Fig. 5.10 (a)), the site weight is $N!/m_n!$.

5) At each corner n of the excited plaquette corresponding to a SU(N) configuration, there is a site weight $N!$ if there are no external dimers or baryons and if $m_n = 0$. Instead, the site weight is $N!\sqrt{N!}$ if there is an external baryon, while it is $N!(N - 1)!$ if there are external dimers or if $m_n = 1$.

The rules (1)-(5) together with the usual strong coupling weights define the $\mathcal{O}(\beta)$ partition function. The new link and site weights induced by the presence of the excited plaquette are graphically represented in Fig. 5.11. To compute the fermionic sign $\sigma_f(\ell)$ of a quark loop ℓ, the procedure described in Sec. 5.2.2 must be followed. At this order the partition functions has a very similar structure to the strong coupling one, with simple combinatorial factors at each site, link and plaquette. Multiple $\mathcal{O}(\beta)$ bubbles are allowed in the ensemble provided that they are disconnected[8]. Qualitatively, the main aspect arising at $\mathcal{O}(\beta)$ is that baryons and mesons are no longer point-like but can extend over one lattice spacing, and can interact via a gluon exchange. This system was studied for the first time via Monte Carlo in [100] for $G = $ SU(3). In Fig. 5.12 we show the evolution of the phase boundaries at finite chemical potential, when the $\mathcal{O}(\beta)$ corrections are included. The chiral transition temperature at $\hat{\mu}_q = 0$ decreases with β, being $aT_c^{\text{NP}} = 0.911(1)$ at $\beta = 0.6$. The various curves at constant β however intersect around the chiral tricritical point which only has a very mild β-dependence at this order. Also, the shape of the line of first order phase transitions is unaffected by the $\mathcal{O}(\beta)$ gauge corrections, and the chiral and nuclear transition are still degenerate. This is of course an artifact of the approximation, and higher orders in β are required to obtain the splitting expected in the continuum limit. However, at higher

---

[8]Two bubbles are connected if they share an edge or a corner.
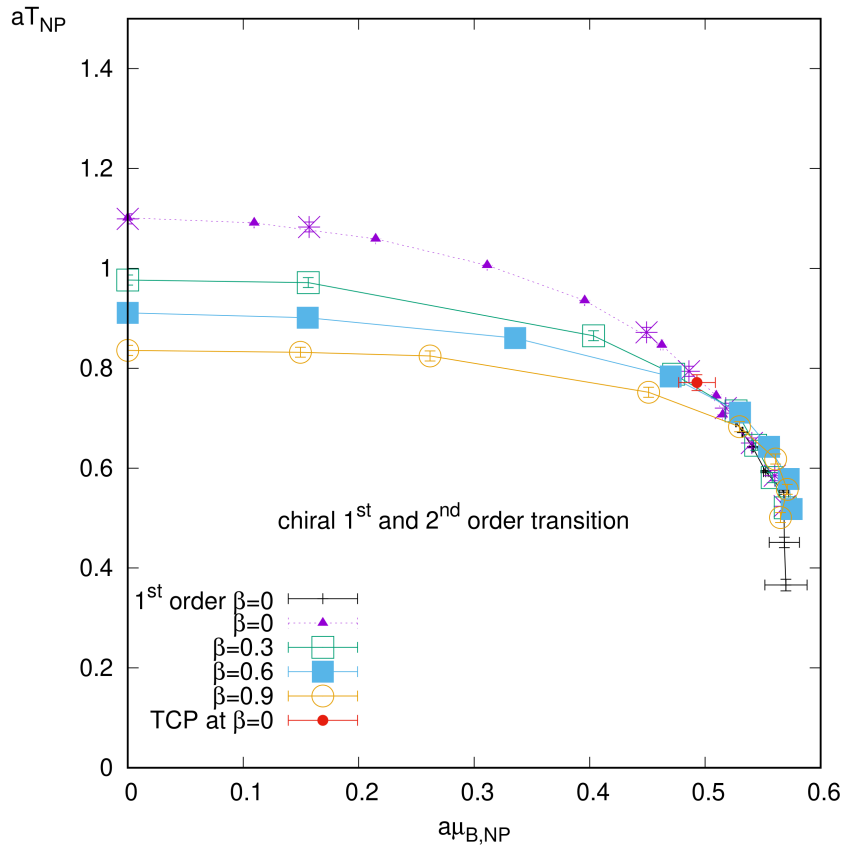
FIGURE 5.12: The chiral phase diagram including $\mathcal{O}(\beta)$ corrections from direct simulations on a $N_\sigma^3 \times 4$ lattice and for $G = SU(3)$. Both temperature aT and baryon chemical potential $\hat{\mu}_B = 3\hat{\mu}_q$ have been rescaled non-perturbatively (NP) as a consequence of the anisotropic calibration at finite β. From [101].

order in β, it is no longer possible to express the partition function only in terms of site and link weights integrating out locally all the DOI. In this case it is necessary to enumerate the bubble diagrams, and check explicitly how many DOI are needed in order to obtain a fully local expression in term of combinatorial factors. At $\mathcal{O}(\beta^2)$, as we are going to show, the structure of the tensor network within the bubbles is sufficiently simple that this number is minimal.

5.3.2 Partition function at $\mathcal{O}\left(\beta^2\right)$

As an application of the formalism we developed, we now consider the partition function at $\mathcal{O}(\beta^2)$ showing how the higher order corrections can be cast in a manageable form for Monte Carlo simulations. At order $\mathcal{O}(\beta^2)$ we allow for bubble contributions $\mathcal{B}_i$ with $\sum_{p \in \mathcal{B}_i} n_p + \bar{n}_p \leq 2$. The plaquette occupation numbers can be distributed within the bubbles,
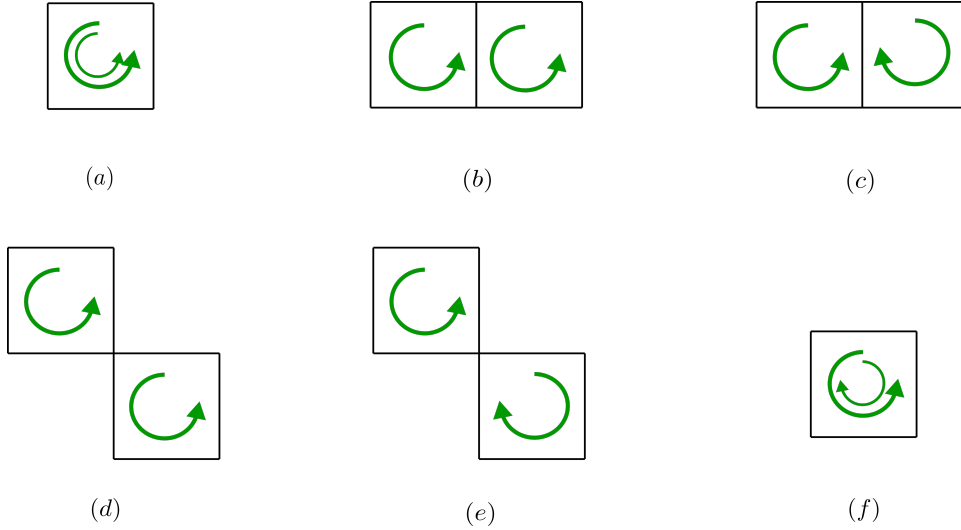
FIGURE 5.13: The six types of diagrams, up to charge conjugation, rotations, and foldings at $\mathcal{O}(\beta^2)$.

as shown in Fig. 5.13, in six different ways[9]. For all of them, except the SU(N) contributions of type (a), and the U(N) contributions of type (f), a fully local expression for their weights can be obtained integrating out locally all the DOI in favor of simple combinatorial factors as we did for the $\mathcal{O}(\beta)$ corrections. Since the procedure is quite involved, we only sketch it for some of the diagrams of type (a) and (b), and then only quote the final result. For the remaining diagrams instead, to obtain local weights we need to leave a number of DOI uncontracted, adding them as dual variables. The power of the decoupling operators is to render this number *minimal*, and the complexity of the resulting partition function is essentially the same as the $\mathcal{O}(\beta)$ one. At the same time it is possible to use directly the bubble weights, i.e. by contracting the (non-trivial) tensor network associated to these diagrams. When their number is not too large (as in this case), the bubbles can be sampled via reweighting. Since they are based on a resummation of DOI, this will always improve on the sign problem. We will show both procedures.

The U(N) contributions of type (a) are of the form depicted in Fig. 5.14 *left*. The great orthogonality theorem still applies, and the form of the tensors T_n^ρ at the corner of the doubly excited plaquette is

$$T_{(0)}^{\rho_{-D}^n \cdots \rho_{+D}^n} = N! \left[\prod_{\mu_{\text{s.c.}}} \frac{1}{\sqrt{D_{\mathbb{1}^{k_n,\mu_{\text{s.c.}}},N}}} \delta_{\rho_{\mu_{\text{s.c.}}}^n, \mathbb{1}^{k_n,\mu_{\text{s.c.}}}} \right] \frac{\delta_{\rho_{+0}^n, \mathbb{1}^{k_n,+0+2}}}{\sqrt{D_{\mathbb{1}^{k_n,+0+2},N}}} \frac{\delta_{\rho_{+1}^n, \mathbb{1}^{k_n,+1+2}}}{\sqrt{D_{\mathbb{1}^{k_n,+1+2},N}}} , \tag{5.59}$$

---

[9]Up to charge conjugation, rotations and foldings.

assuming that $(n, +0)$ and $(n, +1)$ are the two excited links. Hence, the weights of these bubble contributions can be obtained associating the combinatorial factors

$$\hat{w}_\ell^2(k_\ell, f_\ell = \pm 2) = \frac{(N - k_\ell - 2)!}{k_\ell! N!}, \tag{5.60}$$

to each of the excited links[10] since

$$\frac{1}{k_\ell!(k_\ell + 2)!} \frac{1}{D_{\mathbb{1}^{k_\ell + 2}, N}} = \frac{1}{k_\ell!(k_\ell + 2)!} \frac{(k_\ell + 2)!}{N(N-1)\ldots(N - k_\ell - 3)} = \frac{(N - k_\ell - 2)!}{k_\ell! N!}, \tag{5.61}$$

where the first factor on the r.h.s. comes as usual from the Taylor expansion of the staggered action. Concerning the diagrams of type (b), the only non-trivial part might be represented by the tensors at sites n_2 and n_5. For the U(N) contributions (Fig. 5.14 *middle*) however, the tensor network is still trivial because on the $\mathcal{O}(\beta)$ links (i.e. the links attached to only one excited plaquette), just the completely antisymmetric decoupling operator contributes as a consequence of the result derived in the previous subsection. The $\mathcal{O}(\beta)$ combinatorial factors can be thus used on the links surrounding the 2×1 bubble, whereas if the internal link is occupied by k_ℓ dimers, the corresponding link weight is

$$w_\ell^1(k_\ell) = \frac{(N - k_\ell - 1)!}{k_\ell! N!}, \tag{5.62}$$

essentially because the two gluonic color indices of the decoupling operators $P\rho_{-1}^{n_5}$ and $P\rho_{+1}^{n_2}$ combine with the ones of the decoupling operators $P\rho_\mu^{n} = \mathbb{1}^{kn, \mu+1}$ on the $\mathcal{O}(\beta)$ links, forming an additional quark-antiquark pair that gives rise to the factor $w_\ell^1(k_\ell)$. When instead SU(N) contributions are considered, e.g. the one in Fig. 5.14 *right*, although the tensors T_{n_2} and T_{n_5} are in general non-trivial if the internal link is occupied by dimers or traversed by quark fluxes, we can still obtain local weights by resumming *locally* the DOI. This is done observing that the indices of the tensors T_{n_2} and T_{n_5} corresponding to external links do not have multiplicity. The DOI shared by T_{n_2} and T_{n_5} can be thus contracted, and the result cast into modified (trivial) tensors $\tilde{T}_{n_2}$ and $\tilde{T}_{n_5}$ as shown in Fig. 5.15 for the SU(3) diagram in Fig. 5.14 *right*. Then, $\tilde{T}_{n_2}$ and $\tilde{T}_{n_5}$ induce a modification of the site weights at n_2 and n_5. This procedure is generalizable to all diagrams except the U(N) contributions of type (f) and the SU(N) contributions of type (a). The complete list of the resulting modified site and link weights is shown in Fig. 5.16. For the contributions of type (d) and (e) where two excited plaquettes only share a corner, the link weights are as in the $\mathcal{O}(\beta)$ partition function and only a modification of the site weight on the shared corner is induced.

For the U(N) contributions of type (e) and for the SU(N) contributions of type (a) this

---

[10]This statement is also true at $\mathcal{O}(\beta^3)$.

reduction does not work. In the first case there are six possible tensors (for $N = 3$) at the corner of the excited plaquette, depending on the dimer covering (Fig. 5.17). Their values are

$$T_n^{\rho_{+0}^n=1,\rho_{+1}^n}(1) = \begin{pmatrix} 2\sqrt{2} & 2 \end{pmatrix}, \qquad T_n^{\rho_{+0}^n=1,\rho_{+1}^n}(2) = \begin{pmatrix} 0 & 0 & 0 & 0 & 4\sqrt{\frac{2}{3}} & 2\sqrt{\frac{1}{3}} \end{pmatrix},$$

$$T_n^{\rho_{+0}^n,\rho_{+1}^n}(3) = \begin{pmatrix} 1 & \sqrt{2} \\ \sqrt{(2)} & 0 \end{pmatrix}, \qquad T_n^{\rho_{+0}^n,\rho_{+1}^n}(4) = \begin{pmatrix} 0 & 0 & 0 & 0 & 2\sqrt{\frac{1}{3}} & 2\sqrt{\frac{2}{3}} \\ 0 & 0 & 0 & 0 & 2\sqrt{\frac{2}{3}} & -2\sqrt{\frac{1}{3}} \end{pmatrix}, \qquad (5.63)$$

while $T_n(5)$ is a 23×1 matrix having only one non-zero element $T_n^{1,23}(5) = 6$, and trivially $T_n^{1,1}(6) = 6$. In the previous equation, the rows and columns of the matrices identify respectively the value of ρ_{+0}^n and ρ_{+1}^n. Although the tensors are non-trivial and the Boltzmann weights of the bubbles in Fig. 5.17 cannot be rewritten as a product of local combinatorial factors without the DOI, we can see the power of the decoupling operators: many DOI just do not contribute and a completely local expression for the partition function can be obtained considering the few contributing ones as dynamical variables. The full $\mathcal{O}(\beta)$ partition function, considering also the SU(3) contributions of type (a), can be obtained making use of only *six* DOI, associating specific site and link weights to them as shown in Fig. 5.18, where the complete list of the additional combinatorial factors is reported. For each link state there are at most two DOI. In Fig. 5.18 they are indicated with $\rho = \pm$. To obtain such coefficients we also made use of the freedom of rotating the decoupling operators via

$$\left(P'^{\rho'} \right)_i^\ell \equiv \sum_\rho V_{\rho',\rho} \left(P^\rho \right)_i^\ell, \qquad \left(P'^{\rho'} \right)_k^j \equiv \sum_\rho V_{\rho',\rho} \left(P^\rho \right)_k^j, \qquad V \in \mathrm{SO}\left(N_\rho \right). \qquad (5.64)$$

The $\mathcal{I}-$integral is indeed invariant under rotations in the decoupling operators space, and by choosing specific linear combinations one can reduce the number of contributing DOI. In term of the standard dual variables $\{n_p, \bar{n}_p, k_\ell, f_\ell, m_n\}$ and of the additional DOI, the full $\mathcal{O}(\beta^2)$ partition function is

$$\mathcal{Z}_{\beta^2}(\beta, \hat{m}_q, \hat{\mu}_q) = \sum_{\{n_p, \bar{n}_p, f_\ell, k_\ell, m_n, \rho_\mu^n\}} \sigma_f \prod_p \frac{(\beta/2N)^{n_p+\bar{n}_p}}{n_p! \bar{n}_p!} \prod_{\ell=(n,\mu)} \tilde{w}(\ell) \, e^{f_\ell \, \hat{\mu}_q \, \delta_{\mu,0}} \prod_n \tilde{w}(n) \, (2\hat{m}_q)^{m_n},$$

$$(5.65)$$

$$\tilde{w}\left(\ell = (n,\mu)\right) \equiv \tilde{w}\left(k_{n,\mu}, f_{n,\mu}, n_{(n,\mu,\nu)}, \bar{n}_{(n,\mu,\nu)}, \rho_\mu^n \right), \qquad (5.66)$$

$$\tilde{w}(n) \equiv \tilde{w}\left(k_{(n,\pm\mu)}, f_{(n,\pm\mu)}, n_{(n,\mu,\nu)}, \bar{n}_{(n,\mu,\nu)}, \rho_{\pm\mu}^n, m_n \right), \qquad (5.67)$$

where depending on the occupation numbers and on the six DOI ρ_μ^n, the factors $\tilde{w}_\ell$ and $\tilde{w}_n$ are respectively the link and site weights in Figs. 5.16 and 5.18.

At the same time, for the diagrams with non-trivial structure, it is possible to resum the
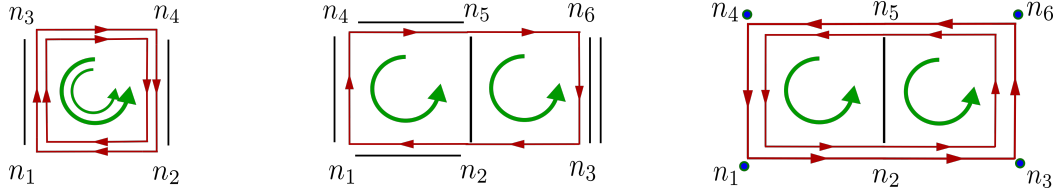
FIGURE 5.14: From left to right we show respectively typical U(3) diagrams of type (a) and (b), and a typical SU(3) contribution of type (c). In all these cases the bubble weights can be obtained associating combinatorial factors to each link and site of the bubble.

DOI in favor of the bubble weights $W_{\mathcal{B}_i}$. This computation has been automatized, and the result is reported in Tab. 5.2. This procedure generalizes to the higher orders. Our strategy is to precompute all tensors that are compatible with the truncation order, storing only the non-zero tensor elements. From the trivial tensors the modification of the site and link weights can be read automatically, while attention should be paid in order to identify the DOI that can be resummed locally. Clearly this computation is performed one time only since the tensor network does not depend on the simulation parameters. So far all $\mathcal{O}(\beta^4)$ tensors in four dimensions have been computed. The bubble weights can be instead obtained on the fly during Monte Carlo. Eventually these objects become too non-local to be effectively sampled via reweighting, and only the description in terms of the DOI should be used. In the latter case indeed the Svistunov-Prokofiev Worm algorithm can be directly applied.

At order $\mathcal{O}(\beta^k)$ with $k \geq 3$, non-planar geometries appear. Examples are provided in Fig. 5.19 for the cubic β corrections. The tensor network that give rise to these bubble diagrams is still very simple, and the number of contributing DOI small. In the case of the diagrams shown, the tensors at sites n_1 and n_2 are

$$T_{n_1}^{\rho_{+1}^{n_1}}(a) = T_{n_2}^{\rho_{-1}^{n_2}}(a) = \begin{pmatrix} 1 & \frac{1}{3} & \frac{\sqrt{2}}{3} \end{pmatrix} \tag{5.68}$$

$$T_{n_1}^{\rho_{+1}^{n_1}}(b) = T_{n_2}^{\rho_{-1}^{n_2}}(b) = \begin{pmatrix} 0 & 0 & 0 & 0 & 0 & \sqrt{\frac{2}{3}} \end{pmatrix}, \tag{5.69}$$

where we only show the non-trivial DOI associated to the link $(n_1, +1) = (n_2, -1)$ shared by the three plaquettes. From the tensors, the modification of the site and link weights is readily obtained in a similar fashion as for the $\mathcal{O}(\beta^2)$ corrections. The orthogonal basis which we used to define the decoupling operators, has the merit of producing a small number of non-zero tensor elements T_n^{ρ}. Although we know that this must be related to the great orthogonality theorem, and in some cases we were able to show this explicitly, we did not succeed obtaining a set of rules to determine *beforehand* what are in general the contributing DOI. The solution to this problem, which requires a better group theoretical understanding of Eq. (5.18), will heavily influence the maximum order reachable in numerical simulations.

$$T_{n_5}^{\rho_{-1}^{n_5},1,1} = 2 \begin{pmatrix} \sqrt{\frac{2}{3}} \\ \frac{1}{\sqrt{3}} \end{pmatrix}$$

$$\tilde{T}_{n_5}^{1,1,1} = 2$$

$$\sum_{\rho_{-1}^{n_5}=\rho_{+1}^{n_2}}$$

$$T_{n_2}^{1,1,\rho_{-1}^{n_2}} = 2 \left(\sqrt{\frac{2}{3}} \quad \frac{1}{\sqrt{3}} \right)$$

$$\tilde{T}_{n_2}^{1,1,1} = 2$$

$$\tilde{T}_{n_2}^{1,1,1} = \tilde{T}_{n_5}^{1,1,1} \equiv \sqrt{T_{n_2}^{1,1,1} T_{n_5}^{1,1,1} + T_{n_2}^{1,1,2} T_{n_5}^{2,1,1}}$$

FIGURE 5.15: Example of resummation of DOI. The only non-trivial part of the tensors $T_{n_2}^{\rho}$ and $T_{n_5}^{\rho}$ corresponds to the DOI ρ in direction $(n_2, +1) = (n_5, -1)$. We contract the two tensors in this direction and cast the result into scalar quantities $\tilde{T}_{n_2} = \tilde{T}_{n_5}$.

5.3.3 Cross checks from exact enumeration

In this section we present our results concerning the comparison between the bubble evaluation in the dual representation, and hybrid Monte Carlo (HMC) simulations. This comparison was carried out as a preliminary step before performing Monte Carlo simulations in order to cross check the correctness of the dual formalism and of our implementation. On a finite volume, the partition function $\mathcal{Z}$ is always a finite polynomial $\mathcal{P}\left(\beta, \hat{m}_q, \hat{\mu}_q\right)$ in β, quark mass $\hat{m}_q$ and fugacity $e^{\hat{\mu}_q}$. For various truncation of the β expansion we exactly computed the polynomials $\mathcal{P}$ on a 2×2 and 4×4 lattice with periodic boundary conditions in all directions. To do so, we first evaluated all tensors T^ρ appearing for a given truncation of the plaquette occupation numbers, and then enumerated all admissible combinations of $\{n_p, \bar{n}_p, k_\ell, d_\ell, m_n\}$ for various gauge groups. For each combination, the corresponding tensor network was then contracted, and the fermionic sign σ_f computed according to the recipe described in Sec. 5.2.2. The resulting value contributes to a given coefficient of the polynomial $\mathcal{P}$, depending on the monomer number m_n, the total quark flux in temporal direction $\sum_n f_{n,0}$, and the plaquette occupation numbers $\sum_p (n_p + \bar{n}_p)$. For fixed truncation $\mathcal{O}(\beta^k)$, the number of admissible configurations grows very large increasing the number of dimensions; hence we could not perform the exact enumeration in dimensions $D + 1 > 2$. Nevertheless, as our dual formulation does not present any fundamental difference when applied to higher dimensions, this cross check gives some indications about its validity in $D + 1 = 3, 4$. Moreover, in doing this comparison we did not take advantage of any resummation of DOI: our main goal was to verify the capability of the dual formulation to correctly reproduce the β dependence of various observables, and to validate our algorithms

FIGURE 5.16: The list of combinatorial factors for all diagrams (a)-(f), excluding the $SU(N)$ contributions of type (a) and the $U(N)$ contributions of type (f). In the upper part of the figure we show the link weights, whereas the bottom part contains the list of the modified site weights. The last two site weights do not depend on how the remaining quark-antiquark pair is distributed on the links attached to the second plaquette. Site states that are not shown, carry the strong coupling factor $N!/m_n!$ while at the corner of a single excited plaquette the combinatorial factors in Fig. 5.11 must be used. The green arrows show the direction of the gauge flux.
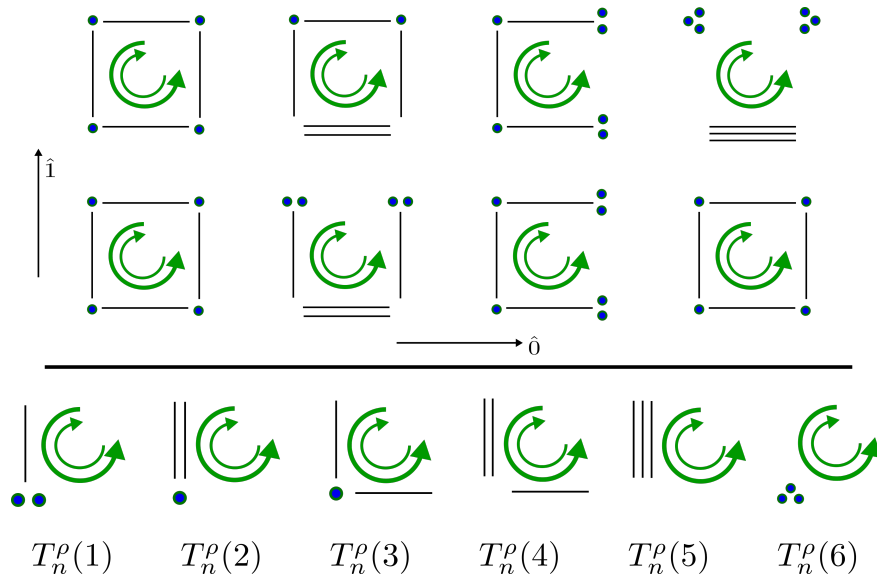
FIGURE 5.17: Depending on the dimer covering, there are six possible tensors at the corner of the plaquette with $n_p = \bar{n}_p = 1$. $T_n^\rho(6)$ is just a scalar because there is only one DOI on the links $(n, +0)$ and $(n, +1)$.
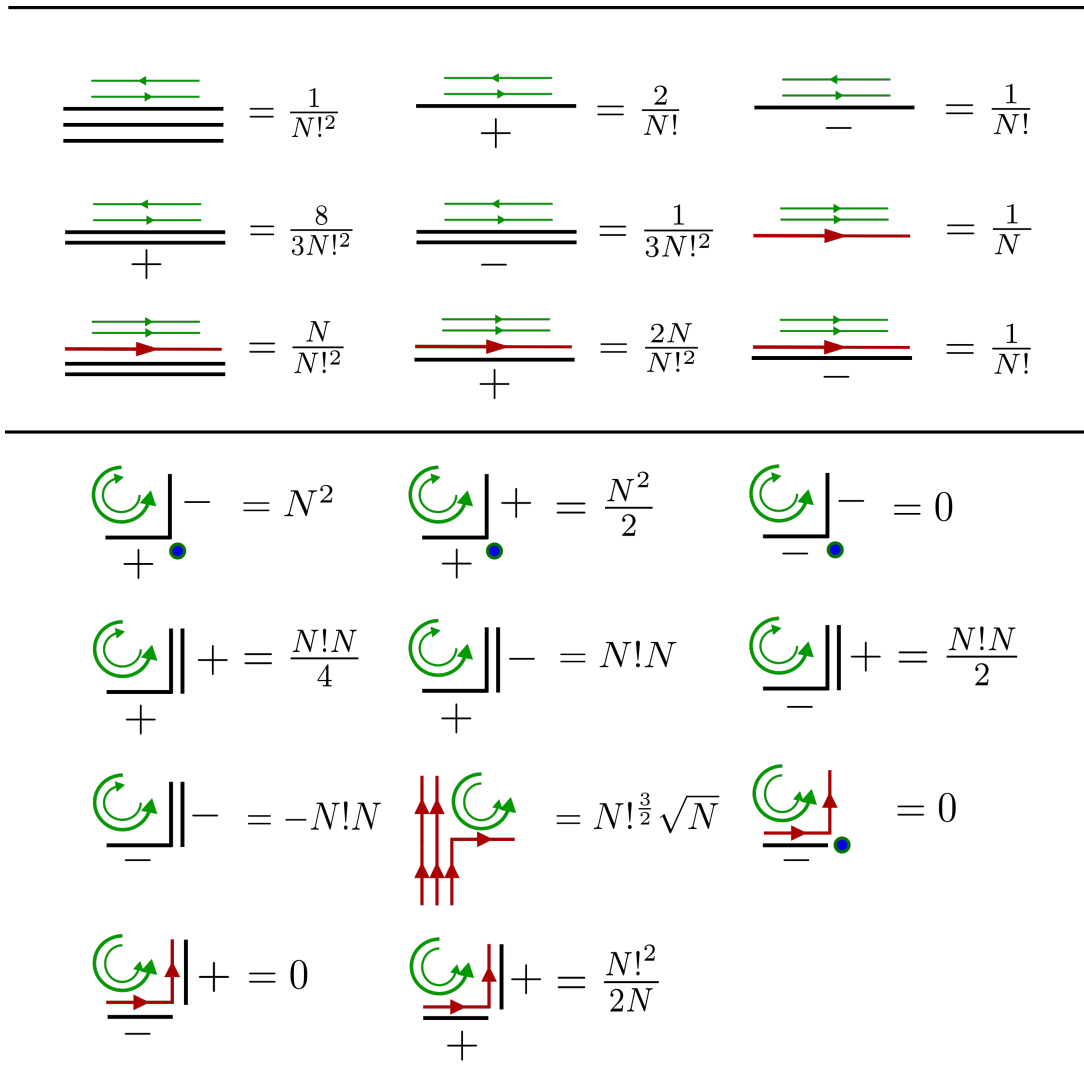
FIGURE 5.18: The list of combinatorial factors for the SU(N) diagrams of type (a) and the U(N) diagrams of type (f). In the upper part of the figure we show the link weights, in the lower the modified site weights. In all cases there are at most two DOI per link, which are identified in the figure by $\pm$. The six DOI appearing can be then made dynamical and sampled along with the standard occupation numbers. Although the N dependence is made explicit, these results only hold for $N = 3$.

$(n_p, \bar{n}_p)$	(k_1, f_1)	(k_2, f_2)	(k_3, f_3)	(k_4, f_4)	$W_{\mathcal{B}_i}$
$(1,1)$	$(0,0)$	$(0,0)$	$(0,0)$	$(0,0)$	1
$(1,1)$	$(3,0)$	$(0,0)$	$(0,0)$	$(0,0)$	1
$(1,1)$	$(2,0)$	$(0,0)$	$(0,0)$	$(0,0)$	3
$(1,1)$	$(1,0)$	$(0,0)$	$(0,0)$	$(0,0)$	3
$(1,1)$	$(1,0)$	$(1,0)$	$(0,0)$	$(0,0)$	6
$(1,1)$	$(1,0)$	$(1,0)$	$(1,0)$	$(0,0)$	12
$(1,1)$	$(1,0)$	$(1,0)$	$(1,0)$	$(1,0)$	17
$(1,1)$	$(2,0)$	$(1,0)$	$(0,0)$	$(0,0)$	3
$(1,1)$	$(2,0)$	$(1,0)$	$(1,0)$	$(0,0)$	6
$(1,1)$	$(2,0)$	$(1,0)$	$(1,0)$	$(1,0)$	5
$(1,1)$	$(2,0)$	$(1,0)$	$(0,0)$	$(1,0)$	3
$(1,1)$	$(2,0)$	$(1,0)$	$(2,0)$	$(0,0)$	3
$(1,1)$	$(2,0)$	$(1,0)$	$(2,0)$	$(1,0)$	2
$(2,0)$	$(0,1)$	$(0,1)$	$(0,-1)$	$(0,-1)$	0.5
$(2,0)$	$(1,1)$	$(0,1)$	$(0,-1)$	$(0,-1)$	1
$(2,0)$	$(1,1)$	$(1,1)$	$(0,-1)$	$(0,-1)$	1
$(2,0)$	$(1,1)$	$(0,1)$	$(1,-1)$	$(0,-1)$	2
$(2,0)$	$(1,1)$	$(1,1)$	$(1,-1)$	$(0,-1)$	1
$(2,0)$	$(1,1)$	$(1,1)$	$(1,-1)$	$(1,-1)$	1
$(2,0)$	$(2,1)$	$(0,1)$	$(0,-1)$	$(0,-1)$	0.5
$(2,0)$	$(2,1)$	$(0,1)$	$(2,-1)$	$(0,-1)$	0.5
$(2,0)$	$(2,1)$	$(0,1)$	$(1,-1)$	$(0,-1)$	1
$(2,0)$	$(0,1)$	$(0,1)$	$(0,-1)$	$(2,0)$	3
$(2,0)$	$(0,1)$	$(1,1)$	$(0,-1)$	$(2,0)$	6
$(2,0)$	$(0,1)$	$(0,1)$	$(2,0)$	$(2,0)$	3
$(2,0)$	$(0,1)$	$(0,-2)$	$(0,-1)$	$(0,2)$	18

TABLE 5.2: The list of bubble weights $W_{\mathcal{B}_i}$ (up to rotations, charge conjugation, and foldings) corresponding to the bubble diagrams of type (a) and (e) for which the tensor network is non-trivial. Since they are all made by a doubly excited plaquette, to identify a given diagram it is sufficient to specify the link states $((k_i, f_i), \ i = 1, \ldots, 4)$ and the corresponding plaquette occupation numbers $(n_p, \bar{n}_p)$. Links are ordered such that $U_p = U_1 U_2 U_3^\dagger U_4^\dagger$. Fermionically disconnected diagrams are not shown since at this order they are the product of their fermionically connected components. The combinatorial factors from the Taylor expansion have been included in the values of the weights $W_{\mathcal{B}_i}$. We only considered bubbles without external dimers. When $k_{n,\mu}$ external dimers are attached to a given site n, the correction factor $m_n!/(m_n - k_{n,\mu})!$ must be included.
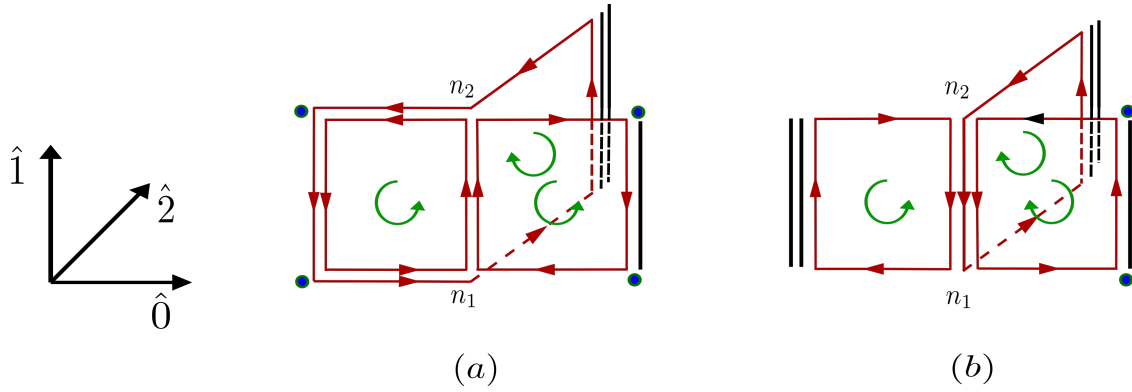
FIGURE 5.19: Example of non-planar bubble diagrams at order $\mathcal{O}(\beta^3)$. The $\mathcal{O}(\beta)$ site and link weights can be used everywhere except at sites n_1 and n_2, and on the link shared by the three excited plaquettes. The modification of the weights can be obtained from the tensors $T^{\rho}_{n_1}$ and $T^{\rho}_{n_2}$ in Eq. (5.68).

G	2×2	4×4
U(2)	$\mathcal{O}(\beta^7)$	$\mathcal{O}(\beta^2)$
U(3)	$\mathcal{O}(\beta^6)$	$\mathcal{O}(\beta^2)$
SU(2)	$\mathcal{O}(\beta^6)$	$\mathcal{O}(\beta^2)$
SU(3)	$\mathcal{O}(\beta^4)$	$\mathcal{O}(\beta^2)$

TABLE 5.3: The maximum order in the β expansion considered, depending on the gauge group G and on the lattice size.

for the computation and contraction of the decoupling operators. We considered four different gauge groups: U(2), U(3), SU(2) and SU(3). The complexity of the enumeration clearly depends on the chosen group, and different orders of the β expansion could be reached depending on G. The list of the maximum orders considered is reported in Tab. 5.3. From the polynomial $\mathcal{P}\left(\beta, \hat{m}_q, \hat{\mu}_q\right)$ several observables can be computed. Derivative observables such as the chiral condensate $\langle \bar{\psi}\psi \rangle$, chiral susceptibility $\chi_{\bar{\psi}\psi}$, average plaquette $\langle P \rangle$ and plaquette susceptibility χ_P, can be determined from the mass and β derivatives of $\mathcal{P}$. The Polyakov loop $\langle L(\vec{n}) \rangle$ can instead be computed as the following ratio

$$\langle L(\vec{n}) \rangle = \frac{1}{N} \frac{\mathcal{P}_{\vec{n}}(\beta, \hat{m}_q, \hat{\mu}_q)}{\mathcal{P}(\beta, \hat{m}_q, \hat{\mu}_q)}, \tag{5.70}$$

where $\mathcal{P}_{\vec{n}}(\beta, \hat{m}_q, \hat{\mu}_q)$ is the polynomial obtained from the modified tensor network with a Polyakov loop insertion at $\vec{n}$, truncated at the same order $\mathcal{O}(\beta^k)$ as $\mathcal{P}$. As we illustrated in Sec. 5.2.3, the presence of the Polyakov loop modifies the gauge constraint on the temporal links $((\tau, \vec{n}), 0)$, and gives rise to the modified tensors $\tilde{T}^{\rho}_{\vec{n}}$. The result of the comparison with HMC simulations on the 2×2 lattice, for the four different gauge groups, is reported in Figs. 5.20 and 5.21 for $G = $ U(2) and U(3), and in Figs 5.22 and 5.23 for SU(2) and SU(3). For

G	$\mathcal{O}(\beta)$	$\mathcal{O}(\beta^2)$	$\mathcal{O}(\beta^3)$	$\mathcal{O}(\beta^4)$	$\mathcal{O}(\beta^5)$	$\mathcal{O}(\beta^6)$	$\mathcal{O}(\beta^7)$
U(2)	55	215	639	2 079	6 007	19 125	55 973
U(3)	155	655	2 279	8 687	31 617	124 680	//
SU(2)	91	379	1 355	4 478	17 370	53 408	//
SU(3)	255	1 499	8 939	52 571	//	//	//

TABLE 5.4: The number of non-zero tensor elements entering the exact evaluation of the polynomials $\mathcal{P}\left(\beta, \hat{m}_q, \hat{\mu}_q\right)$ as a function of the truncation order and of the gauge group G.

the latter two we also plot the behavior of the polynomials $\mathcal{P}_{\hat{\chi}}(\beta, \hat{m}_q, \hat{\mu}_q)$ obtained making use of the character expansion inspired coefficients $\alpha_{n_p, \bar{n}_p}(\beta)$ in place of $\beta^{n_p + \bar{n}_p}/(n_p! \bar{n}_p!)$ (see Sec. 5.2.4). For all gauge groups we show the chiral condensate, the average plaquette and the Polyakov loop. Concerning HMC simulations, 10^5 trajectories were generated for each value of the parameters.

As it is clear from Figs. 5.20, 5.21, 5.22 and 5.23, the higher order terms on the 2×2 lattice correctly reproduce the β dependence of the observables. When the Taylor coefficients $\beta^{n_p + \bar{n}_p}/(n_p! \bar{n}_p!)$ are used, the agreement with the HMC results extends (for the largest order considered) up to $\beta \approx 1.5 - 2$ for U(2) and U(3), and up to $\beta \approx 1 - 1.5$ for SU(2) and SU(3). For the latter the computation was performed only up to $\mathcal{O}(\beta^4)$ because the evaluation of all valid configurations becomes too time consuming in the case of the $\mathcal{O}(\beta^5)$ corrections. Remarkably, when the character expansion inspired coefficients are used (i.e. $\alpha^1(\beta)$ and $\alpha^2(\beta)$), the agreement extends to larger β values and especially in the case of the average plaquette, the analytic curves remain always close to the full result. We recall that the α^2 coefficients only correspond to a truncation of the plaquette occupation numbers up to two. The usage of the α coefficients, which are linear combinations of Bessel function determinants, avoids the presence of the artifact from the definition of the plaquette expectation value in the dual representation (see Sec. 5.2.3), which no longer goes to zero at large β.

On the 4×4 lattice instead, given the very large number of admissible configurations, it was only possible to cross check the $\mathcal{O}(\beta^2)$ corrections for U(2) and U(3), which however correctly reproduce the linear behavior of the average plaquette and of the chiral condensate (Fig. 5.24).

Overall, the main outcome of this comparison is that the higher order corrections correctly reproduce the strong coupling branch for different quark masses. The high number of tensor elements considered (see Tab. 5.4), and the sensitivity of the final result to the correct computation of the fermionic sign σ_f, shows that the tensors T_n^ρ are correctly computed and the formalism we developed can be trusted. Although the computation of the tensor and

of the bubble weights $W_{\mathcal{B}_i}$ has been automatized, and works in principle for every trunca-tion $\mathcal{O}(\beta^k)$, to obtain a representation of the partition function that is applicable in Monte Carlo simulations without invoking the reweighting of the bubbles, it is fundamental to identify the DOI that can be resummed locally (as we did for the $\mathcal{O}(\beta^2)$ corrections in the previous subsection), and disregard the ones that do not contribute. Only in this way nu-merical simulations in large four-dimensional volumes can be feasible. For the $\mathcal{O}(\beta^3)$ and $\mathcal{O}(\beta^4)$ corrections this is still doable by analyzing case by case the structure of the tensor network within the (not so large) number of bubble diagrams appearing. Concerning the higher orders, there are still issue that need to be investigated further. First of all, as we already mentioned, the computation of the tensors T_n^ρ gets more and more time consum-ing. One possible way to mitigate this problem consists in analyzing the group theoretical structure of the contraction of the decoupling operators. An important step in this direction would be to know before the contraction of the color indices, what are the DOI that con-tribute depending on the background of occupation numbers. This would make it easier to identify the DOI that can be resummed, reducing drastically the complexity of the partition function. At the same time, numerical improvements of the contraction routine, and the parallelization of the code we developed, would be desirable.

As a preliminary evaluation of the severity of the sign problem when including higher order corrections, we plotted in Fig. 5.25 the average signs $\langle\sigma\rangle = \langle\sigma_f\sigma_\rho\rangle$ and $\langle\sigma_f\rangle$ for SU(3), as obtained on the 2×2 lattice for various truncation of the β expansion. The first observable encodes the information about the sign fluctuations induced by the fermions and by the tensor network, while $\langle\sigma_f\rangle$ gives information about the severity of the sign problem in the DOI-resummed representation of the partition function. In formulae we have

$$\langle\sigma_f\rangle \equiv \frac{\mathcal{Z}}{\mathcal{Z}_1^{\text{p.q.}}}, \qquad \langle\sigma\rangle \equiv \frac{\mathcal{Z}}{\mathcal{Z}_2^{\text{p.q.}}}, \qquad \langle\sigma\rangle \leq \langle\sigma_f\rangle, \tag{5.71}$$

where $\mathcal{Z}_1^{\text{p.q.}}$ is obtained setting $\sigma_f = 1$, while in $\mathcal{Z}_2^{\text{p.q.}}$ we also take the absolute value of each tensor element $T_n^\rho \rightarrow |T_n^\rho|$. Despite the smallness of the volume considered, which does not give quantitative information about the magnitude of the sign problem in large four-dimensional volumes, it is still worth to compare the behavior of the different orders. As the figure shows, in the DOI resummed representation, by increasing the truncation order, the sign $\langle\sigma_f\rangle$ does not worsen (it slightly improves), making reasonable to expect for the higher order terms, the same sign problem induced by the $\mathcal{O}(\beta)$ corrections. However this result must be taken *cum grano salis*: many fermion loop geometries are not allowed on this small volume, therefore we cannot rule out that on a larger volume the behavior will be different. If this preliminary result turns out to be correct, it will imply that numerical simulations are feasible in four dimensions up to $\beta \approx 1 - 2$, which corresponds to the value

where the $\mathcal{O}(\beta)$ partition function cannot be sampled anymore by sign reweighting. When considering also the negative sign induced by the tensor network (Fig. 5.25 *left*), the signal shows a deterioration for $\beta \geq 1$ both at zero and non-zero density. Whether this constitutes a no-go for numerical simulations employing the partition function with locally resummed DOI (thus with a milder sign problem), it is only to be seen in practice. The Monte Carlo simulations are currently in preparation. The important message is that with respect to the permutation basis in terms of Weingarten functions (Sec. 4.1.2), the improvement is drastic.
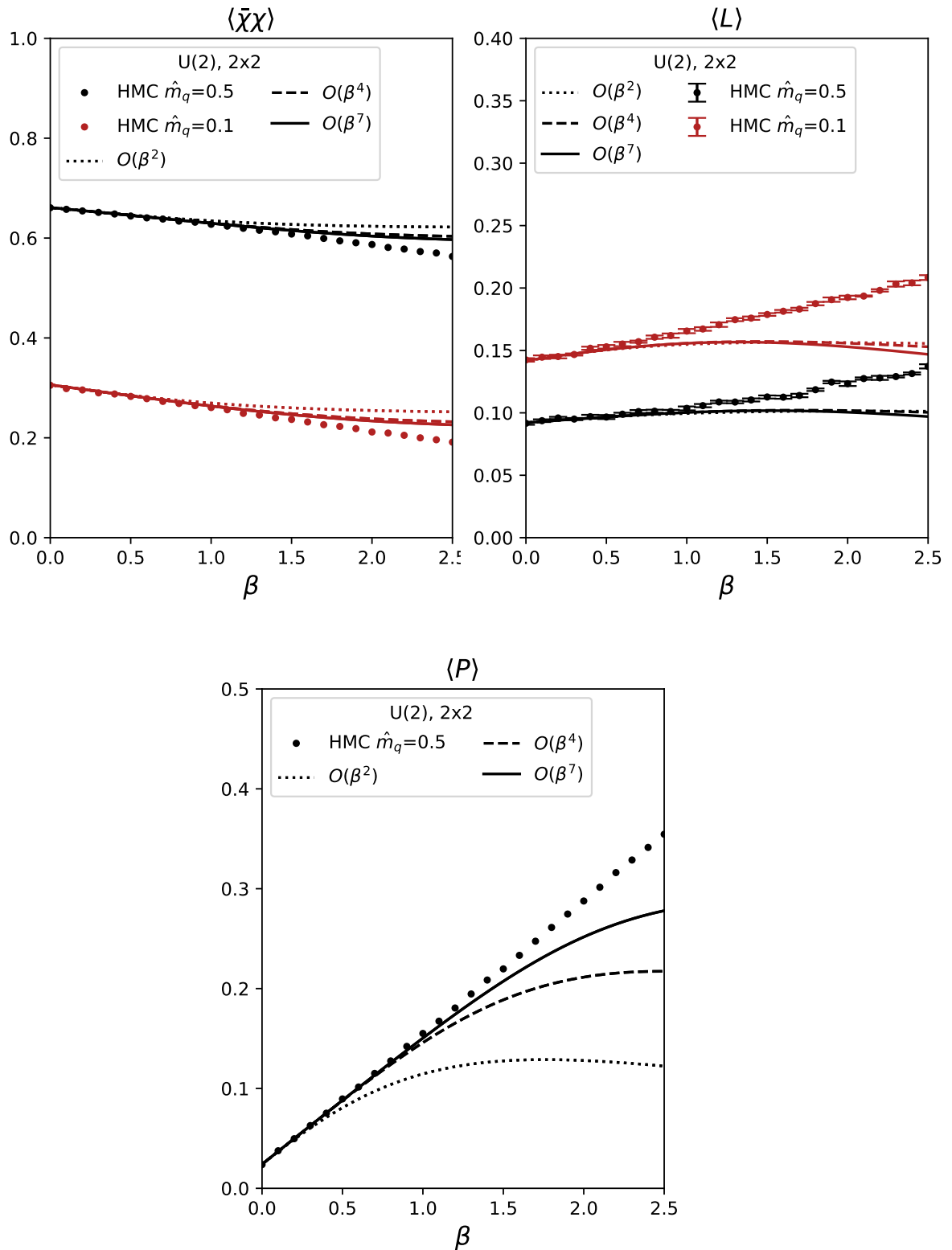
FIGURE 5.20: The chiral condensate $\langle \bar{\chi}\chi \rangle$, the average plaquette $\langle P \rangle$, and the Polyakov loop $\langle L \rangle$ for $G = \mathrm{U}(2)$. The HMC results are plotted against the polynomials $\mathcal{P}(\beta, \hat{m}_q, \hat{\mu}_q)$ for various truncation of the β expansion. The average plaquette $\langle P \rangle$ has only a mild quark mass dependence; hence it is plotted only for one value of the bare quark mass $\hat{m}_q = 0.5$ for visualization purposes. Error bars that are not shown are smaller than the point size.
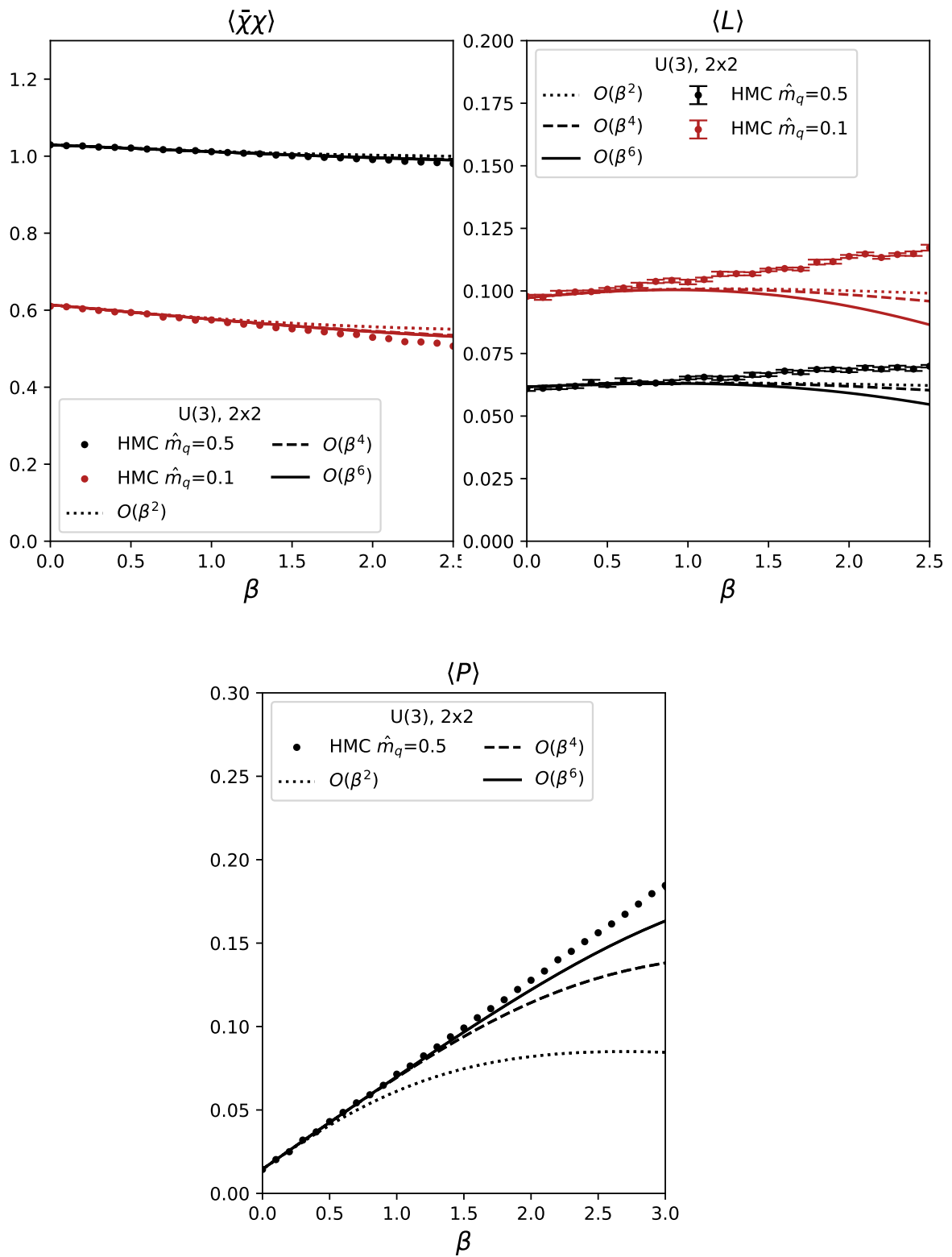
FIGURE 5.21: Same as in Fig. 5.20 for $G = \mathrm{U}(3)$.
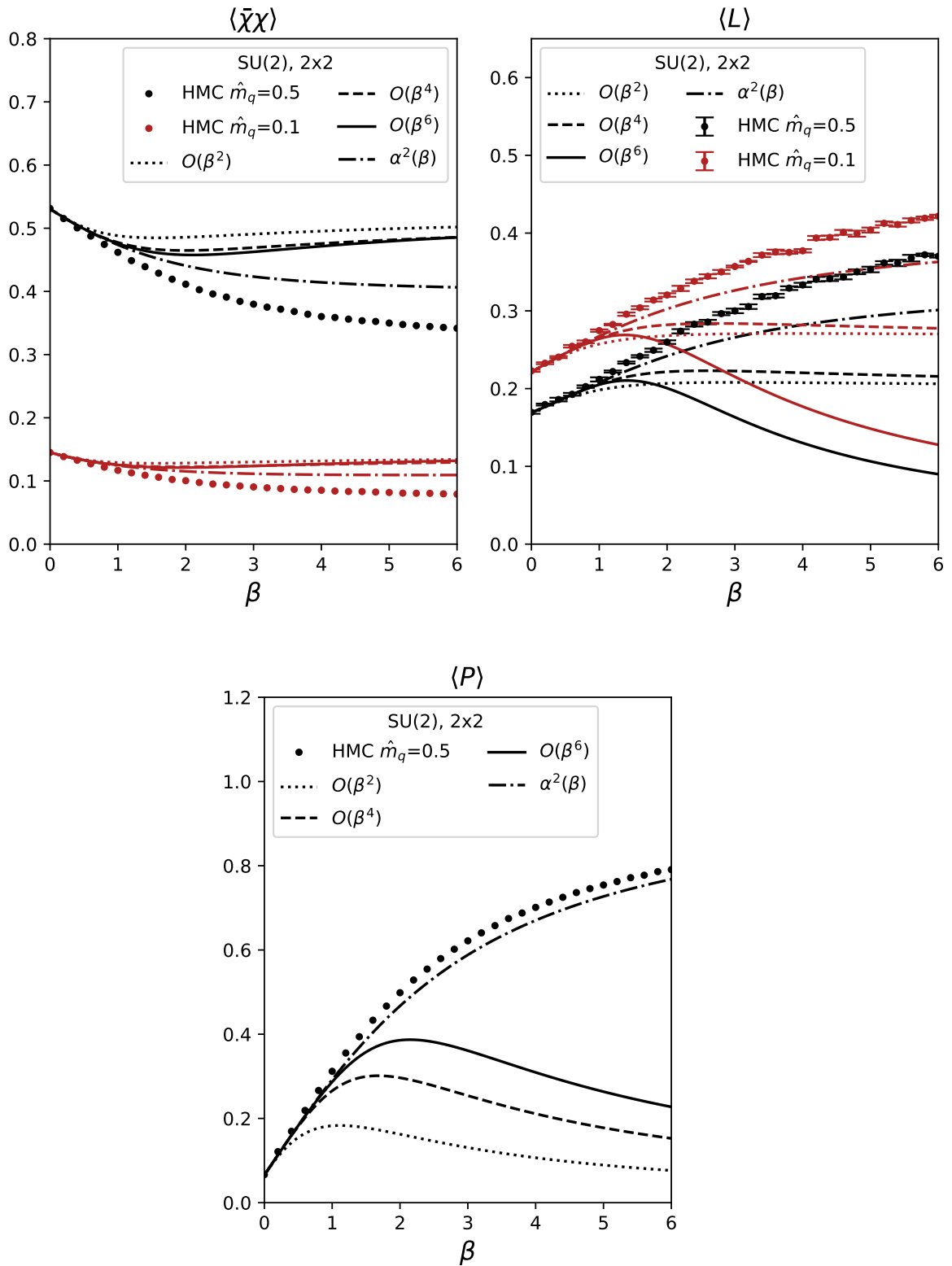
FIGURE 5.22: Same as in Fig. 5.20 for $G = SU(2)$. In this case we also plotted the polynomials $\mathcal{P}_{\hat{\chi}}(\beta, \hat{m}_q, \hat{\mu}_q)$ obtained using the α coefficients. Since the results obtained using $\alpha^{r=1}$ and $\alpha^{r=2}$ are nearly degenerate for $SU(2)$, we decided to show only the case $r = 2$ for the sake of clarity.
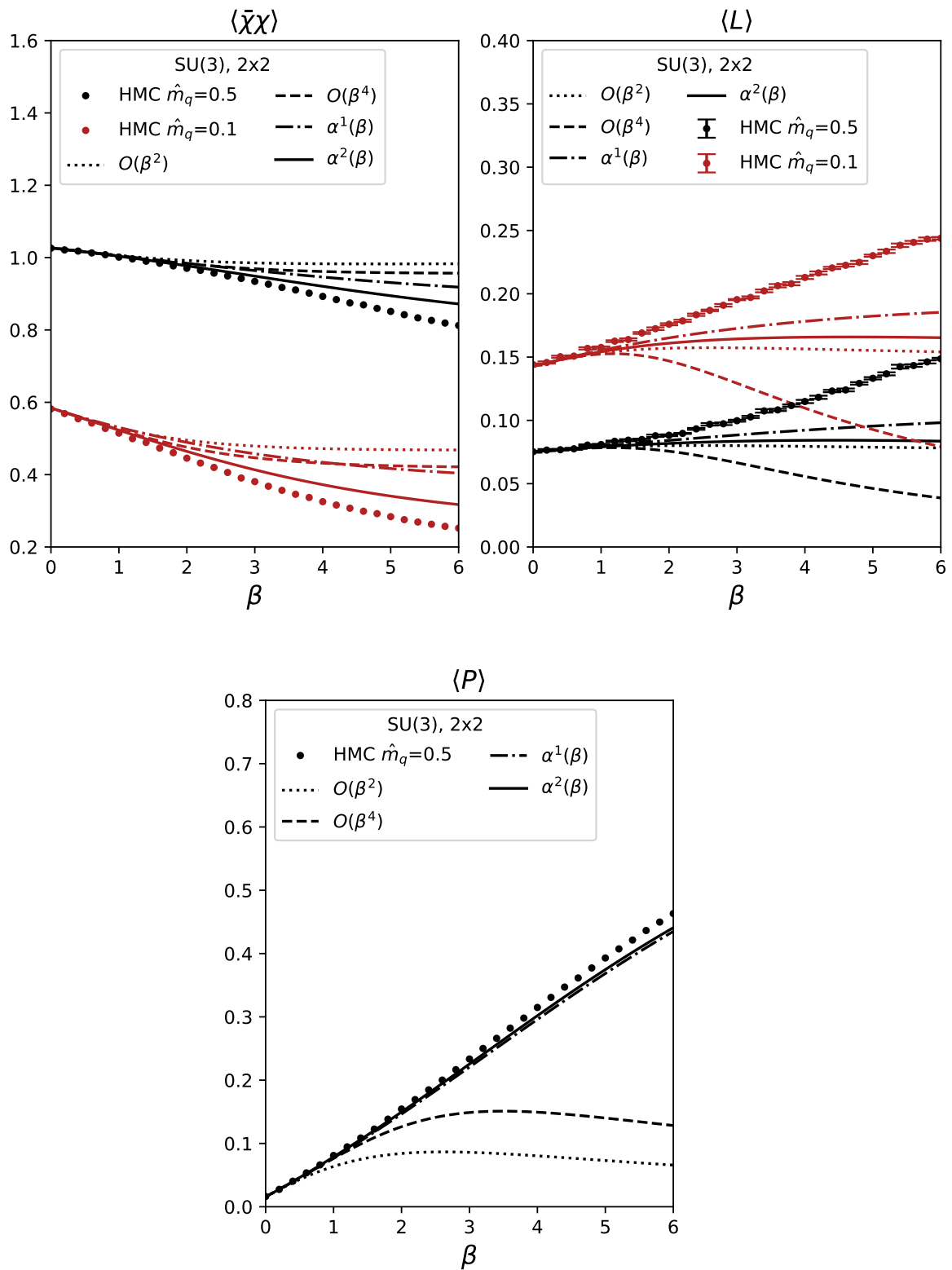
FIGURE 5.23: Same as in Fig. 5.22 for $G = \mathrm{SU}(3)$. In this case we plotted both the results for $\alpha^{r=1}$ and $\alpha^{r=2}$.
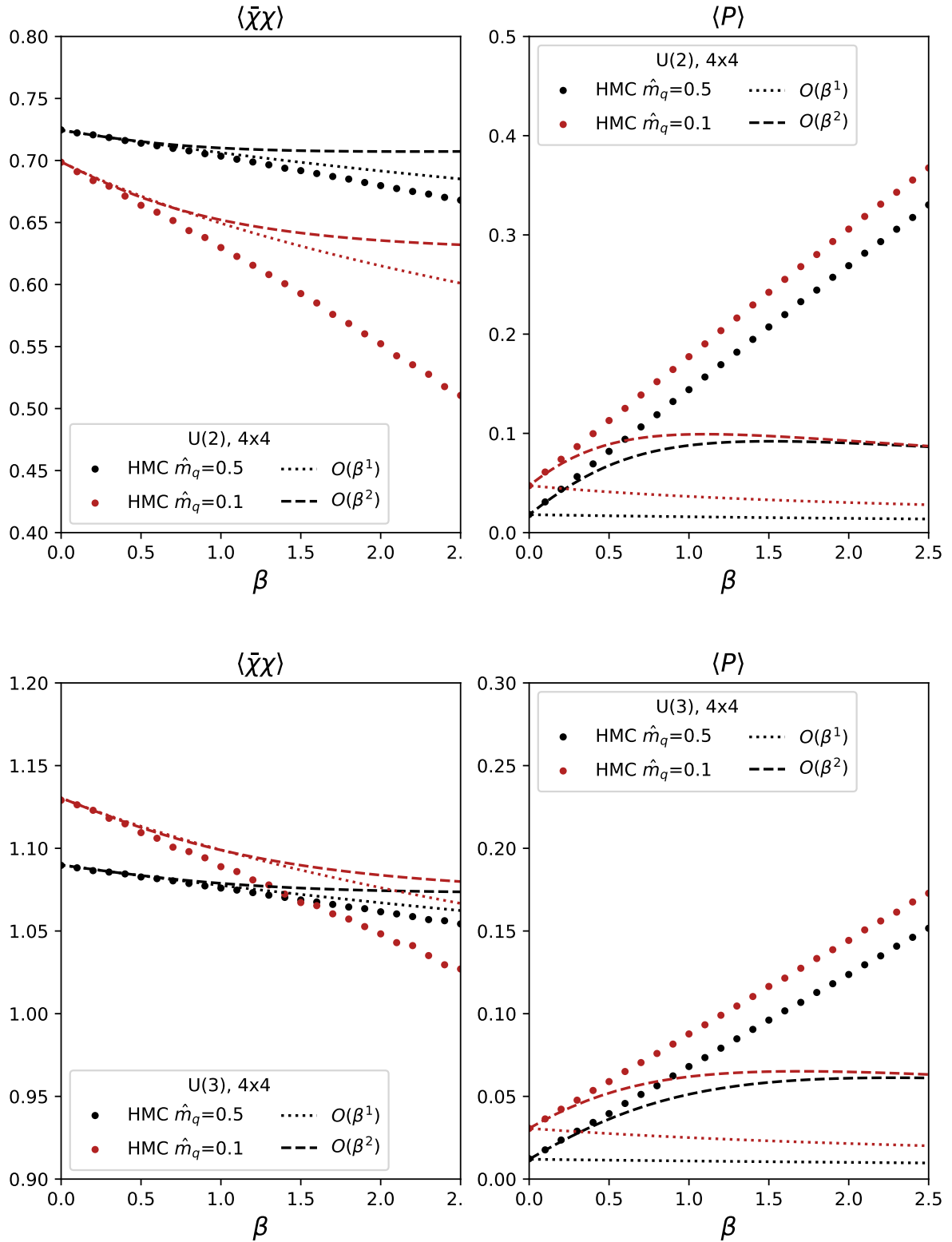
FIGURE 5.24: The chiral condensate $\langle \bar{\chi}\chi \rangle$ and the average plaquette $\langle P \rangle$ on the 4×4 lattice for $U(2)$ and $U(3)$. Given the large number of admissible configurations we were able to determine only the $\mathcal{O}(\beta)$ and $\mathcal{O}(\beta^2)$ polynomials $\mathcal{P}(\beta, \hat{m}_q, \hat{\mu}_q)$. The error bars are not shown because they are smaller than the point size.
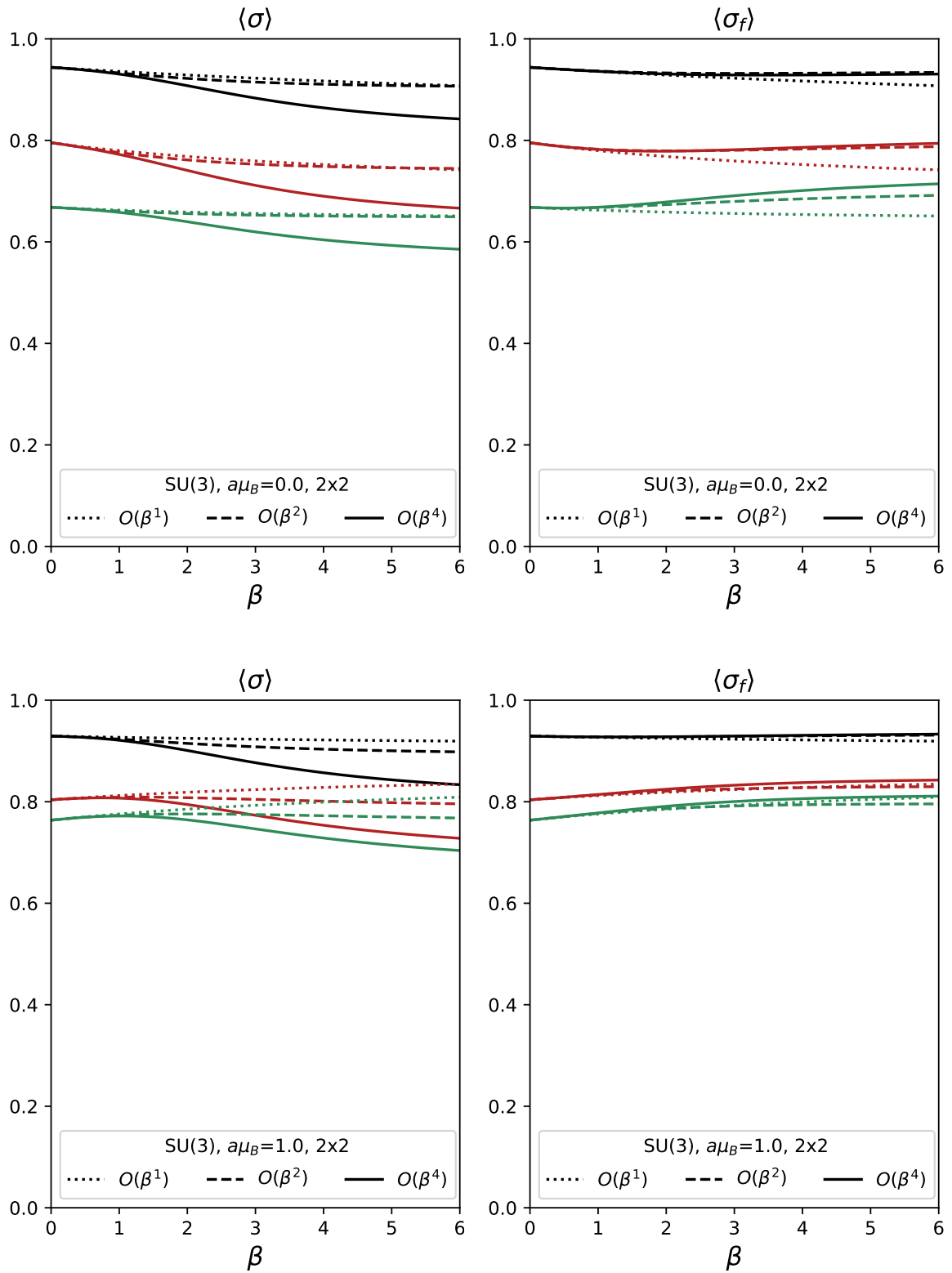
FIGURE 5.25: The average signs $\langle\sigma\rangle$ and $\langle\sigma_f\rangle$ for $G = \mathrm{SU}(3)$ on the 2×2 lattice for various quark masses $\hat{m}_q$ and truncation of the β expansion, and for two values of the baryon chemical potential $\hat{\mu}_B = 0.0$ and $\hat{\mu}_B = 1.0$. Black, red, and green lines correspond respectively to $\hat{m}_q = 0.5, 0.2, 0.0$.

Chapter 6

Conclusion

In this Ph.D. thesis we developed a new method to extend the dual formulation of strong coupling lattice QCD to finite β. We achieved an exact dualization of the all-order strong coupling expansion for general $SU(N)$ (or $U(N)$) gauge group, by making use of what we called *decoupling operators*. These arose from our solution of the polynomial $SU(N)$ one-link integral with open color indices, and is discussed in Ch. 5. The full partition function, after having integrated out both gauge and fermion fields, is organized as a Taylor expansion in β, where the configurations are identified by the same type of occupation numbers already present in the dualization of the Schwinger model, plus a set of additional integer variables, the *decoupling operator indices* (DOI). These are defined on the lattice bonds and correspond to labels for the decoupling operators. The first type of variables, usually referred to as dual variables, obey a number of constraints that in the dual representation reflect the original symmetries of the theory. The Grassmann integral indeed imposes an exact conservation law for the quark fluxes, while the $SU(N)$ Haar measure allows the quark and gauge flux to be present only in specific combinations. In terms of the dual variables and of the DOI, the statistical weights of the dual configurations are calculated as the disjoint product of local site weights, making the dual representation well suited for Monte Carlo simulations. The presence of the DOI, or in general of additional degrees of freedom besides the dual variables, is *unavoidable* in the dualization of non-Abelian gauge theories. The statistical weights of configurations only determined by the dual variables, are indeed non-local and hard to compute. The role of the DOI is to re-express the non-localities as a sum over local quantities which are in principle all computable. Moreover, the dependence of the dual partition function on the parameters of the theory, like quark mass and chemical potential, is particularly simple and only amounts to multiplication by positive factors.

The main reason why this representation is interesting is the possibility to reduce the magnitude of the finite density sign problem, which severely affect the standard formulation in terms of gauge links. This is indeed the case at strong coupling ($\beta = 0$), and our primary goal was to provide a formalism to evaluate the gauge corrections order by order

in the β expansion. The computation of the configuration weights has been automatized to provide this information. Several orders in the β expansions were computed: all statistical weights are now known up to $\mathcal{O}(\beta^4)$ in four dimensions, and up to $\mathcal{O}(\beta^7)$ in two dimensions for the most relevant case of SU(3). Given this result, we explicitly showed, taking as an example the $\mathcal{O}(\beta^2)$ corrections, how the partition function can be further cast in a form directly usable in Worm-type Monte Carlo simulations, in such a way that for small orders in the β expansion the complexity of the system is essentially constant. Several observables obtained in the dual formulations were cross checked in small two-dimensional volumes against the results obtained using hybrid Monte Carlo simulations, proving the capability of our method to reproduce the gauge corrections.

As in the strong coupling limit, also at finite β the dual partition function is not sign problem free. Sign fluctuations induced by gluons and fermions do not cancel. Our preliminary analysis of the sign problem shows that up to $\beta \approx 1$ simulations should be feasible, and that up to $\mathcal{O}(\beta^4)$ the phase diagram can be studied making use of the formalism we developed. An important question that one can then answer concerns the evolution of the critical point (or tricritical point in the chiral limit), as a function of β. At leading order, only a mild dependence on β is observed, while the chiral and nuclear transition are still degenerate. This behavior can change including the $\mathcal{O}(\beta^2)$ corrections for which the numerical simulations are in preparation.

Our dualization strategy is very general and can be applied to different models (e.g. scalar QCD), and possibly to different types of fermion discretizations. Indeed the decoupling operators are insensitive to the matter content of the Lagrangian, which however can affect the complexity of the resulting partition function. To give an example, in the case of Wilson fermions the presence of the additional spin indices produces a much larger tensor network as compared to the staggered one.

An all-order evaluation of the partition function is however not only hindered by a potential sign problem, but computational issues arise due to the high numerical cost of evaluating the statistical weights at large order. An important problem to solve, as a future research plan, is the numerical bottleneck caused by the color contraction of the decoupling operators. A group theoretical analysis of the structure of such contractions can allow us to obtain the site weights without the need of performing the contraction of the decoupling operators explicitly.

Appendix A

Proof of the combinatorial lemma Eq. (4.18)

Here we demonstrate the combinatorial lemma

$$\frac{f_{\lambda+q}}{D_{\lambda,N}} = \frac{(qN+p)!}{p!} \prod_{i=0}^{N-1} \frac{i!}{(i+q)!} \frac{f_{\lambda}}{D_{\lambda,N+q}} , \tag{A.1}$$

valid for $\text{len}(\lambda) \leq N$, which was used to obtain the generating functional in terms of the generalized Weingarten functions. To do so, we will manipulate the l.h.s. of the previous equation using the formulae given in Eq. (4.29) for the dimensions f_{λ} and $D_{\lambda,N}$ of the irreps of the symmetric and unitary group

$$f_{\lambda} = \frac{p!}{\prod_{(i,j)\in\lambda} h_{\lambda}(i,j)} \equiv \frac{p!}{h_{\lambda}} \qquad D_{\lambda,N} = \frac{\prod_{(i,j)\in\lambda}(N+i-j)}{\prod_{(i,j)\in\lambda} h_{\lambda}(i,j)} \equiv \frac{\tilde{D}_{\lambda,N}}{h_{\lambda}} , \tag{A.2}$$

where $\lambda \vdash p$ and the *hook* $h_{\lambda}(i,j)$ were defined in Sec. 4.1.2. The lhs of Eq. (A.1) can be written as

$$\frac{f_{\lambda+q}}{D_{\lambda,N}} = \frac{f_{\lambda+q}}{D_{\lambda+q,N}} = \frac{(qN+p)!}{\tilde{D}_{\lambda+q,N}} , \tag{A.3}$$

because $D_{\lambda,N} = D_{\lambda+q,N}$ as a consequence of

$$R_{\lambda} \otimes (R_{\text{det}})^{\otimes q} \cong R_{\lambda+q} , \tag{A.4}$$

since $D_{\text{det},N} = 1$. The term $\tilde{D}_{\lambda+q,N}$ in the l.h.s. of Eq. (A.3) can be further manipulated as follows

$$\tilde{D}_{\lambda+q,N} = \prod_{i=0}^{N-1} \frac{(N+q-i-1)!}{(N-i-1)!} \tilde{D}_{\lambda,N+q} . \tag{A.5}$$
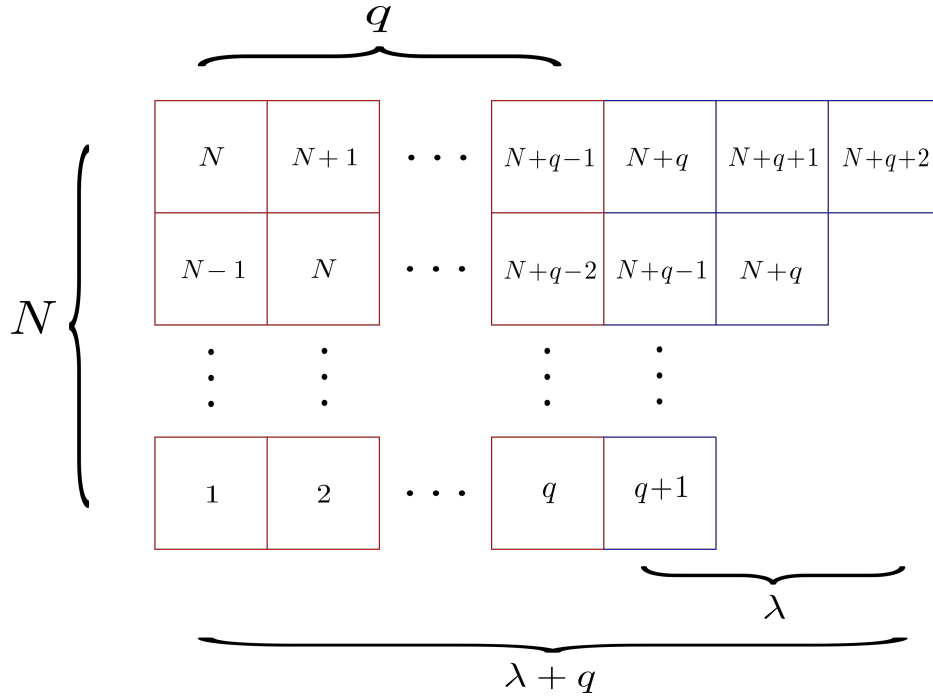
FIGURE A.1: The partitions λ (blue boxes) and $\lambda + q$ (blue and red boxes). The quantity $\tilde{D}_{\lambda+q,N}$ is the product of all numbers within the boxes. The restriction of this product to the blue boxes is clearly $D_{\lambda,N+q}$, therefore $\tilde{D}_{\lambda,N+q} = \alpha(N,q)\tilde{D}_{\lambda,N+q}$, where $\alpha(N,q)$ is the product of all numbers within the red boxes. It is easy to check that $\alpha(N,q) = \prod_{i=0}^{N-1} \frac{(N+q-1-i)!}{(N-i-1)!}$.

The validity of this equality is made clear in Fig. A.1. In conclusion we have

$$
\begin{aligned}
\frac{f_{\lambda+q}}{D_{\lambda,N}} &= \frac{(qN+p)!}{\tilde{D}_{\lambda+q,N}} = \prod_{i=0}^{N-1} \frac{(N-i-1)!}{(N+q-i-1)!} \frac{(qN+p)!}{\tilde{D}_{\lambda,N+q}} = \prod_{i=0}^{N-1} \frac{i!}{(i+q)!} (qN+p)! \frac{1}{h_\lambda} \frac{h_\lambda}{\tilde{D}_{\lambda,N+q}} \\
&= \prod_{i=0}^{N-1} \frac{i!}{(i+q)!} \frac{(qN+p)!}{p!} \frac{p!}{h_\lambda} \frac{h_\lambda}{\tilde{D}_{\lambda,N+q}} = \frac{(qN+p)!}{p!} \prod_{i=0}^{N-1} \frac{i!}{(i+q)!} \frac{f_\lambda}{D_{\lambda,N+q}} \qquad \square. \quad (A.6)
\end{aligned}
$$

Appendix B

List of generalized Weingarten functions

In this appendix we provide the complete list of the generalized Weingarten functions for the symmetric group S_4. In this case the number of conjugacy classes is five.

$$\tilde{\text{Wg}}_N^{q,4}(\{1,1,1,1\}) = \begin{cases} \dfrac{(N+q)^4-8(N+q)^2+24}{(N+q)^2((N+q)^2-1)((N+q)^2-4)((N+q)^2-9)} & N \geq 4 \\[2ex] \dfrac{23(q+3)^3+63(q+3)^2-14(q+3)-48}{4!(q+3)^2((q+3)^2-1)((q+3)^2-4)(q+6)} & N = 3 \\[2ex] \dfrac{14(q+2)^2+46(q+2)+24}{4!(q+2)^2((q+2)^2-1)(q+4)(q+5)} & N = 2 \end{cases}$$

$$\tilde{\text{Wg}}_N^{q,4}(\{2,1,1\}) = \begin{cases} -\dfrac{1}{(N+q)((N+q)^2-1)((N+q)^2-9)} & N \geq 4 \\[2ex] \dfrac{(q+3)^2-15(q+3)-34}{4!(q+3)((q+3)^2-1)((q+3)^2-4)(q+6)} & N = 3 \\[2ex] \dfrac{1}{6(q+2)((q+2)^2-1)(q+5)} & N = 2 \end{cases}$$

$$\tilde{\text{Wg}}_N^{q,4}(\{3,1\}) = \begin{cases} \dfrac{3}{4(N+q)^2((N+q)^2-1)((N+q)^2-9)} & N \geq 4 \\[2ex] -\dfrac{(N+q)^2+11(N+q)+12}{4!(N+q)^2((N+q)^2-1))(N+q+2)(N+q+3)} & N = 2,3 \end{cases}$$

$$\tilde{\text{Wg}}_N^{q,4}(\{2,2\}) = \begin{cases} \dfrac{7(N+q)^2-18}{3(N+q)((N+q)^2-1)((N+q)^2-4)((N+q)^2-9)} & N \geq 4 \\[2ex] -\dfrac{(q+3)^3+9(q+3)^2-18(q+3)-48}{4!(q+3)^2((q+2)^2-1)((q+2)^2-4)(q+6)} & N = 3 \\[2ex] \dfrac{(q+2)^2+5(q+2)+12}{12(q+2)^2((q+2)^2-1)(q+4)(q+5)} & N = 2 \end{cases}$$

$$\tilde{\text{Wg}}_N^{q,4}(\{4\}) = \begin{cases} -\dfrac{(N+q)^2+11}{4(N+q)((N+q)^2-1)((N+q)^2-4)((N+q)^2-9)} & N \geq 4 \\[2ex] \dfrac{(q+3)^2+3(q+3)+20}{4!(q+3)((q+3)^2-1)((q+3)^2-4)(q+6)} & N = 3 \\[2ex] -\dfrac{q+7}{12(q+2)((q+2)^2-1)(q+4)(q+5)} & N = 2 \end{cases}$$

Appendix C

Ariadne-β

In this appendix we briefly describe the main features of our code **Ariadne-β** for the generation of the higher order β contributions to the partition function. The code will be soon available online, and this appendix serves as an overview. The code has two main modes: "COMPUTE_TENSORS" and "EVALUATE_BUBBLES". In the first mode, the code takes as an input the maximum order $\mathcal{O}(\beta^k)$ considered, a gauge group $G = \mathrm{U}(N), \mathrm{SU}(N)$, and the number of spacetime dimensions $D + 1$. The output is the whole list of the non-zero weights entering the partition functions up to that order. Depending on the background of dual variables $\{n_p, \bar{n}_p, k_\ell, f_\ell, m_n\}$, the non-zero tensor elements $T^{\rho-D\cdots\rho_D}$ are all printed. The DOI ρ, as defined in Sec. 4.2.2, are multi-indices. In our code a mapping between the multi-indices $\rho \equiv \{(\alpha, \beta), (T_a, T_b)\}$ and a set of positive integers is used. In particular, the set partition (α, β) that distributes the color indices between the epsilon tensors and the delta functions, are ordered in reverse lexicographic order. In the first partition the fermionic color indices appear always before the gluonic color indices, while the subsequent set partition is generated by the next_permutation function of the $C++$ standard library, which follows the reverse lexicographic order. The pair of standard Young tableaux (T_a, T_b) of shape $\lambda \vdash n$, are similarly ordered by imposing the reverse lexicographic ordering on the partitions $\lambda \vdash n$ (i.e. from $\{n, 0\}$ to $\{1, \ldots, 1\}$), and the Yamanouchi symbols induced ordering for the tableaux T_a and T_b. In total we thus order the DOI ρ via

$$
\begin{aligned}
\rho > \rho' \leftrightarrow &(\alpha, \beta) > (\alpha', \beta') \text{ or} \\
&(\alpha, \beta) = (\alpha', \beta'), \ T_a > T_{a'} \text{ or} \\
&(\alpha, \beta) = (\alpha', \beta'), \ T_a = T_{a'} \ T_b > T_{b'}.
\end{aligned} \tag{C.1}
$$

In this way every DOI ρ is associated to an integer with $\rho \in (1, \ldots, N_\rho)$. The code then generates *only* the set of allowed dual variables surrounding an arbitrary lattice site (call it x), and computes the whole tensor T_x^ρ. The $2(D + 1)$ decoupling operators $P^{\rho_{\pm\mu}^x}$ associated to site x are built calculating only the associated irreducible matrix elements $M_{\lambda;a,b}(\pi)$, which

are stored in maps in order to avoid unnecessary multiple computations. The program actually computes only the matrices $M_\lambda(\tau_k)$ associated to the adjacent transpositions, while the matrix $M_\lambda(\pi)$ is then obtained from the decomposition of π in terms of the τ_k. The contraction of the projectors P^ρ is instead handled via the boost tensor library. The gauge flux between any pair of lattice links is precomputed from the value of the plaquette occupation numbers $n_p, \bar{n}_p$, and the corresponding color indices of the decoupling operators associated to the two lattice links are contracted. In practice we do not build the whole operators P^ρ but contract term by term the product of the Levi-Civita part with a permuting delta function δ_π. This has the drawback of slowing down the execution time, but avoids the intensive use of memory needed to store the whole operator $(P^\rho)_i^j$. When all gluonic color indices are contracted, the color indices that are left out (the fermionic ones) are contracted with the tensor G_n defined in Eq. (5.16). The resulting scalar quantity is then multiplied by the combinatorial factors appearing in the definition of the decoupling operators (Eq. (4.49)). Looping over the permuting delta functions produces the final result that , if non-zero, is stored in different files depending on the background of occupation numbers. When possible, the code makes use of rotational invariance and charge conjugation to speed up the computation.

The second mode computes the bubble diagrams given an arbitrary shape and a set of occupation numbers. The bubble shape is taken as an input, and it is implemented as a network of vertices connected by bonds. In this way bubbles related by rotations correspond to the same shape. The tensors T_n^ρ for all bubble vertex are loaded from the stored files, and the contraction of the tensor network is again performed using the boost tensor library. An external routine computes the fermionic sign associated to the nontrivial quark loop geometries and the result is returned.

Bibliography

[1]   A. Bazavov et al. "Chiral crossover in QCD at zero and non-zero chemical potentials". In: *Phys. Lett.* B795 (2019), pp. 15–21. DOI: 10.1016/j.physletb.2019.05.013. arXiv: 1812.08235 [hep-lat].

[2]   Larry McLerran and Robert D. Pisarski. "Phases of cold, dense quarks at large N(c)". In: *Nucl. Phys.* A796 (2007), pp. 83–100. DOI: 10.1016/j.nuclphysa.2007.08.013. arXiv: 0706.2191 [hep-ph].

[3]   Mark G. Alford et al. "Color superconductivity in dense quark matter". In: *Rev. Mod. Phys.* 80 (2008), pp. 1455–1515. DOI: 10.1103/RevModPhys.80.1455. arXiv: 0709.4635 [hep-ph].

[4]   Ulli Wolff. "Simulating the All-Order Strong Coupling Expansion III: $O(N)$ sigma/loop models". In: *Nucl. Phys.* B824 (2010). [Erratum: Nucl. Phys.B834,395(2010)], pp. 254–272. DOI: 10.1016/j.nuclphysb.2010.03.029,10.1016/j.nuclphysb.2009.09.006. arXiv: 0908.0284 [hep-lat].

[5]   Falk Bruckmann et al. "Dual lattice representations for $O(N)$ and $CP(N-1)$ models with a chemical potential". In: *Physics Letters B* 749 (2015), pp. 495 –501. ISSN: 0370-2693. DOI: https://doi.org/10.1016/j.physletb.2015.08.015. URL: http://www.sciencedirect.com/science/article/pii/S0370269315006164.

[6]   Ydalia Delgado Mercado, Christof Gattringer, and Alexander Schmidt. "Dual Lattice Simulation of the Abelian Gauge-Higgs Model at Finite Density: An Exploratory Proof of Concept Study". In: *Phys. Rev. Lett.* 111.14 (2013), p. 141601. DOI: 10.1103/PhysRevLett.111.141601. arXiv: 1307.6120 [hep-lat].

[7]   Christof Gattringer, Thomas Kloiber, and Vasily Sazonov. "Solving the sign problems of the massless lattice Schwinger model with a dual formulation". In: *Nucl. Phys.* B897 (2015), pp. 732–748. DOI: 10.1016/j.nuclphysb.2015.06.017. arXiv: 1502.05479 [hep-lat].

[8]   C. Itzykson and J. B. Zuber. *Quantum Field Theory*. International Series In Pure and Applied Physics. New York: McGraw-Hill, 1980. URL: http://dx.doi.org/10.1063/1.2916419.

[9] Michael E. Peskin and Daniel V. Schroeder. *An Introduction to quantum field theory*. Reading, USA: Addison-Wesley, 1995. URL: http://www.slac.stanford.edu/~mpeskin/QFT.html.

[10] Jean Zinn-Justin. "Quantum field theory and critical phenomena". In: *Int. Ser. Monogr. Phys.* 113 (2002), pp. 1–1054.

[11] M. Tanabashi et al. "Review of Particle Physics". In: *Phys. Rev. D* 98 (3 2018), p. 030001. DOI: 10.1103/PhysRevD.98.030001. URL: https://link.aps.org/doi/10.1103/PhysRevD.98.030001.

[12] H. J. Rothe. "Lattice gauge theories: An Introduction". In: *World Sci. Lect. Notes Phys.* 43 (1992). [World Sci. Lect. Notes Phys.82,1(2012)], pp. 1–381.

[13] Owe Philipsen and Christopher Pinke. "The $N_f = 2$ QCD chiral phase transition with Wilson fermions at zero and imaginary chemical potential". In: *Phys. Rev.* D93.11 (2016), p. 114507. DOI: 10.1103/PhysRevD.93.114507. arXiv: 1602.06129 [hep-lat].

[14] T. Celik, J. Engels, and H. Satz. "The Order of the Deconfinement Transition in SU(3) Yang-Mills Theory". In: *Phys. Lett.* 125B (1983), pp. 411–414. DOI: 10.1016/0370-2693(83)91314-X.

[15] Robert D. Pisarski and Frank Wilczek. "Remarks on the Chiral Phase Transition in Chromodynamics". In: *Phys. Rev.* D29 (1984), pp. 338–341. DOI: 10.1103/PhysRevD.29.338.

[16] Andrea Pelissetto and Ettore Vicari. "Relevance of the axial anomaly at the finite-temperature chiral transition in QCD". In: *Phys. Rev.* D88.10 (2013), p. 105018. DOI: 10.1103/PhysRevD.88.105018. arXiv: 1309.5446 [hep-lat].

[17] Heng-Tong Ding et al. "Chiral phase transition in (2 + 1)-flavor QCD". In: *PoS* LATTICE2018 (2019), p. 171. DOI: 10.22323/1.334.0171. arXiv: 1905.11610 [hep-lat].

[18] Y. Aoki et al. "The Order of the quantum chromodynamics transition predicted by the standard model of particle physics". In: *Nature* 443 (2006), pp. 675–678. DOI: 10.1038/nature05120. arXiv: hep-lat/0611014 [hep-lat].

[19] Claudia Ratti, Michael A. Thaler, and Wolfram Weise. "Phases of QCD: Lattice thermodynamics and a field theoretical model". In: *Phys. Rev.* D73 (2006), p. 014019. DOI: 10.1103/PhysRevD.73.014019. arXiv: hep-ph/0506234 [hep-ph].

[20] Szabolcs Borsanyi et al. "Fluctuations of conserved charges at finite temperature from lattice QCD". In: *JHEP* 01 (2012), p. 138. DOI: 10.1007/JHEP01(2012)138. arXiv: 1112.4416 [hep-lat].

[21] A. Bazavov et al. "The QCD Equation of State to $\mathcal{O}(\mu_B^6)$ from Lattice QCD". In: *Phys. Rev.* D95.5 (2017), p. 054504. DOI: 10.1103/PhysRevD.95.054504. arXiv: 1701.04325 [hep-lat].

[22] I. Montvay and G. Munster. *Quantum fields on a lattice*. Cambridge Monographs on Mathematical Physics. Cambridge University Press, 1997. DOI: 10.1017/CBO9780511470783. URL: http://www.cambridge.org/uk/catalogue/catalogue.asp?isbn=0521404320.

[23] Christof Gattringer and Christian B. Lang. "Quantum chromodynamics on the lattice". In: *Lect. Notes Phys.* 788 (2010), pp. 1–343. DOI: 10.1007/978-3-642-01850-3.

[24] G. Parisi. "Symanzik's improvement program". In: *Nucl. Phys.* B254 (1985), pp. 58–70. DOI: 10.1016/0550-3213(85)90211-1.

[25] Martin Luscher. "Advanced lattice QCD". In: *Probing the standard model of particle interactions. Proceedings, Summer School in Theoretical Physics, NATO Advanced Study Institute, 68th session, Les Houches, France, July 28-September 5, 1997. Pt. 1, 2.* 1998, pp. 229–280. arXiv: hep-lat/9802029 [hep-lat].

[26] Holger Bech Nielsen and M. Ninomiya. "No Go Theorem for Regularizing Chiral Fermions". In: *Phys. Lett.* 105B (1981), pp. 219–223. DOI: 10.1016/0370-2693(81)91026-1.

[27] John B. Kogut and Leonard Susskind. "Hamiltonian Formulation of Wilson's Lattice Gauge Theories". In: *Phys. Rev.* D11 (1975), pp. 395–408. DOI: 10.1103/PhysRevD.11.395.

[28] Kenneth G. Wilson. "Confinement of Quarks". In: *Phys. Rev.* D10 (1974). [,45(1974); ,319(1974)], pp. 2445–2459. DOI: 10.1103/PhysRevD.10.2445.

[29] Rainer Sommer. "Scale setting in lattice QCD". In: *PoS* LATTICE2013 (2014), p. 015. DOI: 10.22323/1.187.0015. arXiv: 1401.3270 [hep-lat].

[30] Szabolcs Borsanyi et al. "High-precision scale setting in lattice QCD". In: *JHEP* 09 (2012), p. 010. DOI: 10.1007/JHEP09(2012)010. arXiv: 1203.4469 [hep-lat].

[31] P. Hasenfratz and F. Karsch. "Chemical Potential on the Lattice". In: *Phys. Lett.* 125B (1983), pp. 308–310. DOI: 10.1016/0370-2693(83)91290-X.

[32] Rajiv V. Gavai and Sayantan Sharma. "Divergences in the quark number susceptibility: The origin and a cure". In: *Phys. Lett.* B749 (2015), pp. 8–13. DOI: 10.1016/j.physletb.2015.07.036. arXiv: 1406.0474 [hep-lat].

[33] M. A. Clark and A. D. Kennedy. "Accelerating Staggered Fermion Dynamics with the Rational Hybrid Monte Carlo (RHMC) Algorithm". In: *Phys. Rev.* D75 (2007), p. 011502. DOI: 10.1103/PhysRevD.75.011502. arXiv: hep-lat/0610047 [hep-lat].

[34] Martin Hasenbusch. "Speeding up the hybrid Monte Carlo algorithm for dynamical fermions". In: *Phys. Lett.* B519 (2001), pp. 177–182. DOI: 10.1016/S0370-2693(01)01102-9. arXiv: hep-lat/0107019 [hep-lat].

[35] Z. Fodor and S. D. Katz. "A New method to study lattice QCD at finite temperature and chemical potential". In: *Phys. Lett.* B534 (2002), pp. 87–92. DOI: 10.1016/S0370-2693(02)01583-6. arXiv: hep-lat/0104001 [hep-lat].

[36] C. R. Allton et al. "Thermodynamics of two flavor QCD to sixth order in quark chemical potential". In: *Phys. Rev.* D71 (2005), p. 054508. DOI: 10.1103/PhysRevD.71.054508. arXiv: hep-lat/0501030 [hep-lat].

[37] Andre Roberge and Nathan Weiss. "Gauge Theories With Imaginary Chemical Potential and the Phases of QCD". In: *Nucl. Phys.* B275 (1986), pp. 734–745. DOI: 10.1016/0550-3213(86)90582-1.

[38] Philippe de Forcrand and Owe Philipsen. "The QCD phase diagram for three degenerate flavors and small baryon density". In: *Nucl. Phys.* B673 (2003), pp. 170–186. DOI: 10.1016/j.nuclphysb.2003.09.005. arXiv: hep-lat/0307020 [hep-lat].

[39] Massimo D'Elia and Maria-Paola Lombardo. "Finite density QCD via imaginary chemical potential". In: *Phys. Rev.* D67 (2003), p. 014505. DOI: 10.1103/PhysRevD.67.014505. arXiv: hep-lat/0209146 [hep-lat].

[40] Dénes Sexty. "Simulating full QCD at nonzero density using the complex Langevin equation". In: *Phys. Lett.* B729 (2014), pp. 108–111. DOI: 10.1016/j.physletb.2014.01.019. arXiv: 1307.7748 [hep-lat].

[41] Gert Aarts et al. "Controlling complex Langevin dynamics at finite density". In: *Eur. Phys. J.* A49 (2013), p. 89. DOI: 10.1140/epja/i2013-13089-4. arXiv: 1303.6425 [hep-lat].

[42] Marco Cristoforetti, Francesco Di Renzo, and Luigi Scorzato. "New approach to the sign problem in quantum field theories: High density QCD on a Lefschetz thimble". In: *Phys. Rev.* D86 (2012), p. 074506. DOI: 10.1103/PhysRevD.86.074506. arXiv: 1205.3996 [hep-lat].

[43] Andrei Alexandru et al. "Sign problem and Monte Carlo calculations beyond Lefschetz thimbles". In: *JHEP* 05 (2016), p. 053. DOI: 10.1007/JHEP05(2016)053. arXiv: 1512.08764 [hep-lat].

[44] Christian Schmidt and Felix Ziesché. "Simulating low dimensional QCD with Lefschetz thimbles". In: *PoS* LATTICE2016 (2017), p. 076. DOI: 10.22323/1.256.0076. arXiv: 1701.08959 [hep-lat].

[45] F. Di Renzo and G. Eruzzi. "One-dimensional QCD in thimble regularization". In: *Phys. Rev.* D97.1 (2018), p. 014503. DOI: 10.1103/PhysRevD.97.014503. arXiv: 1709.10468 [hep-lat].

[46] Kurt Langfeld, Biagio Lucini, and Antonio Rago. "The density of states in gauge theories". In: *Phys. Rev. Lett.* 109 (2012), p. 111601. DOI: 10.1103/PhysRevLett.109.111601. arXiv: 1204.3243 [hep-lat].

[47] Michael Fromm et al. "Onset Transition to Cold Nuclear Matter from Lattice QCD with Heavy Quarks". In: *Phys. Rev. Lett.* 110.12 (2013), p. 122001. DOI: 10.1103/PhysRevLett.110.122001. arXiv: 1207.3005 [hep-lat].

[48] Jonas Glesaaen, Mathias Neuman, and Owe Philipsen. "Equation of state for cold and dense heavy QCD". In: *JHEP* 03 (2016), p. 100. DOI: 10.1007/JHEP03(2016)100. arXiv: 1512.05195 [hep-lat].

[49] Owe Philipsen and Jonas Scheunert. "Baryonic or quarkyonic matter?" In: *PoS* Confinement2018 (2018), p. 057. DOI: 10.22323/1.336.0057. arXiv: 1812.02014 [hep-lat].

[50] Fei Gao and Jan M. Pawlowski. "QCD phase structure from functional methods". In: (2020). arXiv: 2002.07500 [hep-ph].

[51] H. A. Kramers and G. H. Wannier. "Statistics of the two-dimensional ferromagnet. Part 1." In: *Phys. Rev.* 60 (1941), pp. 252–262. DOI: 10.1103/PhysRev.60.252.

[52] H. A. Kramers and G. H. Wannier. "Statistics of the Two-Dimensional Ferromagnet. Part II". In: *Phys. Rev.* 60 (1941), pp. 263–276. DOI: 10.1103/PhysRev.60.263.

[53] Robert Savit. "Duality in Field Theory and Statistical Systems". In: *Rev. Mod. Phys.* 52 (1980), p. 453. DOI: 10.1103/RevModPhys.52.453.

[54] Robert Lohmayer and Rajamani Narayanan. "Phase structure of two-dimensional QED at zero temperature with flavor-dependent chemical potentials and the role of multidimensional theta functions". In: *Phys. Rev.* D88.10 (2013), p. 105030. DOI: 10.1103/PhysRevD.88.105030. arXiv: 1307.4969 [hep-th].

[55] Nikolay Prokof'ev and Boris Svistunov. "Worm Algorithms for Classical Statistical Models". In: *Phys. Rev. Lett.* 87 (2001), p. 160601. DOI: 10.1103/PhysRevLett.87.160601. arXiv: cond-mat/0103146 [cond-mat].

[56] Daniel Göschl et al. "Simulation strategies for the massless lattice Schwinger model in the dual formulation". In: *Nucl. Phys.* B924 (2017), pp. 63–85. DOI: 10.1016/j.nuclphysb.2017.09.006. arXiv: 1708.00649 [hep-lat].

[57] Christof Gattringer and Thomas Kloiber. "Lattice study of the Silver Blaze phenomenon for a charged scalar ϕ^4 field". In: *Nucl. Phys.* B869 (2013), pp. 56–73. DOI: 10.1016/j.nuclphysb.2012.12.005. arXiv: 1206.2954 [hep-lat].

[58] K. E. Eriksson, N. Svartholm, and B. S. Skagerstam. "On Invariant Group Integrals in Lattice QCD". In: *J. Math. Phys.* 22 (1981), p. 2276. DOI: 10.1063/1.524760.

[59] Michael Fromm. "Lattice QCD at strong coupling". PhD thesis. Zurich, ETH, 2010. DOI: 10.3929/ethz-a-006414247. URL: http://e-collection.library.ethz.ch/view/eth:2616.

[60] Pietro Rossi and Ulli Wolff. "Lattice QCD With Fermions at Strong Coupling: A Dimer System". In: *Nucl. Phys.* B248 (1984), pp. 105–122. DOI: 10.1016/0550-3213(84)90589-3.

[61] F. Karsch and K. H. Mutter. "Strong Coupling QCD at Finite Baryon Number Density". In: *Nucl. Phys.* B313 (1989), pp. 541–559. DOI: 10.1016/0550-3213(89)90396-9.

[62] David H. Adams and Shailesh Chandrasekharan. "Chiral limit of strongly coupled lattice gauge theories". In: *Nucl. Phys.* B662 (2003), pp. 220–246. DOI: 10.1016/S0550-3213(03)00350-X. arXiv: hep-lat/0303003 [hep-lat].

[63] Philippe de Forcrand and Michael Fromm. "Nuclear Physics from lattice QCD at strong coupling". In: *Phys. Rev. Lett.* 104 (2010), p. 112005. DOI: 10.1103/PhysRevLett.104.112005. arXiv: 0907.1915 [hep-lat].

[64] Philippe de Forcrand, Wolfgang Unger, and Helvio Vairinhos. "Strong-Coupling Lattice QCD on Anisotropic Lattices". In: *Phys. Rev.* D97.3 (2018), p. 034512. DOI: 10.1103/PhysRevD.97.034512. arXiv: 1710.00611 [hep-lat].

[65] John L. Cardy. *Finite-size Scaling*. Current physics. North-Holland, 1988. URL: https://books.google.de/books?id=lqPvAAAAMAAJ.

[66] K. Binder and D. P. Landau. "Finite-size scaling at first-order phase transitions". In: *Phys. Rev. B* 30 (3 1984), pp. 1477–1485. DOI: 10.1103/PhysRevB.30.1477. URL: https://link.aps.org/doi/10.1103/PhysRevB.30.1477.

[67] Jooyoung Lee and J. M. Kosterlitz. "Finite-size scaling and Monte Carlo simulations of first-order phase transitions". In: *Phys. Rev. B* 43 (4 1991), pp. 3265–3277. DOI: 10.1103/PhysRevB.43.3265. URL: https://link.aps.org/doi/10.1103/PhysRevB.43.3265.

[68] Massimo Campostrini et al. "Critical behavior of the three-dimensional xy universality class". In: *Phys. Rev.* B63 (2001), p. 214503. DOI: 10.1103/PhysRevB.63.214503. arXiv: cond-mat/0010360 [cond-mat].

[69] Philippe de Forcrand et al. "The Phase Diagram of Strong Coupling QCD including Gauge Corrections". In: *PoS* LATTICE2013 (2014), p. 142. DOI: 10.22323/1.187.0142. arXiv: 1312.0589 [hep-lat].

[70] J. Wade Cherrington, Dan Christensen, and Igor Khavkine. "Dual computations of non-Abelian Yang-Mills on the lattice". In: *Phys. Rev.* D76 (2007), p. 094503. DOI: 10.1103/PhysRevD.76.094503. arXiv: 0705.2629 [hep-lat].

[71] J. Wade Cherrington. "A Dual Algorithm for Non-abelian Yang-Mills coupled to Dynamical Fermions". In: *Nucl. Phys.* B794 (2008), pp. 195–215. DOI: 10.1016/j.nuclphysb.2007.11.006. arXiv: 0710.0323 [hep-lat].

[72] J. Wade Cherrington. "Dual Non-Abelian Yang-Mills Simulations in Four Dimensions". In: (2009). arXiv: 0910.1890 [hep-lat].

[73] Christof Gattringer and Carlotta Marchis. "Abelian color cycles: a new approach to strong coupling expansion and dual representations for non-abelian lattice gauge theory". In: *Nucl. Phys.* B916 (2017), pp. 627–646. DOI: 10.1016/j.nuclphysb.2017.01.025. arXiv: 1609.00124 [hep-lat].

[74] Carlotta Marchis and Christof Gattringer. "Dual representation of lattice QCD with worldlines and worldsheets of abelian color fluxes". In: *Phys. Rev.* D97.3 (2018), p. 034508. DOI: 10.1103/PhysRevD.97.034508. arXiv: 1712.07546 [hep-lat].

[75] Christof Gattringer, Daniel Göschl, and Carlotta Marchis. "Kramers–Wannier duality and worldline representation for the SU(2) principal chiral model". In: *Phys. Lett.* B778 (2018), pp. 435–441. DOI: 10.1016/j.physletb.2018.01.065. arXiv: 1709.04691 [hep-lat].

[76] Don Weingarten. "Asymptotic Behavior of Group Integrals in the Limit of Infinite Rank". In: *J. Math. Phys.* 19 (1978), p. 999. DOI: 10.1063/1.523807.

[77] Jean-Michel Drouffe and Jean-Bernard Zuber. "Strong Coupling and Mean Field Methods in Lattice Gauge Theories". In: *Phys. Rept.* 102 (1983), p. 1. DOI: 10.1016/0370-1573(83)90034-0.

[78] Michael Creutz. "On Invariant Integration over SU(N)". In: *J. Math. Phys.* 19 (1978), p. 2043. DOI: 10.1063/1.523581.

[79] I. Bars. "U(N) Integral for Generating Functional in Lattice Gauge Theory". In: *J. Math. Phys.* 21 (1980), p. 2678. DOI: 10.1063/1.524368.

[80] Itzhak Bars and Frederic Green. "Complete Integration of U (N) Lattice Gauge Theory in a Large N Limit". In: *Phys. Rev.* D20 (1979), p. 3311. DOI: 10.1103/PhysRevD.20.3311.

[81] Richard Brower, Paolo Rossi, and Chung-I Tan. "The external field problem for QCD". In: *Nuclear Physics B* 190.4 (1981), pp. 699 –718. ISSN: 0550-3213. DOI: https://doi.org/10.1016/0550-3213(81)90046-8. URL: http://www.sciencedirect.com/science/article/pii/0550321381900468.

[82] Jesse Carlsson. "Integrals over SU(N)". In: (2008). arXiv: 0802.3409 [hep-lat].

[83] Benoit Collins. *Moments and Cumulants of Polynomial random variables on unitary groups, the Itzykson-Zuber integral and free probability*. 2002. arXiv: math-ph/0205010 [math-ph].

[84] Benoît Collins and Piotr Śniady. "Integration with Respect to the Haar Measure on Unitary, Orthogonal and Symplectic Group". In: *Communications in Mathematical Physics* 264.3 (2006), pp. 773–795. DOI: 10.1007/s00220-006-1554-3. arXiv: math-ph/0402073 [math-ph].

[85] Benoît Collins and Sho Matsumoto. *Weingarten calculus via orthogonality relations: new applications*. 2017. arXiv: 1701.04493 [math.CO].

[86] Jonathan Novak. *Complete homogeneous symmetric polynomials in Jucys-Murphy elements and the Weingarten function*. 2008. arXiv: 0811.3595 [math.CO].

[87] Marcel Novaes. *Elementary derivation of Weingarten functions of classical Lie groups*. 2014. arXiv: 1406.2182 [math-ph].

[88] Jean-Bernard Zuber. "Revisiting SU(N) integrals". In: *Journal of Physics A: Mathematical and Theoretical* 50.1 (2016), p. 015203. DOI: 10.1088/1751-8113/50/1/015203. URL: https://doi.org/10.1088%2F1751-8113%2F50%2F1%2F015203.

[89] Giuseppe Gagliardi and Wolfgang Unger. "Towards a Dual Representation of Lattice QCD". In: *PoS* LATTICE2018 (2018), p. 224. DOI: 10.22323/1.334.0224. arXiv: 1811.02817 [hep-lat].

[90] O. Borisenko, S. Voloshyn, and V. Chelnokov. "SU(N) polynomial integrals and some applications". In: (2018). arXiv: 1812.06069 [hep-lat].

[91] D. E. Knuth. *The Art of Computer Programming: Fascicles 0-4*. 1st. Addison-Wesley Professional, 2009.

[92] D. E. Littlewood and A. R. Richardson. "Group Characters and Algebra". In: *Philosophical Transactions of the Royal Society of London. Series A, Containing Papers of a Mathematical or Physical Character* 233 (1934), pp. 99–141. ISSN: 02643952. URL: http://www.jstor.org/stable/91293.

[93] F. D. Murnaghan. "On the Representations of the Symmetric Group". In: *American Journal of Mathematics* 59.3 (1937), pp. 437–488. ISSN: 00029327, 10806377. URL: http://www.jstor.org/stable/2371574.

[94] T. Nakayama. "On some modular properties of irreducible representations of a symmetric group, I". In: *Japanese journal of mathematics :transactions and abstracts* 17 (1940), pp. 165–184. DOI: 10.4099/jjm1924.17.0_165.

[95] Wei Wu and Qianer Zhang. "The orthogonal and the natural representation for symmetric groups". In: *International Journal of Quantum Chemistry* 50.1 (1994), pp. 55–67. DOI: 10.1002/qua.560500105. URL: https://onlinelibrary.wiley.com/doi/abs/10.1002/qua.560500105.

[96] G.D. James and A. Kerber. *The Representation Theory of the Symmetric Group*. Encyclopedia of Mathematics and its Applications. Cambridge University Press, 1984. URL: https://books.google.de/books?id=yWa_RaqkLUsC.

[97] Morton Hamermesh. "Group Theory and its Applications to Physical Problems". In: *American Journal of Physics* 30.10 (1962), pp. 774–775. DOI: 10.1119/1.1941790. URL: https://doi.org/10.1119/1.1941790.

[98] Giuseppe Gagliardi and Wolfgang Unger. "New dual representation for staggered lattice QCD". In: *Phys. Rev.* D101.3 (2020), p. 034509. DOI: 10.1103/PhysRevD.101.034509. arXiv: 1911.08389 [hep-lat].

[99] N. Cabibbo and E. Marinari. "A New Method for Updating SU(N) Matrices in Computer Simulations of Gauge Theories". In: *Phys. Lett.* 119B (1982), pp. 387–390. DOI: 10.1016/0370-2693(82)90696-7.

[100] Philippe de Forcrand et al. "Lattice QCD Phase Diagram In and Away from the Strong Coupling Limit". In: *Phys. Rev. Lett.* 113.15 (2014), p. 152002. DOI: 10.1103/PhysRevLett.113.152002. arXiv: 1406.4397 [hep-lat].

[101] Jangho Kim, Marc Klegrewe, and Wolfgang Unger. "Gauge Corrections to Strong Coupling Lattice QCD on Anisotropic Lattices". In: (2019). arXiv: 2001.06797 [hep-lat].

Acknowledgements

First of all, I would like to thank my supervisor Dr. Wolfgang Unger for having supported me, for all the inspiring discussions we had, and for giving me the possibility to attend many conferences and schools in the past years.

I also want to thank Prof. Dr. Owe Philipsen for agreeing to be the second referee of this Ph.D. thesis.

I thank all the members of the group "Lattice QCD at strong coupling" for the many interesting discussions.

I am grateful to the whole physics department for the friendly working atmosphere. A special thanks goes to Gudrun Eickmeyer and Susi v. Reder who helped me dealing with the German bureaucracy, and finding an apartment in Bielefeld. During the last three years I made many new friends. I thank you all for the fun physics-related discussions, and for all the time we spent together inside and outside the university. In particular I want to thank my friend and office-mate Lorenzo: I had a lot of fun sharing the office with you despite your annoying and precious spring. I am also indebted to my friend David Clarke for proof-reading this thesis.

Without the support of my girlfriend I would have never managed to overcome the difficulties of this doctorate. Thank you Sofia for your kind help during all these years.

To my parents: thank you for your support, for the many phone calls, and for your constant preoccupation for my daily diet.